



HAL
open science

Energy-efficient cooperative techniques for wireless body area sensor networks

Viet-Hoa Nguyen

► **To cite this version:**

Viet-Hoa Nguyen. Energy-efficient cooperative techniques for wireless body area sensor networks. Networking and Internet Architecture [cs.NI]. Université Rennes 1, 2016. English. NNT : 2016REN1S011 . tel-02384923

HAL Id: tel-02384923

<https://theses.hal.science/tel-02384923>

Submitted on 28 Nov 2019

HAL is a multi-disciplinary open access archive for the deposit and dissemination of scientific research documents, whether they are published or not. The documents may come from teaching and research institutions in France or abroad, or from public or private research centers.

L'archive ouverte pluridisciplinaire **HAL**, est destinée au dépôt et à la diffusion de documents scientifiques de niveau recherche, publiés ou non, émanant des établissements d'enseignement et de recherche français ou étrangers, des laboratoires publics ou privés.



THÈSE / UNIVERSITÉ DE RENNES 1
sous le sceau de l'Université Européenne de Bretagne

pour le grade de
DOCTEUR DE L'UNIVERSITÉ DE RENNES 1

Mention : Traitement du Signal et Télécommunications

École doctorale MATISSE

présentée par

Viet-Hoa NGUYEN

préparée à l'unité de recherche UMR6074 IRISA

Institut de recherche en informatique et systèmes aléatoires - GRANIT

École Nationale Supérieure des Sciences Appliquées et de Technologie

**Energy-efficient
cooperative techniques
for Wireless Body Area
Sensor Networks**

Thèse à soutenir à Lannion

09 Février 2016

devant le jury composé de :

CANCES Jean-Pierre

Professeur à l'Université de Limoges / rapporteur

DIOURIS Jean-François

Professeur à l'Université de Nantes / rapporteur

GORCE Jean-Marie

Professeur à l'INSA de Lyon / examinateur

BERDER Olivier

Professeur à l'Université de Rennes 1 / directeur de thèse

VRIGNEAU Baptiste

Maître de Conférences à l'Université de Rennes 1 /
co-directeur de thèse

LANGLAIS Charlotte

Maître de Conférences à Télécom Bretagne /
co-directeur de thèse

Contents

List of Figures	v
List of Tables	ix
Acronyms	xii
Notations	xvi
Abstract	1
Introduction	4
1 Communication in WBAN	14
1.1 Overview on WBAN	16
1.1.1 WBAN architecture	16
1.1.1.1 Network topology	16
1.1.1.2 Types of devices	17
1.1.1.3 Transmission scenarios	17
1.1.1.4 Intra-BAN communication	18
1.1.1.5 Extra-BAN communication	20
1.1.2 WBAN channel characteristics	21
1.1.2.1 Body tissues	21
1.1.2.2 Antenna effect	21
1.1.2.3 Path loss	22
1.1.2.4 Fading	22
1.2 Cooperative technique	25

1.2.1	Cooperative relay	26
1.2.1.1	Decode and Forward relaying	28
1.2.1.2	Amplify and Forward relaying	29
1.2.1.3	Compress and Forward relaying	30
1.2.2	Opportunistic relay	31
1.2.2.1	Without feedback selection	31
1.2.2.2	With feedback selection	33
1.2.3	Cooperative open-loop MIMO	34
1.3	Conclusion	36
2	How to benefit from channel feedback	38
2.1	Closed-loop precoding for co-located MIMO system	40
2.1.1	Virtual channel transformation	41
2.1.1.1	Noise whitening	41
2.1.1.2	Channel diagonalization	41
2.1.1.3	Dimensionality reduction	42
2.1.2	Existing precoders	42
2.1.2.1	(Unweighted) MMSE Design	42
2.1.2.2	Equal-error Design	43
2.1.2.3	QoS-Based Design	43
2.1.2.4	Beam forming Design	44
2.1.2.5	Waterfilling Design	44
2.1.2.6	X- and Y- codes precoder	44
2.1.3	Max- d_{\min} precoder	45
2.1.3.1	The max- d_{\min} precoder solution for BPSK modulation	46
2.1.3.2	The max- d_{\min} precoder solution for QPSK modulation	47
2.1.3.3	The max- d_{\min} precoder solution for 16-QAM modulation	47
2.1.3.4	General expression of max- d_{\min} precoder for high QAM modulation levels	48
2.1.4	Feedback link requirement	49

2.1.4.1	Direct feedback	51
2.1.4.2	Limited feedback	51
2.2	Distributed max- d_{\min} precoding (DMP)	54
2.2.1	System model	55
2.2.2	Decode and Forward relaying (DMPDF)	57
2.2.3	Amplify and Forward relaying (DMPAF)	58
2.2.3.1	Factor multiplying	59
2.2.3.2	Channel customizing	60
2.2.4	Energy model	61
2.2.4.1	Circuit energy consumption model	61
2.2.4.2	Transmission power consumption	62
2.2.4.3	Spectral efficiency and bit rate	62
2.2.5	Simulation results	63
2.3	Conclusion	67
3	Distributed max-d_{\min} precoding: Decode-and-Forward	69
3.1	Introduction	70
3.2	Decode and Forward for the distributed max- d_{\min} precoding	71
3.2.1	Distributed scheme description	71
3.2.2	System model	72
3.2.3	Precoder design	74
3.2.4	Theoretical error probability	74
3.3	Performance analysis	75
3.3.1	Definition of the different hypothesis	75
3.3.2	Study of hypothesis Θ_0	76
3.3.3	Study of Hypothesis Θ_1 & Θ_2	77
3.3.4	Study of hypothesis Θ_3	79
3.3.5	Interference investigation	79
3.3.6	Solution 1: Derive an upper-bound	81
3.3.6.1	Solution 2: Estimate the pdf	82
3.4	Results and discussions	84

3.5	Decoder design with the side information	89
3.6	Conclusion	92
4	Distributed max-d_{\min} precoding: Amplify-and-Forward	94
4.1	Introduction	95
4.2	System description	96
4.3	Euclidean distance distribution analysis	99
4.3.1	The case of \mathbf{F}_{r_1}	103
4.3.2	The case of \mathbf{F}_{octa}	104
4.3.3	The complete form of d_{\min}^2	105
4.4	Euclidean distance based evaluation	108
4.4.1	Ergodic capacity and power allocation strategy	108
4.4.1.1	The values of v_i	109
4.4.1.2	The values of τ_i	110
4.4.1.3	The average ergodic capacity	110
4.4.2	Outage probability	112
4.4.2.1	The case of \mathbf{F}_{r_1}	112
4.4.2.2	The case of \mathbf{F}_{octa}	112
4.4.3	Power allocation	113
4.4.3.1	Capacity based power allocation	113
4.4.3.2	Outage based power allocation	114
4.4.3.3	Simulation results	114
4.5	Conclusion	117
	Conclusions and Future works	119
	Appendices	126
A	Calculation of $E\{ f_{21} ^4\}$ and $E\{ f_{22} ^4\}$	127
A.1	The case of \mathbf{F}_{r_1}	127
A.2	The case of \mathbf{F}_{octa}	128
B	Proof of pdf of d_{\min}^2 for precoder \mathbf{F}_{octa}	131

List of Figures

1	An overview of BoWI project [1]	8
2	Zyggie prototype, version 1	9
1.1	Two common topologies used in WBAN	16
1.2	Two categories of communication in WBAN: red dash arrow denotes the intra-BAN and green solid arrow denotes the extra-BAN	19
1.3	The distribution fitting for the extra-BAN channel: the transmitter on the chest and receiver on the external	24
1.4	The distribution fitting for intra-BAN channel: the transmitter on the chest and receiver on the wrist	24
1.5	Relaying system model with source S , destination D and n relays $R_1..R_n$	27
1.6	Three common types of relaying: dashed arrow denotes the first time slot, the solid arrow denotes the second time slot	28
1.7	A simple cooperative MIMO system with one cooperative node at the transmission side and one cooperative node at the reception side	35
2.1	System model of the MIMO precoding technique	40
2.2	The virtual representation of a linear precoding system	43
2.3	BER performance of different precoding designs	50
2.4	BER performance of direct feedback and limited feedback in comparison to a perfect CSIT system for max- d_{\min} precoder.	53
2.5	System model of a distributed precoded scheme	56
2.6	BER performance comparison: DMP vs. traditional schemes	64
2.7	BER performance comparison of DMP schemes	65

2.8	Total energy consumption vs. distance (10^{-5} BER)	65
2.9	The <i>crossing points</i> for different path loss exponents	67
3.1	Distributed scheme description with a source node, a relay node and a destination.	72
3.2	Illustration the correlation between d_{\min}^2 and r in the hypothesis 1 (similar results for both remaining hypothesis)	80
3.3	Close values of the expectations in different hypothesis.	81
3.4	Distribution of $r_1(i)$ in Hypothesis 1: decoding erroneously the first symbol and correctly the second one	83
3.5	Distribution of $r_2(i)$ in Hypothesis 2: correctly decoding the first symbol and erroneously the second one	84
3.7	BER performance comparison between simulation result, upper bound and interfering estimation method in the configuration of $d_{SC} =$ $5\%d_{SD}, d_{CD} = 97.5\%d_{SD}$	84
3.6	Distribution of $r_3(i)$ in Hypothesis 3: decoding erroneously both sym- bols	85
3.8	BER performance comparison between simulation result, upper bound and interfering estimation method in the configuration of $d_{SC} =$ $25\%d_{SD}, d_{CD} = 85\%d_{SD}$	86
3.9	BER performance comparison between simulation result, upper bound and interfering estimation method in the configuration of $d_{SC} =$ $50\%d_{SD}, d_{CD} = 60\%d_{SD}$	86
3.10	Power allocation parameter β_0 for best performance	87
3.11	DMP vs. conventional schemes	88
3.12	Relay position impact on DMP performance	89
3.13	Performance comparison between different ML decoders for different values of β	91
4.1	Distributed scheme description with a source node, a relay node and a destination.	97

4.2	The pdf of d_{\min}^2 for \mathbf{F}_{r1} simulation approach vs. theoretical approach. The network is set as $d_{SD} = d_{CD}$, $d_{SC} = 5\%d_{SD}$; $E_b/N_0 = 0dB$; and $\beta = 0.05$. The solid line denotes for theoretical results, the cross mark denotes for simulations	104
4.3	The pdf of d_{octa}^2 : simulation vs. theoretical approach. The network is set as $d_{SD} = d_{CD}$, $d_{SC} = 5\%d_{SD}$; $E_b/N_0 = 0dB$; and $\beta = 0.05$. The solid line denotes for approximations, the cross mark denotes for simulations	105
4.4	The pdf of d_{\min}^2 : theoretical vs. simulation approach. The network is set as $d_{SD} = d_{CD}$, $d_{SC} = 5\%d_{SD}$; $E_b/N_0 = 0dB$; and $\beta = 0.05$. The solid line denotes for approximations, the cross mark denotes for simulations	106
4.5	The pdf of d_{\min}^2 : theoretical vs. simulation approach. The network is set as $d_{SD} = d_{CD}$, $d_{SC} = 5\%d_{SD}$; $E_b/N_0 = 0dB$; and $\beta = 0.25$. The solid line denotes for approximations, the cross mark denotes for simulations	107
4.6	The pdf of d_{\min}^2 : theoretical vs. simulation approach. The network is set as $d_{SD} = d_{CD}$, $d_{SC} = 5\%d_{SD}$; $E_b/N_0 = 0dB$; and $\beta = 0.5$. The solid line denotes for approximations, the cross mark denotes for simulations	107
4.7	The ergodic capacity performances: comparison between the equal and optimal power allocation, $d_{SD} = d_{CD}$, $d_{SC} = 5\%d_{SD}$	115
4.8	The outage probability for simulation and theoretical approximation with $\beta = 0.5$ and two values of threshold $R=1; 2$ bit/s/Hz; the network is set as $d_{SD} = d_{CD}$, $d_{SC} = 5\%d_{SD}$; blue and black color denote for the OPA and EPA, respectively; the solid line with mark denotes the simulation result, and the dash line denotes the theoretical result.	116
4.9	Values of β_0 versus E_b/N_0 to obtain the maximum capacity in the context of WBAN: $d_{SD} = d_{CD}$, $d_{SC} = 5\%d_{SD}$	117
4.10	Sphere decoding principle	124
4.11	Wake Up Radio overview	125

List of Tables

1.1	List of scenarios in WBAN and their frequency band	18
1.2	The AIC for the considered models, the minimum value determines the best fitting model	25
2.1	Parameter values for max- d_{\min} precoder in 16-QAM modulation . . .	48
2.2	Spectral efficiency of different cooperative schemes with QPSK	63
2.3	Parameter values of the consumption model [20]	66
3.1	Value of N_b and N_n for QPSK and 16-QAM	75
3.2	Complexity comparison between different ML decoder	92

Acronyms

AF	Amplify-and-Forward.
AIC	Akaike Information Criterion.
AP	Access Point.
ARQ	Automatic Repeat reQuest.
AWGN	Additive White Gaussian Noise.
BCU	Body Control Unit.
BER	Bit-Error-Rate.
BoWI	Body World Interaction.
BPSK	Binary Phase Shift Keying.
CC	Coded Cooperation.
CF	Compress-and-Forward.
CSI	Channel State Information.
CSIT	Channel State Information at the Transmitter.
CTS	Clear To Send.
DF	Decode-and-Forward.
DMP	Distributed max- d_{\min} Precoding.
DMPAF	Distributed max- d_{\min} Precoding Amplify and Forward.
DMPDF	Distributed max- d_{\min} Precoding Decode and Forward.
DSTC	Distributed Space-Time Coding.

ECG	electrocardiogram.
EEG	electroencephalogram.
EGC	Equal Gain Combining.
EPA	Equal Power Allocation.
ICT	Information and Communications Technology.
LLR	Log-Likelihood Ratio.
LOS	Line Of Sight.
LPT	Local Precoded Transmission.
LQI	Link Quality Indicator.
LST	Local Successive Transmission.
MIMO	Multiple-Input Multiple-Output.
ML	Maximum Likelihood.
MMSE	Minimum Mean Square Error.
MRC	Maximal Ratio Combining.
NLOS	Non Line Of Sight.
OPA	Optimal Power Allocation.
PAR	Peak-to-Average Ratio.
PDA	Personal Digital Assistance.
pdf	probability density function.
PRR	Packet Received Rate.
PSD	Power Spectral Density.
QAM	Quadrature Amplitude Modulation.
QoS	Quality of Service.
QPSK	Quadrature Phase Shift Keying.

RF	Radio Frequency.
RSSI	Received Signal Strength Indicator.
RTS	Request To Send.
SC	Selection Combining.
SIMO	Single Input Multiple Output.
SISO	Single Input Single Output.
STBC	Space-Time Block Code.
STTC	Space-Time Trellis Code.
UWB	Ultra-Wide Band.
VNA	Vector Network Analyzer.
WBAN	Wireless Body Area Network.
WSN	Wireless Sensor Network.

Notations

C_{octa}	instantaneous ergodic capacity in the case of <i>octa</i> .
C_{r_1}	instantaneous ergodic capacity in the case of r_1 .
C	instantaneous ergodic capacity.
G_{CD}	relative distance power gain of $C \rightarrow D$ with respect to $S \rightarrow D$.
G_{RD}	relative distance power gain of $R \rightarrow D$ with respect to $S \rightarrow D$.
G_{SC}	relative distance power gain of $S \rightarrow C$ with respect to $S \rightarrow D$.
G_{SR}	relative distance power gain of $S \rightarrow R$ with respect to $S \rightarrow D$.
G_r	antenna gain of reception side.
G_t	antenna gain of transmission side.
M_l	link margin.
N_b	average of difference bits between two neighbors.
N_n	average number of neighbor.
N_f	receiver noise figure.
N_{sr}	statistical variance of n_{sr} .
P_{ADC}	power consumption of analog-digital converter.
P_{DAC}	power consumption of digital-analog converter.
P_{IFA}	power consumption of intermediate frequency amplifier.
P_{LNA}	power consumption of low noise amplifier.
P_{filr}	power consumption of filter at the receiver.
P_{filt}	power consumption of filter at the transmitter.
P_{mix}	power consumption of mixer.
P_{out}^{octa}	outage probability in the case of <i>octa</i> .
$P_{out}^{r_1}$	outage probability in the case of r_1 .
P_{out}	outage probability.

P_{pa}	power consumption of power amplifier.
P_{trans}	transmission power consumption.
R_b	bit rate.
R	predefined rate.
$SINR$	signal to interference plus noise ratio.
SNR	signal to noise ratio.
$\Gamma(\cdot)$	the gamma function.
$\Sigma_{\mathbf{n}_{total}}$	variance of total noise vector.
α_{sr}^2	statistical variance of h_{sr} .
β	power allocation parameter.
ϵ	symbol error rate of local exchange phase.
η_S	spectral efficiency.
γ_0	channel angle threshold.
γ_{inc}	lower incomplete gamma function.
γ	channel angle.
\hat{E}_b	needed energy per bit for a BER target.
\hat{s}	detected signal of s .
\mathbf{F}_d	precoding matrix.
\mathbf{F}_v	virtual precoding matrix.
\mathbf{F}_{octa}	precoding matrix for the case <i>octa</i> .
\mathbf{F}_{r_1}	precoding matrix for the case r_1 .
\mathbf{F}	complete precoding matrix.
\mathbf{G}_v	virtual decoding matrix.
\mathbf{G}	decoding matrix.
\mathbf{H}_v	virtual channel matrix.
\mathbf{H}	MIMO channel matrix.
\mathbf{n}_c	noise vector at the cooperative node.
\mathbf{n}_{total}	total noise vector.
\mathbf{n}	noise vector.
\mathbf{s}	transmit vector.
\mathbf{y}_c	received vector at the cooperative node.

\mathbf{y}	received vector.
\mathcal{E}_d	the energy of second transmission phase (or precoding transmission phase).
\mathcal{E}_l	the energy of first transmission phase (or local exchange phase).
\mathcal{E}	the total energy to transmit one symbol.
\mathcal{F}_d	set of matrices \mathbf{F}_d for limited feedback.
\mathcal{F}_v	set of matrices \mathbf{F}_v for limited feedback.
\mathcal{F}	set of matrices \mathbf{F} for limited feedback.
$\mathcal{Q}(\cdot)$	Q function.
\mathcal{S}	modulated constellation.
erfc	complementary error function.
ϕ	scaling parameter of precoder.
ψ	power allocation parameter of precoder.
ρ	channel gain.
σ_i	singular values of channel matrix in decreasing order.
θ	rotation parameter of precoder.
\tilde{C}	average ergodic capacity.
\tilde{P}_e	average bit error probability.
b	number of data streams.
d_{CD}	distance from the cooperative node to the destination.
d_{RD}	distance from the relay to the destination.
d_{SC}	distance from the source to the cooperative node.
d_{SD}	distance from the source to the destination.
d_{SR}	distance from the source to the relay.
d_{\min}	minimum Euclidean distance.
$f_{d_{\min}^2}^{octa}$	pdf of d_{\min}^2 in the case of <i>octa</i> .
$f_{d_{\min}^2}^{r_1}$	pdf of d_{\min}^2 in the case of r_1 .
$f_{d_{\min}^2}$	pdf of d_{\min}^2 .
f_{ij}	entries of \mathbf{F} .
g, g_i	amplifying factor.
h_{ij}	entries of \mathbf{H} .
h_{rd}	channel of the transmission from the relay to destination.

h_{sd}	channel of the transmission from the source to destination.
h_{sr}	channel of the transmission from the source to relay.
h	local channel.
k	modulation level of QAM.
n_R	number of receive antennas.
n_T	number of transmit antennas.
n_{rd}	noise at the destination of the transmission from the relay to destination.
n_{sd}	noise at the destination of the transmission from the source to destination.
n_{sr}	noise at the relay of the transmission from the source to relay.
s_{pre}	precoded signal.
s	signal of the source.
y_{rd}	received signal at the destination from the relay.
y_{sd}	received signal at the destination from the source.
y_{sr}	received signal at the relay from the source.
E_b	energy per bit.
N_0	noise power.
$ \cdot ^*$	the complex conjugate.

Abstract

The Wireless Body Area Network (WBAN), consisting of multiple small wireless sensor nodes embedded on human body, represent a remarkable milestone of personal network. This network widely enhances the quality of life not only in the entertainment industry, multimedia, sport training, military, security... but also in the medical domain, where it provides an innovative method to monitor the health more flexibly and more efficiently. As wireless communications represent the major energy consumption in the network, the objective of this thesis is to propose a high energy-efficient transmission protocol that is suitable for the WBAN.

The latter induces severe channel fading that can be counterbalanced by the diversity provided by relay and MIMO techniques. Moreover, precoding techniques are investigated to adapt the signals to be transmitted to the propagation channel. Owing to the difficulty of embedding several antennas in a small-size sensor node, the cooperation manner has to be adopted to deploy the MIMO precoding technique into WBAN. Regarding the performance, the minimum Euclidean distance based precoding is chosen due to its advantages in reducing the error probability.

In this thesis, we propose therefore the deployment of a minimum Euclidean distance based precoding, called Distributed max-dmin Precoding (DMP) into WSN in general and in WBAN in particular. We will especially focus on the link between the WBAN and a base station equipped with two antennas, and two relaying protocols are considered: Decode-and-Forward (DF) and Amplify-and-Forward (AF). By nature of the spatial multiplexing, the DMP offers higher spectral efficiency than a distributed Space Time Coding (STC). As far as the DMP-AF is concerned, we introduce different manners to handle the local channel that changes significantly the precoder. The latter can be designed taking into account this local channel or adapted afterwards, and we can exchange two symbols in once or consecutively [68], [70]. The Monte Carlo simulations show out impressive performance of proposed transmission schemes in comparison to conventional scheme such as Single Input Single Output (SISO) and Single Input Multiple Output (SIMO). An energy model, taking into account the circuit consumption and transmission consumption, was used to compare the considered DMP and the existing protocols in terms of energy consumption. The results point out the interest of using the DMP

for medium distances between transmitter and receiver. Besides these simulations, the theoretical performance of our DMP schemes is derived. For the DF relaying, the system can be transformed equivalently to an interference system, where the appearing interference is determined to be signal-dependent. As a result, the combination of interference approach and the minimum Euclidean distance distribution allows adopting the upper bound for the error probability in the DMP-DF [69]. For the AF relaying, we carry out an equivalent system model, taking the local channel into account of precoding design, before the analysis on Euclidean distance distribution is established. Based on that, the evaluation on the ergodic capacity and outage probability are performed [70]. The performance analysis not only confirms the simulation results but also does help to allocate the power more efficiently, for both DMP-DF and DMP-AF. Moreover, in the DMP-DF, we propose new maximum likelihood decoder at the destination that improves the receiving performance [69]. This decoder considers the decoding information of relay to adjust the log-likelihood ratio, hence the decoding error is reduced.

Introduction

Over the past couple of decades, the life expectancy of people has increased to a great extent due to the amelioration of science and medicine especially in the developed countries [61]. This is a result of the quality of life and medical improvement through the new treatments for sicknesses as well as the advancement in technology. Accordingly people have started living longer, leading to the increasing of an aging population. This means in near future people will be facing to the overload of the health care systems. Besides the growth of health care demands for elderly people, medical researches [101] have proved that most of the diseases for instance cancers, asthma, chronic or fatal diseases, can be prevented if they are detected in their early stages. This requires a new medical treatment that allows to track the physiology data in real time. Fortunately, recent technology achievements as integrated circuits, wireless protocols, physiological sensors will allow us to tackle with these demands. These motivations create a new type of Wireless Sensor Network (WSN): Wireless Body Area Network (WBAN) [21, 41, 51, 72, 76]. Along with the rapid growth of micro-electronic technology, personal electronic devices are more diverse and modern. Meanwhile, a significant improvement in terms of miniaturization allows putting electronic devices onto/into the human body. Basically, the WBAN is a specific kind of WSN, targeted to the human body. The WBAN, which is known as a new way of doing things, does not only provide a new health care generation but also can be used in other areas such as: home entertainment, office application, sport training, and security supports...

The WBAN uses small light smart sensors placed on/in the human skin. The term "smart" herein refers their capability to collect, process information; communicate each other, and sometimes assist the medical treatment. These sensors have the task of taking the vital information to help analyzing the health situation of the object being tracked. In medicine, physiological sensors collect data of temperature, blood pressure, heart rate, electrocardiogram (ECG), electroencephalogram (EEG), respiration rate . . . In a conventional health care, these parameters are usually obtained by medical tests that suffer many inconveniences in terms of cost, flexibility and timeliness. With the growth of aging population, the current medical system will not be able to sustain this expansion, and WBAN are seen as a potential

solution.

A WBAN provides a monitoring method that prevents patients from sudden infant death syndromes or enables proper dosing and reduces the risk of fainting for diabetes patient. In addition, data provided by WBAN is continuous, real-time and during a large-interval time, therefore its medical information should be more accurate and complete. Besides, WBAN also offers intelligent solution to support patients in the emergency situation or assist people with disabilities. For example, a paralyzed patient can recover the ability to move by the interaction of a sensors network that connect the nerves system and muscles of patients with an artificial actuator. The WBAN integrated within an overall eHealth solution could bring a step change in the remote management of patient healthcare. Generally speaking, there are two types of devices; sensors which are used to measure certain parameters of the human body, either externally or internally, and actuators which act as a drug delivery system according to the data they receive from the sensors or through interaction with the user. The medicine can be delivered on predetermined moments, triggered by an external source, in other words a doctor who analyzes the data, or when a sensor notices a problem. For example, if a patient suffering from diabetes has a sudden drop of glucose, a signal will be sent to the actuator in order to start an injection of insulin. In short, WBANs will be a key solution in early diagnosis, monitoring and treatment of patients with possibly fatal diseases of many types, including diabetes, hypertension and cardiovascular related disease.

Besides medical applications, the WBAN can also be found in non-medical domains. The first one is the real time streaming which involves video streaming, audio streaming as well as stream transfer which are used for vital sign and body information-based entertainment service, body gesture motion capture, remote control of entertainment devices, identification, emotion detection and to monitor forgotten things by sending an alert to the owner. Nexts are the entertainment applications, which consist of gaming applications and social networking. The devices integrated in WBANs are appliances such as microphones, MP3-players, cameras and advanced computer. They can be used in virtual reality, personal item tracking, exchanging digital business card, consumer electronics and gaming purposes, for

instance game control with hand gesture (such as wii's or xbox's games) or mobile body motion game and virtual world game. The third one is called emergency (non-medical), which are on-body sensors capable of detecting a non-medical emergency such as fire or poisonous gas to urgently warn the user in that emergency condition. Furthermore, there is the emotion detection which, via simple bio-sensors, measures the induction of physical manifestations throughout the body. The last one is called Secure Authentication; it uses both physiological and behavioral biometrics such as iris recognition, fingerprints and facial patterns. This is one of the key applications of WBANs due to duplicability and forgery, which has motivated the use of new physical characteristics of the human body.

Sensors in the WBAN are required at key positions to enable effective monitoring of the relevant physiological conditions. They operate cooperatively, forming a sensor network, which is a deployment of several devices equipped with sensors that perform a collaborative measurement process. A WBAN needs a communication module that supports a wireless protocol such as wifi, bluetooth, zigbee... The wireless nature will not only help the network be more flexible for daily activities but also facilitate the communication to an external system such as a surveillance system, internet, and cellular networks. On the other hand, it also brings real challenges on communication reliability, security, safety, and power consumption. Given the WBAN context, this thesis focuses on the study of communication, especially on energy consumption aspects. In practice, the wireless communication has to deal with more complex problems than the wired one. Firstly, the wireless channels should be subject to various unfavorable factors such as fading, shadowing, attenuating... Energy loss when wireless communication performed on human body is stronger due to the absorption of body tissues. Furthermore, the nature of daily application, human movement and posture changes will affect substantially the wireless channels. A further constraint on size has to be taken into consideration, leading to the limitation of energy source, e.g. batteries. Consequently the optimization of energy must be ultimately focused. Moreover, reducing the transmit power also offers the advantage in limiting the interference between devices as well as networks. In addition, the safety standards on microwave power must be an

important consideration. Thereby, for wireless personal devices, the radiated waves have to be controlled to prevent the damage to the vital organs and tissues. The low power constraint allows a long life battery capability, which is a key requirement because a patient could have to undergo an operation each time of battery failure.

BoWi project: Body World Interactions [1]

BoWi is a CominLabs project, focused on the society challenge called Digital Environment for the Citizen. It is also related to the social challenge Information and Communications Technology (ICT) for Personalized Medicine and to the research track Energy Efficiency in ICT.

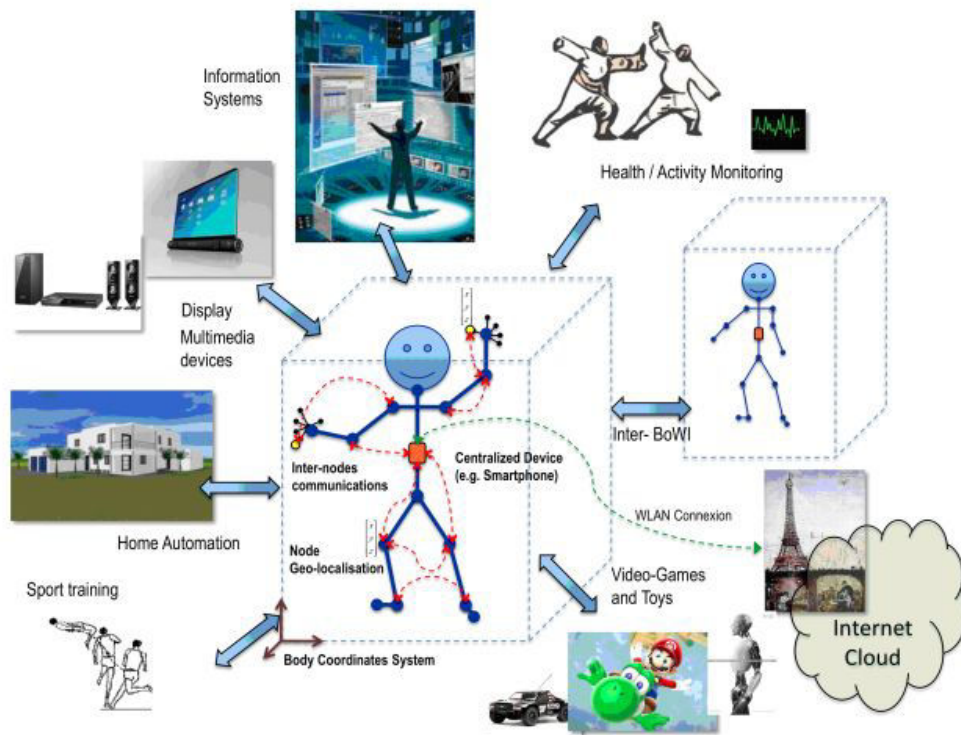


Figure 1: An overview of BoWi project [1]

The main objective of the BoWi project is to develop a pioneer interfaces for an emerging interacting world based on smart environments (house, media, information and entertainment systems...). The Wireless Body Areas Sensor Networks is

focused for the aim of estimating accurately the gesture and body movement. The ultimate requirements are determined on the device size and the ultra-low power consumption. In BoWI, the geolocation approach will be the combination of the radio communication distance measurement and inertial sensors data. The health care, activity monitoring, and environment control can be considered as applications of BoWI.

In the first step, the Zyggye (Figure 2) prototype was developed as a wearable device. Three sensors are integrated inside: the accelerometer, gyrometer, and magnetometer. The project's initial task is to use the data from these sensors to detect the posture. To do so, Zyggye nodes will be set on a specific location then transmit its data to the station. This station gathers and analyzes data then gives out the posture/gesture. This thesis's objective is to propose a high energy efficient wireless communication protocol that is suitable for BoWI project.



Figure 2: Zyggye prototype, version 1

Within BoWI, four works are proposed to be investigated. The first one is aiming to design an ultra-low power architecture for WBAN. The configurable architecture is considered and the ultra-low power can be achieved by the aggressive use of dynamic power management [1]. On another aspect, the antenna and propagation are tackled. The objective is to obtain the channel models of WBAN by measurements, and afterwards use them in order to design an antenna that is suitable for the Zyggye prototype. In addition, a work on the multi-sensor and radio based geolocation is carried out. The aim is to propose an algorithm that exploits effectively the data of inertial sensors (magnetometer, accelerometer, and gyroscope) to detect the user's gesture. In the next step, the Ultra-Wide Band (UWB) geolocation can be studied for more accuracy and probably more energy efficiency.

This thesis is in charge of the wireless communication which is the key factor connecting devices in BoWI project. The ultimate objective is to reduce the power consumption meanwhile maintain the reliability. To manage these requirements, the spatial diversity is a good approach to study. However, the size constraint of WBAN cannot allow to equip multiple antennas to deploy the spatial diversity. For this reason, the cooperative technique is proposed to be investigated. In fact, this technique is already well-studied in the WSN context, and exists almost in two main categories: cooperative relay and cooperative Multiple-Input Multiple-Output (MIMO). Our contribution is to go in deep on the implementation of a MIMO precoding into the WBAN via the cooperative technique. In this term, we set an eye on the minimum Euclidean distance based precoding with an impressive performance in reducing the error probability.

Thesis contributions

- Thanks to measurements on the channel characteristics for BoWI prototype (Zyggie), the nature of channel fading in WBAN is analyzed. The distribution fitting process is carried out to obtain the suitable model for the considered system.
- With the aim to obtain a high energy efficient network, we focus on the wireless communication protocol. As a result, we have proposed and investigated the distributed precoding scheme, based on the cooperative deployment of a minimum Euclidean distance precoder. Two forwarding strategies are considered: Decode-and-Forward and Amplify-and-Forward. In terms of DMP-AF, we introduce different uses of signal processing in the local exchange phase. The numerical evaluation (Matlab simulation) pointed out the outperformance of the proposed protocol compared to the conventional system such as SISO, MISO, distributed Space-Time Block Code (STBC) in terms of error rate, or energy efficiency. An energy model has been studied for the DMP scheme, the comparison to conventional schemes is derived afterwards. Thereby, the energy consumption is in favor of the DMP for medium distances (several

meters).

- As far as DMP-DF is concerned, the performance analysis approach is carried out based on the classification of hypothesis, occurring in the cooperative node when decoding. As a result, an equivalent system is presented with the appearance of the interference. The upper bound on the error probability is then achieved. Based on that the power allocation can be accomplished.
- If the decoding information at the cooperative node is available at the destination, an advanced Maximum Likelihood (ML) decoder will be performed, taking the decoding error of cooperative node into the computation of Log-Likelihood Ratio (LLR). In expense of higher complexity, the new decoder offers significantly a performance improvement.
- Regarding the DMP-AF, to obtain the performance analysis, we transformed the system model to achieve the corresponding system. The spectral-advantageous AF scheme was picked up, then the distribution of minimum Euclidean distance was investigated. Afterward, some evaluations were derived, based upon the probability density function (pdf) of d_{\min} such as: ergodic capacity and outage probability. We performed the power allocation analytically, aiming to maximizing the system capacity.

Thesis structure

Chapter 1: Communication in WBAN

Aiming to develop a network that is easily deployable on human body, the wireless communication is an important requirement, but it suffers from the effects of the channel such as path loss, fading, shadowing... In WBAN these factors are even more particular due to the nature of human body environment and the mobility induced by the daily activities (walking, running, standing...). Thus, in this chapter a view on the elements that affect the wireless communication will be described. Regarding the existing communication protocols, a literature review will be provided on well-known cooperative protocols, such as cooperative relay and cooperative MIMO.

Chapter 2: How to benefit from channel feedback

Looking at the MIMO categories, the precoding technique emerges as a closed-loop system that can use the channel feedback efficiently. Moreover, by nature of a spatial multiplexing system, this technique achieves an impressive spectral efficiency, compared to the STBC. More advantageously, the feedback information can be exploited to satisfy a pertinent requirement such as: Minimum Mean Square Error (MMSE), equal-error, Quality of Service (QoS), SNR-maximization, maximization of capacity...

An overview of MIMO precoding techniques is introduced in this chapter, and the idea to bring the MIMO precoding into the WSN via the cooperation manner is tackled. In this latter work, we mention an application of a minimum Euclidean distance based precoding with the huge advantage in diminishing the error rate. The numerical evaluation on the performance and energy efficiency is also provided.

Chapter 3: Distributed maxdmin precoding: Decode and Forward

In this chapter, we specifically consider the Decode-and-Forward structure. We address the performance analysis of the distributed precoding scheme, deploying the Euclidean distance based precoding via cooperative technique in a general WSN; the implementation into WBAN is totally similar. The decode-and-forward relaying is focused on the basic case with one single relay node, one source node and a destination which possesses two co-located antennas. The given methodology in this chapter, is obviously extendable for larger systems. These extensions might be considered in the future works with more relay nodes and/or more antennas at the destination.

In addition, we propose to examine the possibility to use the information of the relay performance at the destination. This information is adopted in calculating the log-likelihood ratio to detect more efficiently the symbol in the maximum likelihood (ML) decoder at the destination. A new maximum likelihood decoder is introduced, exploiting the decoding error probability of the relay to enhance the detection at the destination. In the light of the fact that the complexity of ML decoder augments severely in a full use of this information, we propose a suboptimal and less complex

solution taking advantage of the max-log approximation.

Chapter 4: Distributed maxdmin precoding: Amplify and Forward

Similarly to the previous chapter, the Amplify-and-Forward scheme performance analysis is derived, to further obtain the practical power allocation. The *Local precoded transmission* with the channel customizing scheme will be selected due to its spectral efficiency and performance. The theoretical performance analysis on the channel capacity and outage probability are carried out, based upon the statistical distribution of minimum Euclidean distance between two received vectors. We address out also the power allocation strategy, defining the power apportionment between two phases of a distributed scheme that offers the best channel capacity performance.

Chapter 1

Communication in WBAN

Introduction

The WBAN can be considered as a specific type of WSN where the devices, network topology, communication scenarios are different. Aiming to develop a network that is easily deployable on human body, the wireless property is an important requirement. The communication in WBAN therefore is carried out via the wireless channel. Unlike the wire communication, the wireless communication suffers from affects of the channel such as path loss, fading, shadowing... Especially, in WBAN these factors are more particular due to the nature of human body environment.

In WBAN, one of most important constraint is the ultra-low power consumption. Regarding this term, two components are considered: circuit and transmission consumption. Like other electronic system, the components such as processor, amplifier, mixer, filter... consumes the energy for signal processing. In recent years, the explosive growth of micro-electronic technology empowers the processing capability while reduces the power consumption. This positive trend offers more opportunity to obtain a flexible, powerful WBAN with small size and long-term operation. The second kind of power consumption is due to wireless wave propagation. According to the nature of wireless, we emit wirelessly an electromagnetic wave to create the communication among devices. The energy consumed by this operation depends on the physical algorithm, environment, frequency band, etc. In the light of the fact that the consumption of the circuit is more and more diminished along with the semiconductor technology advancement, the transmission takes an important part in the energy diagram. For this reason, to propose an ultra low power wireless network, it is obvious to focus on the wireless communication. In general, the wireless communication is more complicated than the wire one owing to the sophisticated channel. Especially in WBAN, this issue becomes more difficult due to the human body is not an ideal media for radio frequency propagation.

Consequently, in this chapter a view on the elements of a WBAN is provided including the description of the wireless communication aspects in section 1.1. Afterwards, the state of the art of cooperative technique that is capable to reduce the transmission power, is described in section 1.1.2. Section 1.3 finally concludes the

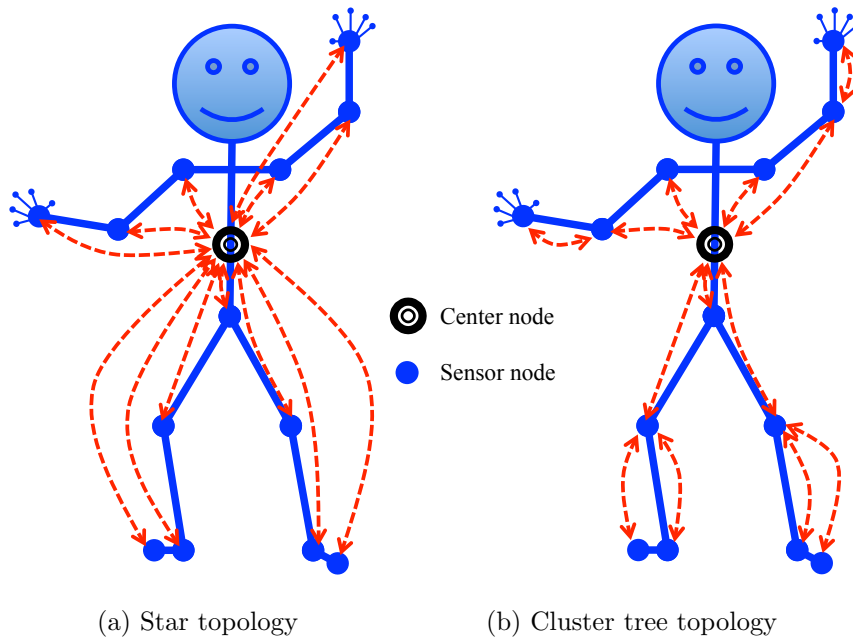


Figure 1.1: Two common topologies used in WBAN

chapter.

1.1 Overview on WBAN

1.1.1 WBAN architecture

1.1.1.1 Network topology

Generally, the WBAN can be organized as a star, cluster tree, mesh or ring topology. However, the two former topologies star and cluster tree are used most commonly in WBAN. Star topology (see Figure 1.1a) is suitable for applications supported by small network, whereas cluster tree (see Figure 1.1b) one is more convenient for larger scale physical size network. Obviously, the star topology is well suitable for WBAN due to the dimensions. All nodes in network are connected to a central coordinator (center node), this node responds to gather, process, and forward the data to an access point that is capable to analyze them. Consequently, the center node in this topology is supposed to be more powerful in terms of energy, processing capability, and memory than the other nodes in the network.

1.1.1.2 Types of devices

1. Sensor node: This device is mounted on the body. All information such as vital signal, location data, environment condition, audio, video signal. in WBAN is recorded by this device. Additionally, a sensor node must be capable to do some simple signal processing and transmit wirelessly the data to an external access point [4]. Two kinds of sensor node are existing: implant and on-body sensor. Most of implant nodes are used in medical application to monitoring the vital signal, whereas on-body nodes can be used for both medical or non-medical application.
2. Actuator node: In general, an actuator node is similar to a sensor node (also on-body device), except it is able to execute some particular task according to the information it receives or the order from external access point [48].
3. Personal access point: This device responds to gather all data in a network then forward to the external access point, located far away from human body. In some cases, it is used to inform user for warning or providing information. Basically, a personal access point acts like a center node in a WBAN. As a result, it is more powerful than the other node in terms of processing capability, memory, energy resource [86]. In some applications, the smart phone or the Personal Digital Assistance (PDA) can be personal access point.
4. External access point: This device is the center of the network, it undertakes the analysis of all data received from the sensors, and keeps them for the future needs. It can also take decisions or make the data available on the internet.

1.1.1.3 Transmission scenarios

The potential of WBAN is evident, it is still in the early time of development. Therefore, the subgroup IEEE 802.15.6 was formed, aiming to develop WBAN for medical and non-medical devices. In summary, four main scenarios are listed by this standard in the Table 1.1 [105]:

The BoWI project considers only on-body sensors: accelerometer, gyro-meter,

Scenarios	Description	Frequency Band
S1	Implant to Implant	402-405 MHz
S2	Implant to Body Surface	402-405 MHz
S3	Implant to External	402-405 MHz
S4	Body Surface to Body Surface	13.5, 50, 400, 600, 900 MHz, 2.4, 3.1-10.6 GHz
S5	Body Surface to External	900 MHz, 2.4, 3.1-10.6 GHz

Table 1.1: List of scenarios in WBAN and their frequency band

magnetometer. The data from these sensors, combined with Received Signal Strength Indicator (RSSI) information is collected by an external Access Point (AP) (computer). This AP is supposed to be a powerful station with outstanding capability in terms of processing, memory and energy. Therefore, two transmission scenarios are concerned to be studied herein. The first one is the communication among on-body nodes in a WBAN, called *intra-BAN*. This scenario is crucially affected by human body, the surround environment as well as the gesture. The second scenario is the communication between the center node and the AP. This kind of communication is called: *extra-BAN*.

1.1.1.4 Intra-BAN communication

For the reason that WBAN is a small network, the star topology is advantageous. Consequently, there is only the connection between the center node and sensor nodes (sensor nodes do not communicate to each other). The most important constraint on this communication is the simplicity, not only to reduce energy consumption and delay time but also because the distance between two nodes is small. A simple direct transmission SISO is an obvious possibility. This is the simplest way to transmit a signal, therefore we drain less energy for the circuit. However the drawback is that to obtain a sufficient performance, we emit a significant power. Besides, the multi-hop transmission could be considered. This protocol is used popularly in a

tree or cluster-tree topology. For example, in [49] a cascading multi-hop scheme proposes low delays, low packet loss and high energy efficiency while the flexibility is preserved. In another study [82], a scheduling provides multihop support through the division of the network into timezones. Thanks to this, a shortest path routing from a node to the gateway is obtained.

In addition, the gesture and human movement have important impact on the channel properties and the path loss. Adapting the transmission protocol with the change of the gesture provides the opportunity to enhance the link quality and reduce the energy consumption. For example, in [29] a packet transmission scheduling is addressed, based on the behavior of RSSI between transmitter and receiver. Thanks to some periodical movement of the human body, this protocol predicts the peak in the RSSI diagram to send packets. As a result, the Packet Received Rate (PRR) between 50% and 90% of an outdoor intermediate link is increased to above 90%. Moreover, a power control mechanism can be used to manage the transmit power in function of the link quality [44, 80]. Specifically, based on the information about RSSI/Link Quality Indicator (LQI), the transmission power is adapted to prevent the energy waster in the case the link is strong and assure the link reliability when the link goes bad. Furthermore, the power control can also be deployed using the knowledge of body posture on the transmission.

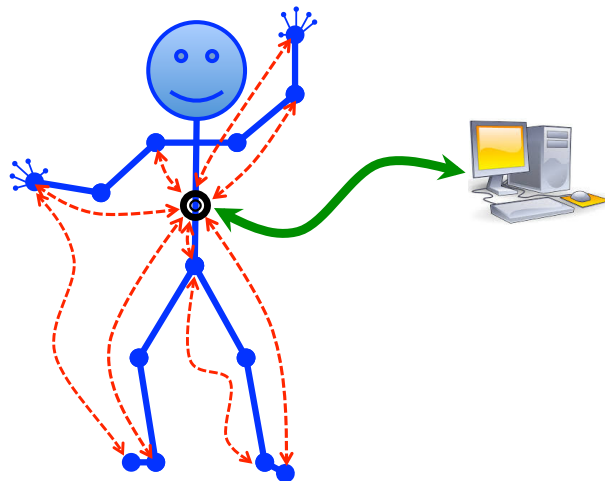


Figure 1.2: Two categories of communication in WBAN: red dash arrow denotes the intra-BAN and green solid arrow denotes the extra-BAN

Instead of using radio frequency wave to transmit the signal, the human body can be used as a transmission medium for electrical signals [107], call *intra-body communication*. Therefore, the body becomes a channel to perform a coupling between transmitter and receiver. In general, we can classify the coupling of intra-body communication into 2 main categories: capacitive coupling [23,24,27,77,78,107] and galvanic coupling [28, 50, 71]. In the first method the use of the near field and the capacitive coupling of human body to its environment make the human body acting as a transmission medium. Whereas, the latter method exploits the coupling current into human body via two electrodes. This intra-body coupling proposes an ultra-low power transmission, benefiting from the utilization of dielectric body parameters to send the data. In contrast, its drawback is that the data rate is limited and the system is less convenient due to the requirement of direct contact of sensor node and human tissue.

1.1.1.5 Extra-BAN communication

The requirement of sending out the data to the external station makes the extra-BAN communication happening (see Figure 1.2). The extra-BAN is defined as the communication between a node in WBAN and an external AP. In WBAN, there is a center node responds to gather and send out all data in the network. Different to the intra-BAN communication, the channel in extra-BAN communication is less particular. It can be considered similarly as the context of cellular network or any personal device network. Basically, the direct transmission SISO and multi-hop technique are applicable. Nonetheless, the demand on a low-power system make them less feasible due to the reason that they require significant power to obtain a sufficient performance. On this aspect, the MIMO is considered as a good candidate in proposing the spatial diversity to increase the performance with the same power level as the conventional protocols. However, the constraint on the physical size of sensor node limits this spatial diversity technique (the most feasible diversity technique) to enhance the communication quality. To overcome this challenge, the need of cooperation is obvious [11]. This technique exploits the help of one or multiple additional nodes to create the spatial diversity. We provide the state of the

art on the cooperative technique in the section 1.2.

1.1.2 WBAN channel characteristics

In order to deploy the wireless communication, the obligation is to investigate the wireless channel, in which the electromagnetic wave is propagated. To study the physical layer, the channel model, consisting of characteristics such as path loss, fading, shadowing, power delay profile..., is required. In this section, we discuss some typical characteristics of propagation channel in the WBAN.

1.1.2.1 Body tissues

The human body, in general, got many characteristics that influence on the radio frequency propagation such as conductive factors, dielectric constant, impedance... As a result, the wireless transmission suffers high losses caused by the power absorption, frequency shift, radiation pattern destruction... The effects are obvious, however the variation of human tissue characteristics (owing to the different body size, sex, age, fat percentage. . .) makes the investigation more complicated.

1.1.2.2 Antenna effect

Basically, human body possesses strong dielectric characteristic, thus it affects significantly on the antenna radiation pattern. Moreover this characterization varies with different individual body, causing the difficulty in being described in a unique manner. The change of human gesture and posture affect also the propagation nature of antenna. Therefore, it is obliged to understand all these aspects to adapt the wireless communication into body area environment. In addition, the antenna design is strongly depending on the application of WBAN. That means the form, the size, and the characteristic of antenna must be suitable with the purpose and situation. For example, for the on-body node, the dipole antenna might be suitable, whereas, in pacemaker implant, the circular antenna might be selected. In conclusion, the antenna design must take into account the dielectric elements of human body tissues as well as the application in which it is being used.

1.1.2.3 Path loss

Regarding the extra-BAN links, the path loss is easily modeled as a distance-dependent model. In other words, this link is totally similar to other classical systems such as cellular network, multimedia communication, wifi communication... Unlikely, the intra-BAN links propose the complicated attenuation behavior. The reason is not only the sophisticated absorption of body tissues (due to different tissue characteristics: body size, sex, age...), but also the continuous gesture that changes in daily activities. The attempt to model the path loss in function of separated distance is poorly suitable [58,92]. A path loss model must take into account not only the distance, but also the sensor placement and human movement.

1.1.2.4 Fading

Due to many reasons, the wireless signal in WBAN is faded. The fading phenomenon might be created by the multipath of surround environment, the energy absorption, the reflection, or the shadowing of body parts. The fading causes the deviation of the attenuation affecting the received signal. In a wireless system, the principle of the fading behavior must be determined in order to evaluate a certain transmission protocol. In literature, there are some studies on modeling the statistical channel distribution [92,93], [85], [22], [91], [18] for WBAN. These investigations attempted to fit the measured or simulated data of the channel gain with the fading distributions such as Rayleigh, Ricean, lognormal, Weibull... Generally, the on-body channel can be modeled as a lognormal fading in most of cases. Besides, the Weibull or gamma distribution can be listed for providing the quite good fitting. Two well-known distributions Rayleigh or Nakagami seems to be poor-fitting in the context of WBAN. Regarding the indoor environment, the most applicable case for the WBAN, the Weibull and gamma distribution are two best candidatures.

On attempting to study the characteristics on the fading property which crucially affect the wireless communication, we carry out some measurements on the on-body channels. These measurements are implemented with the Zyggie prototype [1], with the help of the Vector Network Analyzer (VNA). The environment is supposed to be indoor. Two scenarios will be focused: 1) *extra-BAN*: between a node on the chest

and an external node; 2) *intra-BAN*: between a node on the chest and a node on the wrist. The channel gain will be recorded by the VNA at 2.45 GHz. To determine the best-fitting fading distribution, the minimum Akaike Information Criterion (AIC) is applied [3]. This parameter is computed based on the data of 1000 channel gains collected in each scenarios. The following models (with their pdf) will be selected to be examined:

1. Lognormal

$$f(x|\mu, \sigma) = \frac{1}{x\sigma\sqrt{2\pi}} e^{-\frac{(\ln(x)-\mu)^2}{2\sigma^2}} \quad (1.1)$$

2. Gamma

$$f(x|a, b) = \frac{1}{b^a\Gamma(a)} x^{a-1} e^{-\frac{x}{b}} \quad (1.2)$$

3. Weibull

$$f(x|a, b) = \frac{x}{b^2} e^{-\frac{x}{b^2}} \quad (1.3)$$

4. Rayleigh

$$f(x|b) = \frac{x}{b^2} e^{-\frac{x}{b^2}} \quad (1.4)$$

5. Nakagami-m

$$f(x|m, \Omega) = \frac{2m^m}{\Gamma(m)\Omega^m} x^{2m-1} e^{-\frac{mx^2}{\Omega}}, \quad (1.5)$$

where $\Gamma(\cdot)$ is the gamma function. Thereby, the AIC is expressed as

$$AIC = -2 \ln(l(\hat{\delta}/data)) + 2Z + \frac{2Z(Z+1)}{n_\delta - Z - 1}, \quad (1.6)$$

where $\ln(l(\hat{\delta}/data))$ denotes the maximum log-likelihood over unknown parameters δ , given the data and the model; Z is number of parameters in the model; and n_δ is number of sampling data.

In Figure 1.3, the distribution fitting for the extra-BAN channel is illustrated. As we can see for the case of Line Of Sight (LOS), the channel varies slightly. In this situation, the Rayleigh fading proposes the worst fitting. The best candidates would be lognormal or gamma fading. If the LOS can not be performed, the channel gain deviation becomes stronger, and the fading behavior changes. At this point, the Weibull can be the best-fitting distribution. The lognormal and gamma fading

are probably considered as a good model for this channel. In intra-BAN, for a communication between the chest and the wrist, the transmitter is placed on the chest, the receiver is on the wrist. Two situations are studied: the body stands still, and the body moves. As can be seen in the Figure 1.4, the lognormal, Weibull, gamma and Nakagami fading can be the candidates.

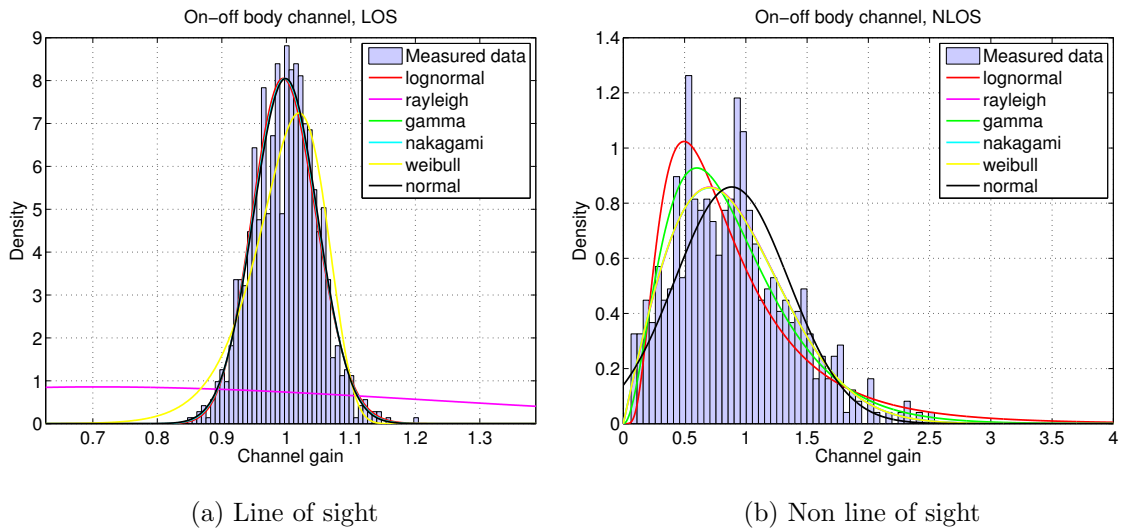


Figure 1.3: The distribution fitting for the extra-BAN channel: the transmitter on the chest and receiver on the external

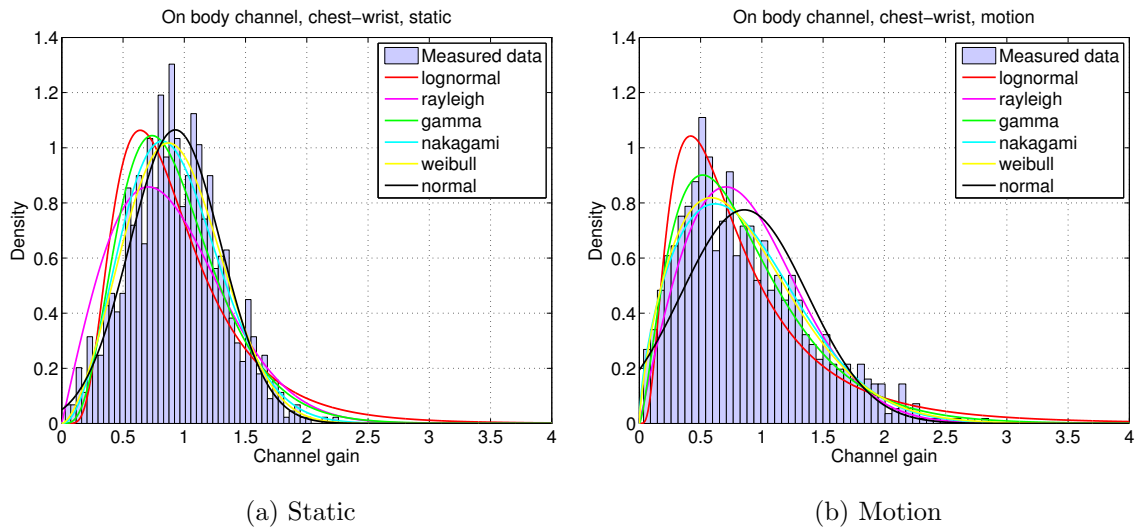


Figure 1.4: The distribution fitting for intra-BAN channel: the transmitter on the chest and receiver on the wrist

Table 1.2: The AIC for the considered models, the minimum value determines the best fitting model

Model	AIC			
	extra-BAN	extra-BAN	intra-BAN	intra-BAN
	LOS	NLOS	static	motion
Lognormal	0.1972	5.9700	5.5158	6.1649
Gamma	0.9245	5.2522	4.9686	5.3265
Weibull	0.3789	5.2198	4.8763	5.3203
Rayleigh	2.6203	3.2037	2.9805	3.3492
Nakagami-m	0.2029	5.2198	4.8933	5.3255

To determine the best-fitting model, the table of AIC for each model is provided (see table 1.2). Based upon that, we can select the lognormal for the extra-BAN channel with LOS and the Rayleigh fading for the remaining cases.

1.2 Cooperative technique

The demand on high data rate communication or less energy consumption leads to the use of some diversity techniques that provide multiple versions of data helping to enhance the transmission quality. The diversity techniques can be classified into three main categories: frequency diversity, time diversity and spatial diversity. The latter technique that exploits the space by using typically multiple antennas, is most commonly used. The data, transmitted by different paths, is therefore assured to be more reliable than a single path with the direct transmission SISO. In a co-located point to point system, the spatial diversity is obtained thanks to a MIMO technique, where each terminal could be equipped by multiple antennas. However, in WSN (WBAN in particular), the sensor size constraint does not allow to put two or more antennas on a sensor, so a classical MIMO technique could not be directly applied. Thus, to perform the diversity technique, the cooperative technique can be carried out.

1.2.1 Cooperative relay

The cooperative relay is the well-known cooperative technique in the early time. This technique is first introduced by E.C. van der Meulen [102], using a relay to assist the transmission between a transmitter and a receiver. Afterward, many works have studied its achievable advantages [19], [47], [88], [89]. In principle, the relay system is described in the Figure 1.5. Whereby, it consists of one or multiple relays that forward the signal from the source to the destination. Based on the signal processing at relays, some categories could be listed: Decode-and-Forward (DF), Amplify-and-Forward (AF), Compress-and-Forward (CF), Coded Cooperation (CC). The advantage of a relaying technique is to enhance the diversity since the destination receive two or more versions of information from the source and from relays. Consequently, the transmission quality (such as error rate, outage probability, channel capacity...) is improved. Thanks to this, the energy consumption is decreased for a target quality requirement.

To deploy a relaying system, two main bases are considered: repetition-based and Distributed Space-Time Coding (DSTC)-based. In the repetition-based relaying, relays receive the information from the source, they forward afterward identically that information to the destination. The received information at the destination thereby includes different versions from independent paths (relays and source). Therefore, the probability that the destination fails to detect the signal is reduced. Whereas, the DSTC-based relaying benefits from the space time coding protocol to obtain the quality enhancement.

The cooperative relay technique can be realized in many areas: cellular network, ad-hoc network, satellite communication, radio media and WSN. Different from the other systems, a WSN in general and a WBAN in particular, is restricted by many constraints, especially in terms of size, and energy source. Due to the small-size, each sensor can be equipped only with a single antenna. Thus, in order to obtain the uniformity and the consistence with our context, from this moment we focus only on the node with single antenna . Whereas, the center AP can be supposed to be a robust station. That means the constraint in terms of computation and power could be ignored. Furthermore, two or more antennas could be equipped on AP

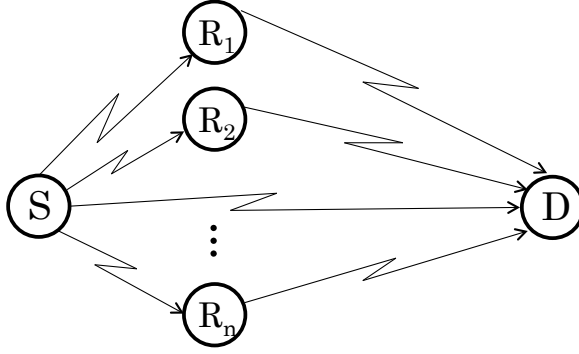


Figure 1.5: Relaying system model with source S , destination D and n relays $R_1..R_n$

that supports facilitating the space diversity in the reception side.

We consider a simple relaying system with a source node, a relay node and a destination (see Figure 1.6a). The role of relay is to help forwarding the signal from the source to destination. The transmission in a relaying system consists of two phases. In the first time-slot, the source transmit its data to both relay node and the destination. The destination buffers the data from the source and waits for the second version of it in next time slot. In the second time slot, the relay node after receiving the data from source node, will forward it to the destination. At the destination, two versions of data are obtained, afterward some techniques of combination can be used such as Selection Combining (SC), Maximal Ratio Combining (MRC), Equal Gain Combining (EGC) [12]...

Let us define d_{SR} , d_{SD} , d_{RD} the distances from $S \rightarrow R$, $S \rightarrow D$, $R \rightarrow D$, respectively. Due to the difference in distance, the transmission links $S \rightarrow R$ and $R \rightarrow D$ obtain gains G_{SR} , G_{RD} in power in respect with $S \rightarrow D$ link. Considering that these gains depend on the path loss environment, let K be the path loss exponent. The mentioned gains are expressed as

$$G_{SR} = \left(\frac{d_{SD}}{d_{SR}} \right)^K, \quad (1.7)$$

$$G_{RD} = \left(\frac{d_{SD}}{d_{RD}} \right)^K. \quad (1.8)$$

Owing to existing of two transmission phases, the power allocation must be regarded. To be fair, let us define \mathcal{E} the total energy to transmit one symbol. This energy will be divided into two parts: \mathcal{E}_l , and \mathcal{E}_d for first and second time slot, respectively.

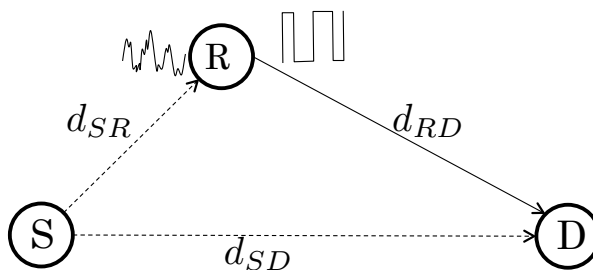
1.2.1.1 Decode and Forward relaying

In DF relaying, the relay detects the received signal from the source then re-transmits the detected signal to the destination. Let s be the signal from the source, in the first time slot the relay and the destination receive, respectively:

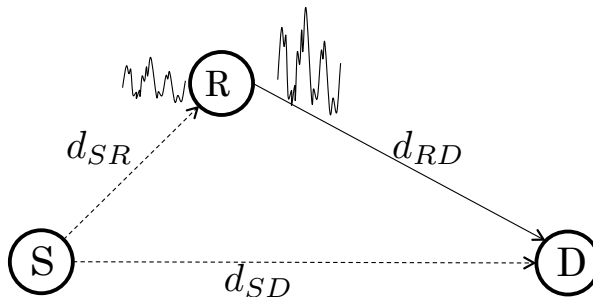
$$y_{sr} = \sqrt{\mathcal{E}_l G_{SR}} h_{sr} s + n_{sr}, \quad (1.9)$$

$$y_{sd} = \sqrt{\mathcal{E}_l} h_{sd} s + n_{sd}, \quad (1.10)$$

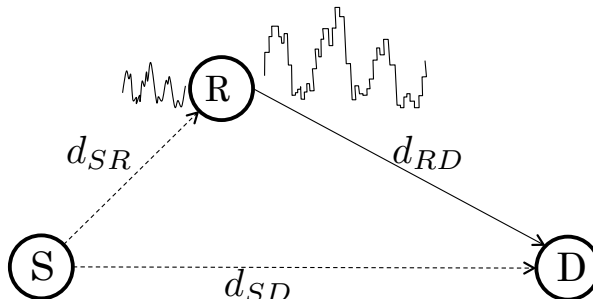
where h_{sr} denotes the source to relay channel, h_{sd} denotes the source to destination channel; n_{sr} , n_{sd} are the Additive White Gaussian Noise (AWGN) at the relay and destination, correspondingly.



(a) Decode-and-Forward



(b) Amplify-and-Forward



(c) Compress-and-Forward

Figure 1.6: Three common types of relaying: dashed arrow denotes the first time slot, the solid arrow denotes the second time slot

In the second time slot, after receiving the signal from the source node, the relay node uses the ML decoder to detect it. The detected signal \hat{s} then is resent to the destination through the channel h_{rd} . The received signal at the destination is:

$$y_{rd} = \sqrt{\mathcal{E}_d G_{RD}} h_{rd} \hat{s} + n_{rd}, \quad (1.11)$$

where n_{rd} denotes the AWGN in this phase at the destination. From two versions of data from source and from relay, a MRC scheme is supposed to be utilized. The combined signal is expressed as

$$y_{com} = y_{sd} h_{sd}^* + y_{rd} h_{rd}^* = |h_{sd}|^2 s + |h_{rd}|^2 \hat{s} + n_{sd} h_{sd}^* + n_{rd} h_{rd}^*, \quad (1.12)$$

where $|\cdot|^*$ denotes the complex conjugate. Apparently, two possibilities happen: the relay node decodes s correctly, meaning $\hat{s} = s$, or wrongly $\hat{s} \neq s$. As a result, in the case the link between source and relay is good, the DF relay improves the performance at the destination, with respect to a single direct transmission. In contrast, if the signal is decoded imperfectly, it will affect the MRC.

1.2.1.2 Amplify and Forward relaying

In general, this technique is similar to the previous technique. However at the relay node, the signal is not decoded. Instead, it is amplified then retransmitted to the destination (see Figure 1.6b). Depending on the availability of the channel information at the relay, it can choose one corresponding amplifying factor among the cases as follows:

- If, at the relay, the instantaneous Channel State Information (CSI) is not present, except its statistical parameter, the amplifying factor is given as [38]

$$g = \sqrt{\frac{\mathcal{E}_d}{\mathcal{E}_l G_{SR} \alpha_{sr}^2 + N_{sr}}}, \quad (1.13)$$

where α_{sr}^2 is the statistical variance of the channel h_{sr} , and N_{sr} denotes the noise variance at the relay node in the transmission from the source node. Using this amplifying factor, the average energy is balanced, whereas the instantaneous power might exceed or fall behind the average value.

- In the case the CSI is known at the relay, we can use the following amplifying factor [39]

$$g = \frac{h_{sr}^*}{|h_{sr}|} \sqrt{\frac{\mathcal{E}_d}{\mathcal{E}_l G_{SR} \alpha_{sr}^2 + N_{sr}}}. \quad (1.14)$$

- Also in the case the relay is capable to obtain the channel coefficient, it uses the amplifying factor:

$$g = \frac{h_{sr}^*}{|h_{sr}|} \sqrt{\frac{\mathcal{E}_d}{\mathcal{E}_l G_{SR} |h_{sr}|^2 + N_{sr}}}, \quad (1.15)$$

to assure the output power at the relay is always controlled [5].

Therefore, the destination will receive the signal from the relay as

$$y_{rd} = \sqrt{g \mathcal{E}_d G_{RD}} h_{rd} s + n_{rd}. \quad (1.16)$$

The combining scheme is performed the same way as the DF relaying. Apparently, the noise at the relay is also amplified along with the signal. However, two versions of data are obtained at the destination. The diversity is consequently enhanced, helping improving the detection at the destination.

1.2.1.3 Compress and Forward relaying

Totally corresponding to the name, this technique compresses the data at the relay, then forward it to the destination. This idea is first introduced in [19]; instead of retransmitting a replica of the signal, we can consider quantizing and sending it as a sequence of bits. Thanks to this, the relay observation could be reconstructed at the destination.

In CF relaying [33], [90], the source node sends a message which is encoded into n symbols: $s(1), \dots, s(n)$. The relay therefore receives

$$y_{sr}(i) = h_{sr} s(i) + n_{sr}(i). \quad (1.17)$$

In order to aid the transmission between source and destination, the relay node encodes its received signal y_{sr} into s_r . This encoded message is built successively,

meaning $s_r(i)$ is constructed by $y_{sr}(1), \dots, y_{sr}(i-1)$. At the destination, the received signal could be expressed as

$$y_d(i) = h_{sd}s(i) + h_{rd}s_r(i) + n_d(i), \quad (1.18)$$

where n_d denotes the AWGN at the destination. Then the decompression is performed at the destination with the aim to model the signal from relay and from source as a reconstructed relay observation.

In conclusion, each kind of relaying, in practice, will be suitable for a certain network configuration. Given that the link between the source and destination is weak, whereas relay offers a reliable path. The DF relaying, in this case, takes the advantage since the detection at the relay proposes very few errors. In contrast, when the link between source and relay does not allow to decode the signal properly, the CF or AF scheme can be selected.

1.2.2 Opportunistic relay

By creating the cooperation between the source and relay node, relaying techniques will suffer from the inter-node propagation channel. This effect degrades the performance comparing to a co-located system with the same diversity technique. Moreover, regarding the network, there are many nodes operating simultaneously but all of them can not participate at the same time to cooperate with source node. This leads to the idea, called opportunistic relaying, to select the more suitable nodes in network to aid the communication between source and destination node [9]. It is considered as an advanced relaying technique. Therefore, it can be combined with all kinds of relaying DF, AF or CF. To select the relay nodes, two main approaches are proposed: with or without the feedback from the destination.

1.2.2.1 Without feedback selection

This technique of selection does not require the channel information from the destination. In other words, it is open loop opportunistic relay. Thereby the relay is chosen, based on the simple information from preamble phase, geographic char-

acteristic, residual power source... Herein, we present some well-known selections technique without the feedback from the destination.

Simple relay selection :

In [7], the authors describe a relay section based on the instantaneous SNR information at the source node among all its possible relays in the network. Hereby, all nodes will decode the signal from the source, and decide if they will be in the possible relay set. This decision is addressed out based on the correct detection of its received signal. In this set, the source then determines the relay that proposes the strongest SNR.

Power-aware relay selection :

The power-aware relay selection aims to extend the network lifetime [13]. Specifically, the optimal power allocation will be applied to determine the optimal transmit power at the potential relays and source. The source then calculates the timeout based on this transmit power and the residual power on each node, and a node is decided to be the relay so that the network lifetime is maximized.

Geographic based relay selection :

As the name of this technique, the relay selection is based on the geographical information of the network [104]. Thereby, the distance between the nodes is assumed to be available. Then to determine the best relay, the source derives a minimization of a metric which is computed in function of the distances and modulation scheme. The objective is to maximize the cooperation gain, thus reduce the error rate at the destination.

CSI-timer mapping relay selection In this method [9], the channel information is deduced by the received Request To Send (RTS), or Clear To Send (CTS) sequences at the potential relays. Afterward, an initial timer value is set in function of the source - relay and relay - destination channel. A node which has the timer reaches to zero first, is selected. When a node knows its timer expires first, it broadcasts a flag packet to claim itself as the relay for the source. The remaining nodes

then stop their timer and back off.

1.2.2.2 With feedback selection

When feedback information is available at the transmission side, the transmitter can choose its relay more efficiently. In return, the feedback process is required, causing an expense on power consumption as well as the delay time.

Switched and examined node selection :

This selection [35] is almost similar to the CSI-timer mapping relay selection in the previous section. Meaning a node considers the channel information between source-itself and itself-destination to claim itself to be the relay. However, in the case of collision when there are two or more nodes declare as the relay, this technique can reduce the collision thanks to the information from the feedback data to the source. In return, it consumes more energy.

Opportunistic relay with limited feedback :

In this scheme [98], the source broadcasts its signal to the potential relays and the destination. All potential relays confirm the success or failure of its signal detection to the destination. Secondly, based on the value of SNR, the destination determines the relay with the strongest SNR among relays that acknowledgedly receive the signal from the source node. Then it informs its decision to all relays. This protocol could achieve the same diversity-multiplexing trade-off as the space-time coding.

Opportunistic cooperative diversity with feedback :

This protocol consists of two main principles: the timer mapping selection (similar to the CSI-timer mapping relay selection) and the Automatic Repeat reQuest (ARQ) [10]. After selecting the best candidate for relaying, the destination will send back a bit, indicating that the received message from source is decoded correctly or not. In the case the message is unsuccessfully received at the destination, the relay transmits the signal to help the destination. In the contrary case, the transmission from relay is unnecessary, and the relaying phase does not occur, saving energy efficiency.

Incremental transmission relay selection :

In this protocol [99], firstly, the source broadcasts its signal to all potential relays and destination. If the detection at the destination is successful, there is no need to pick up a relay. If the reception failed, then the destination selects among the potential relays that successfully receive the message, and even the source. If a relay is chosen, it forwards the signal to the destination. In another case, the source retransmits its message.

Outage optimal relay selection :

When the transmission from the source to the destination is unsuccessful, the relaying or retransmitting is required. Thus, the outage optimal relay selection identifies the relay as the node that offers the minimum outage probability with the destination (i.e the node that has the maximum mutual information with the destination) [97]. The set of potential relays is determined as all the nodes in the network that successfully detect the signal from the source. If there is not a relay that could receive the signal from source, the destination demands the source to retransmit.

1.2.3 Cooperative open-loop MIMO

In recent years, the explosive growth of media demands the high data rate communication. Therefore, the MIMO technology is well-known as a technique that exploits multiple antennas to increase the rate and quality of communication. Benefiting from the spatial diversity, the MIMO technology offers undeniable advantages. They can be used to enhance the link quality, the data rate at the same transmission power level, or reduce the power consumption at the same quality target. The MIMO technology is applied more and more widely such as in wireless ad hoc, cellular network, satellite communication [46,75,79]. . . However, in the WSN, in general, and in WBAN, in particular, this technique can not be deployed directly due to the limitation on the size of sensor as mentioned in the beginning of this section. This obstacle leads us to the potential of cooperation to realize the MIMO technology in WSN. Specifically, to carry out the MIMO technique in WSN, we use a set of nodes

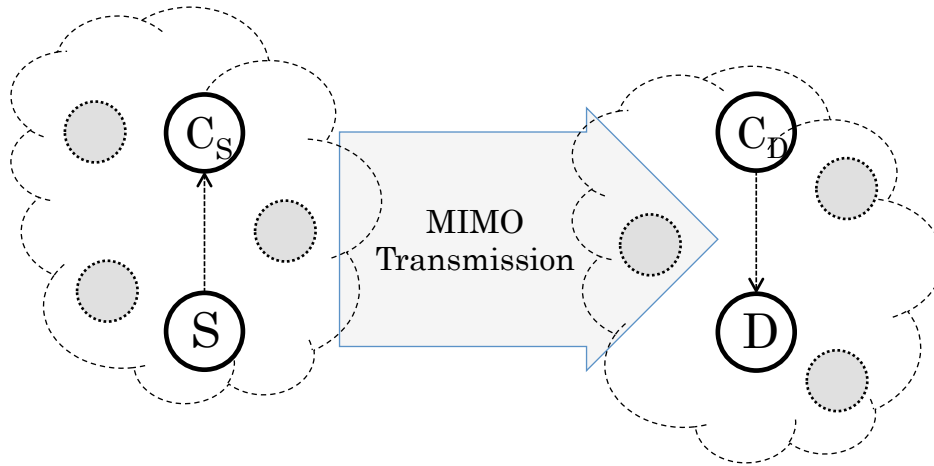


Figure 1.7: A simple cooperative MIMO system with one cooperative node at the transmission side and one cooperative node at the reception side

in the reception side and transmission side as multiple antennas. In other words, each relay plays the role of an antenna in the point-to-point system.

A simple system model is illustrated in the Figure 1.7, where we only have the virtual 2×2 MIMO system. The source node cooperates with its neighbor node to form a virtual multiple antenna transmitter, and the destination cooperates with its neighbor node to form a virtual multiple antenna receiver. Afterward, a MIMO transmission can be applied. To accomplish this transmission, three steps are obliged to be performed.

1. Step 1: Local data exchange

The data of the source node will be shared with its cooperative node

2. Step 2: Cooperative MIMO transmission

After receiving the data, the cooperative node will encode it by a MIMO coding such as STBC, Space-Time Trellis Code (STTC)... with the source node. In the second time slot, the encoded signals are transmitted simultaneously to the reception side.

3. Step 3: Cooperative reception

Each node in the reception set will receive the data from the two transmis-

sion nodes. The destination's cooperative node then forward its received data to the destination. The destination decodes the MIMO signal to obtain the information.

Generally, the cooperative MIMO is an attempt to deploy the MIMO technique in the distributed manner when the antennas can not be located in the same component. Even though it benefits from the advantage of spatial diversity, it also suffers the impairment of inter-channel between the cooperative nodes and the need of precise synchronization of transmitters when applying STBC.

1.3 Conclusion

In this chapter, we attempt to characterize the context of this thesis: wireless body area sensor network. It can be seen as a particular type of WSN with typical features such as: wireless operation, small-scaling network, dedicated to human body, strictly small size nodes... Focusing on the wireless communication aspect, the WBAN wireless nature is briefly described. Thereby, the communication can be classified into 2 categories: intra-BAN and extra-BAN. The channel properties are also investigated by measurements according to each kind of communication. Firstly, the intra-BAN channel can be considered as log-normal fading in most of cases of body posture. The attenuation behavior between two terminals on WBAN can not be distance-dependent as common wireless system. It is possibly addressed as gesture-based path loss model. Whereas, the extra-BAN can be seen less special, and the Rayleigh fading might be selected for most of situations (except the case of static and LOS).

The focal point of this thesis is to propose a high energy-efficient communication protocol. Literally, this issue of intra-BAN communication can be coped by cascading multi-hop transmission, RSSI/LQI based scheduling, or intra-body coupling method. Regarding the extra-BAN communication, we suggest the cooperative technique as the solution. Basically, some existing cooperative schemes can be performed in the WBAN context such as: cooperative relay and distributed STBC. The spatial diversity created by these techniques is undeniable to obtain better

performance. However, we are setting the eyes on the more promising approach: distributed precoding. Profiting from the CSI at the transmitter, the MIMO precoding can manage to reduce the bad effects of fading channel, thereby improving the Bit-Error-Rate (BER). Moreover, thanks to the spatial multiplexing protocol, the data rate can be upgrade up to twice compared to a distributed STBC system. In the next chapter, an overview on the precoding system will be introduced. Based upon that, we propose its implementation into the WBAN.

Chapter 2

How to benefit from channel feedback

Introduction

Since the MIMO technology has been proposed so far, it is more and more widely applied in wireless communications. Benefiting from the spatial diversity, this technique provides the huge advantage to improve the transmission quality. Basically, MIMO techniques can be classified into two main categories: spatial multiplexing (or data rate maximization) and space-time coding (or diversity maximization). The first category aims to increase the transmission speed thanks to the simultaneous transmission of multiple independent data via multiple antennas. Meanwhile, the space-time block coding system obtains a better diversity when transmitting multiple versions of a data. This diversity gain reduces the error rate at the destination advantageously, equivalently enhance the communication quality [25].

Within the spatial multiplexing category [100], [26], the MIMO precoding [43, 59, 84, 95] technique exploits the Channel State Information at the Transmitter (CSIT) to deal with the impairments of propagation channel. This technique is also called as closed-loop MIMO technique. Generally, the CSI is estimated at the receiver in the training phase then the transmitter can obtain this information via a feedback link. Based on CSIT, we precode the transmit signal in order to decrease the negative effects of the fading channel. At the destination, the decoding process allows to obtain the signal in better condition, compared to the conventional transmission. As expected with the nature of a spatial multiplexing system, the MIMO precoding technique proposes high data rate, whereas error rate is prevented thanks to the use of CSIT to cope with the fading channel. The design of the precoder can be quite various, relying on the system requirement. We can list some well-known precoding designs as follows: MMSE, equal-error, QoS-Based, beamforming, waterfilling... More details on these precoders will be given in the next section.

In this chapter, we provide an overview of MIMO precoding techniques. Firstly, some existing well-known precoding designs are presented. After that, the idea to bring the MIMO precoding into the WSN via the cooperation manner is tackled. In this latter work, we present our first contribution that consists in the application of minimum Euclidean distance based precoding to a AF and DF protocol in a WBAN.

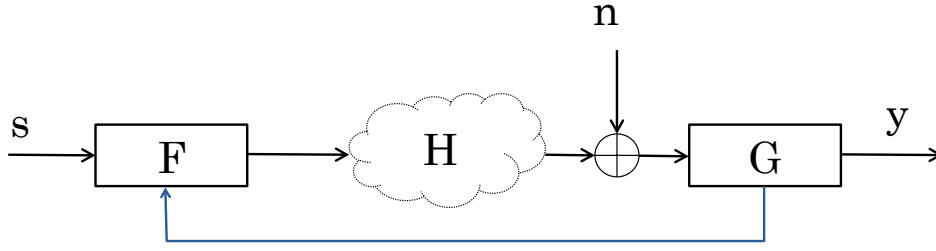


Figure 2.1: System model of the MIMO precoding technique

2.1 Closed-loop precoding for co-located MIMO system

The system model of a closed-loop precoding is shown in the Figure 2.1. The transmitter, after receiving the CSIT from the receiver via the feedback link, will generate a precoder \mathbf{F} . The transmit signal is encoded by this precoder, then propagated through the fading channel \mathbf{H} . At the destination, the receiver decodes the signal thanks to the decoding matrix \mathbf{G} , which is paired with the precoding matrix \mathbf{F} . Thus, the system model is expressed as follows

$$\mathbf{y} = \mathbf{GHFs} + \mathbf{Gn}, \quad (2.1)$$

where \mathbf{y} , \mathbf{s} , \mathbf{n} denote the received, transmit, and AWGN vector, respectively. Assuming that the transmitter and receiver possess n_T , n_R antennas, respectively. If b is the number of data streams, then the constraint on b is set as $b \leq \min(n_T, n_R)$. In the literature, the precoding design exists mostly in the form of linear precoding. The virtual transformation of the channel is generally applied to obtain a diagonalized virtual channel composed of the singular values. As a result, we obtain a virtual channel composed of the singular values of the real channel. Thanks to these values, the precoding design is built based on a specific criterion among those described in section 2.1.2

2.1.1 Virtual channel transformation

When the channel knowledge is available at the transmitter, we can fully generate 2 matrices \mathbf{F}_v , \mathbf{G}_v to make the channel matrix diagonal. This new matrix is called the virtual channel, given as

$$\mathbf{H}_v = \mathbf{G}_v \mathbf{H} \mathbf{F}_v \quad (2.2)$$

This transformation undergoes three steps [16]: noise whitening, channel diagonalization and dimensionality reduction.

2.1.1.1 Noise whitening

The noise covariance matrix is eigenvalue-decomposed:

$$E[\mathbf{nn}^*] = \mathbf{R}_n = \mathbf{Q} \mathbf{\Lambda} \mathbf{Q}^* \quad (2.3)$$

where \mathbf{Q} is a unitary matrix and $\mathbf{\Lambda}$ is a diagonal matrix. Let us define

$$\mathbf{F}_1 = \mathbf{I}_{n_T}, \quad \mathbf{G}_1 = \mathbf{\Lambda}^{-\frac{1}{2}}, \quad \mathbf{H}_{v1} = \mathbf{G}_1 \mathbf{H} \mathbf{F}_1. \quad (2.4)$$

2.1.1.2 Channel diagonalization

After noise whitening, we obtain the matrix $\mathbf{H}_{v1} = \mathbf{G}_1 \mathbf{H} \mathbf{F}_1$. The singular value decomposition (SVD) is used to diagonalize the intermediate channel matrix \mathbf{H}_{v1} :

$$\mathbf{H}_{v1} = \mathbf{A}_2 \mathbf{\Sigma}_2 \mathbf{B}_2^* \quad (2.5)$$

where \mathbf{A}_2 and \mathbf{B}_2 are unitary matrices, and $\mathbf{\Sigma}_2$ is a diagonal matrix whose elements represent the square roots of all eigenvalues of the matrix $\mathbf{H}_{v1} \mathbf{H}_{v1}^*$. One should note that these eigenvalues are real positive numbers and sorted in decreasing order. We continue defining two matrices \mathbf{F}_2 and \mathbf{G}_2 :

$$\mathbf{F}_2 = \mathbf{B}_2, \quad \mathbf{G}_2 = \mathbf{A}_2^* \quad (2.6)$$

The second intermediate channel matrix can be expressed as

$$\mathbf{H}_{v2} = \mathbf{G}_2 \mathbf{H}_{v1} \mathbf{F}_2 \quad (2.7)$$

2.1.1.3 Dimensionality reduction

The matrix \mathbf{H}_{v2} is in the diagonal form and presents the gains of the channel. In this step, we need to reduce the dimension corresponding to the number of data-streams b . To obtain the dimensionality reduction, two matrices \mathbf{F}_3 and \mathbf{G}_3 are defined as

$$\mathbf{F}_3 = \begin{pmatrix} \mathbf{I}_b \\ 0 \end{pmatrix} \quad \text{and} \quad \mathbf{G}_3 = (\mathbf{I}_b \quad 0) \quad (2.8)$$

These operations are only available if $b \leq \min(n_T, n_R)$. The obtained virtual channel matrix is given by

$$\mathbf{H}_v = \mathbf{G}_3 \mathbf{H}_{v2} \mathbf{F}_3 \quad (2.9)$$

Finally, the system model becomes:

$$\mathbf{y} = \mathbf{G}_d \mathbf{H}_v \mathbf{F}_d \mathbf{s} + \mathbf{G}_d \mathbf{n}_v \quad (2.10)$$

where $\mathbf{H}_v = \mathbf{G}_3 \mathbf{G}_2 \mathbf{G}_1 \mathbf{H} \mathbf{F}_1 \mathbf{F}_2 \mathbf{F}_3 = \mathbf{G}_v \mathbf{H} \mathbf{F}_v$ is the diagonal virtual channel matrix, $\mathbf{n}_v = \mathbf{G}_v \mathbf{n}$ is the $b \times 1$ virtual noise vector. Following all transformations above, we have $\mathbf{F}_v^* \mathbf{F}_v = \mathbf{I}$, thus the power constraint of the considered precoding system is described as

$$\text{trace}(\mathbf{F} \mathbf{F}^*) = \text{trace}(\mathbf{F}_d \mathbf{F}_d^*) = 1. \quad (2.11)$$

After performing the virtual transformation, the virtual channel is under the following form:

$$\mathbf{H}_v = \text{diag}(\sigma_1, \dots, \sigma_b), \quad (2.12)$$

where σ_i denotes the subchannel gain and is sorted in the decreasing order. The equivalent system is shown in Fig. 2.2. In order to satisfy the requirement of system, the precoding matrix \mathbf{F}_d is designed to optimize a pertinent criterion. The next subsection will provide some well-known precoding designs that are popularly used in MIMO systems so far.

2.1.2 Existing precoders

2.1.2.1 (Unweighted) MMSE Design

The MMSE (minimum mean-square error) precoder is presented to minimize the sum of the symbol estimation errors across all subchannels [84]. This kind of design

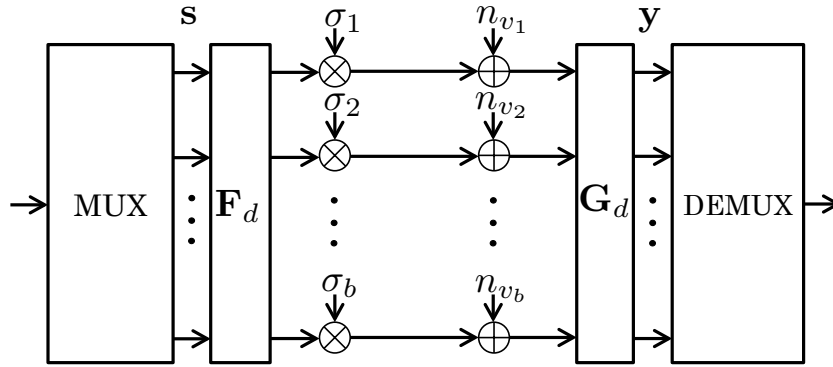


Figure 2.2: The virtual representation of a linear precoding system

does not minimize MSE for each subchannel. So maybe the best subchannel can have a higher MSE than the worst subchannel. Moreover, the MMSE precoder can cancel the weakest subchannel and pour the power to the others.

2.1.2.2 Equal-error Design

Different from MMSE design precoder, Equal-error design guarantees the same error for all subchannels. For fixed rate systems that require the reliable transmission of b symbol streams using identical modulation and coding scheme, we need that all b subchannels have equal errors. In this case, each subchannel is poured power. More power is allocated to the weakest subchannel, while less power is poured to the strongest subchannel to make sure that all MSEs remain the same [84].

2.1.2.3 QoS-Based Design

The QoS (Quality of service)-based precoder forces each datastream to a certain target performance required by the application. For example, the multimedia signal consists of video and audio signal that have different quality requirements. Therefore, the use of QoS-based precoding allows to adapt each data stream to its demand

2.1.2.4 Beam forming Design

This precoder pours the power only on the strongest subchannel corresponding to the maximum eigenvalue [43]. The structure of this design is simple but the data rate is decreased because only one symbol is transmitted in each time slot.

2.1.2.5 Waterfilling Design

The Water-filling precoder is presented to maximize the system capacity. The data rate can be improved significantly. Similar to the beam forming precoder, the Water-filling precoder removes some subchannels and pours power on the others.

2.1.2.6 X- and Y- codes precoder

In order to improve the diversity gain of the precoding scheme, prior to the singular value decomposition, the X- and Y- codes precoder has been proposed by jointly coding information across a pair of subchannels [59]. The X-, Y-Codes/Precoders achieve higher diversity gains at lower encoding/decoding complexity for both well- and ill-conditioned channels.

The system model can be simply described as follows: the original signal is first mapped to the information vector $\mathbf{s} = (s_1, \dots, s_b)$, then mapped by using matrix $\mathbf{F}_c : \mathbf{z} = \mathbf{F}_c \mathbf{s}$. So, the received signal is expressed as

$$\mathbf{y} = \mathbf{H}_v \mathbf{F}_c \mathbf{s} + \mathbf{n}, \quad (2.13)$$

where \mathbf{n} is the noise. The matrix \mathbf{F}_c is characterized by the list of pairings and the 2×2 encoder matrices for each pair.

Each information vector consists of b symbols, and they are divided into $b/2$ pairs. The k -th pair of information symbols, s_{i_k} and s_{j_k} , is jointly coded by using a real 2×2 matrix $\mathbf{A}_k = a_{k,i,j}$ and each \mathbf{A}_k is a submatrix of coding matrix \mathbf{F}_c

$$\begin{cases} f_{i_k, i_k} = a_{k,1,1} & f_{i_k, j_k} = a_{k,1,2} \\ f_{j_k, i_k} = a_{k,2,1} & f_{j_k, j_k} = a_{k,2,2} \end{cases} \quad (2.14)$$

For example, in the case $b = 6$ the X-codes structure is written as

$$\mathbf{F}_c = \begin{pmatrix} a_{1,1,1} & & & & & a_{1,1,2} \\ & a_{2,1,1} & & & & a_{2,1,2} \\ & & a_{3,1,1} & a_{3,1,2} & & \\ & & a_{3,1,1} & a_{3,1,2} & & \\ & a_{2,1,1} & & & a_{2,1,2} & \\ a_{1,1,1} & & & & & a_{1,1,2} \end{pmatrix}. \quad (2.15)$$

Among the diverse precoding techniques, we found an interesting idea in [16], where the minimum Euclidean distance (d_{\min}) between two received point is targeted. Thereby, this distance will be maximized by a precoding matrix, leading to a significant improvement of system performance. Next subsection will describe in details.

2.1.3 Max- d_{\min} precoder

Some recent studies [16], [65], [63], [2], [62], [64] mention about a precoding design that proposes very impressive performance in terms of reducing the error rate of MIMO system. This precoder is based on the maximization of the minimum Euclidean distance (max- d_{\min}) between signal points at the reception side. Thanks to this advantage, the decoder at the receiver has a lower probability to detect erroneously since the received constellation is stretched out. In general, the solution for max- d_{\min} precoder depends on the modulation structure used at transmitter (BPSK, QPSK, QAM). The higher level of modulation requires a more complicated solution to obtain the maximum Euclidean distance. Moreover, the number of data streams (representing the dimension of MIMO spatial multiplexing) likewise affects the maximization. Currently, the solution is available for solely two and three data streams. For larger dimensions, the max- d_{\min} precoder could be organized under multiple sub-systems of two or three data streams.

From the received signal in equation (2.1), the minimum squared Euclidean distance (d_{\min}^2) is accordingly defined as [16]

$$d_{\min}^2 = \min_{\mathbf{s}_k, \mathbf{s}_l \in \mathcal{S}, \mathbf{s}_k \neq \mathbf{s}_l} \|\mathbf{H}_v \mathbf{F}_d (\mathbf{s}_k - \mathbf{s}_l)\|^2 \quad (2.16)$$

where $\mathbf{s}_k, \mathbf{s}_l$ are two different transmit signals, \mathcal{S} is the set of all possible transmit vectors. The max- d_{\min} precoder is therefore obtained by maximizing this distance:

$$\mathbf{F}_{d_{\min}} = \arg \max_{\mathbf{F}'_d} d_{\min}, \quad (2.17)$$

under the power constraint: $\text{trace}\{\mathbf{F}_d \mathbf{F}_d^*\} = 1$. As mentioned above, the solution for the precoders depends on the modulation level and channel knowledge. Let us consider the system with 2 datastreams, after the virtual transformation, the virtual channel matrix is given by

$$\mathbf{H}_v = \begin{pmatrix} \sigma_1 & 0 \\ 0 & \sigma_2 \end{pmatrix} = \rho \begin{pmatrix} \cos \gamma & 0 \\ 0 & \sin \gamma \end{pmatrix} \quad (2.18)$$

where $\rho = \sqrt{\sigma_1^2 + \sigma_2^2}$ is called channel gain and $\gamma = \text{atan} \frac{\sigma_2}{\sigma_1}$ is called channel angle. Apparently, because $\sigma_1 \leq \sigma_2$, the channel angle is always $0 \leq \gamma \leq \pi/4$ because the diagonal line of \mathbf{H}_v is in decreasing order. The general precoder solution can be expressed by the product of power allocation, rotation, and scaling matrices as shown as

$$\mathbf{F}_d = \sqrt{E_s} \begin{pmatrix} \cos \psi & 0 \\ 0 & \sin \psi \end{pmatrix} \begin{pmatrix} \cos \theta & \sin \theta \\ -\sin \theta & \cos \theta \end{pmatrix} \begin{pmatrix} 1 & 0 \\ 0 & e^{i\phi} \end{pmatrix}, \quad (2.19)$$

where ψ, θ, ϕ stand for the power allocation, rotation and scaling parameter, respectively. They will be generated in function of channel condition. Otherwise, the solution for the max- d_{\min} precoding matrix is also relying on the modulation scheme. In the following, we present the max- d_{\min} precoding design for the common modulation scenarios in wireless communication.

2.1.3.1 The max- d_{\min} precoder solution for BPSK modulation

The precoding matrix is expressed as follows [16]

$$\mathbf{F}_d = \sqrt{\frac{p_0}{2}} \begin{pmatrix} 1 & i \\ 0 & 0 \end{pmatrix} \quad (2.20)$$

After passing the numerical search for the values of ψ, θ , and φ , the authors from [16] have confirmed that whatever the channel condition, i.e, for all channel

angle γ , the precoder solution that maximizes the minimum Euclidean distance is obtained for $\psi = 0^\circ$, $\theta = 45^\circ$ and $\varphi = 90^\circ$. It can be seen that the precoder for BPSK modulation only uses the strongest eigenmode of the channel. In other words this design is equivalent to the beamforming design.

2.1.3.2 The max- d_{\min} precoder solution for QPSK modulation

The solution for QPSK modulation can be divided into two cases. If the channel angle stays under the channel angle threshold γ_0 , the precoder can be seen as a beamforming design, similar to to BPSK modulation case. Otherwise, if the channel angle is larger than the threshold, the precoder leads to an octagonal constellation at the receiver.

If $0 \leq \gamma \leq \gamma_0$ (γ is channel angle) [16]:

$$\mathbf{F}_d = \mathbf{F}_{r_1} = \begin{pmatrix} \sqrt{\frac{3+\sqrt{3}}{6}} & \sqrt{\frac{3+\sqrt{3}}{6}} e^{i\frac{\pi}{12}} \\ 0 & 0 \end{pmatrix} \quad (2.21)$$

If $\gamma_0 \leq \gamma \leq \pi/4$:

$$\mathbf{F}_d = \mathbf{F}_{octa} = \sqrt{\frac{E_s}{2}} \begin{pmatrix} \cos \psi & 0 \\ 0 & \sin \psi \end{pmatrix} \begin{pmatrix} 1 & e^{i\frac{\pi}{4}} \\ -1 & e^{i\frac{\pi}{4}} \end{pmatrix} \quad (2.22)$$

$$\text{where } \begin{cases} \psi = \text{atan} \frac{\sqrt{2}-1}{\tan \gamma} \\ \gamma_0 \simeq 17,28^\circ \end{cases}$$

2.1.3.3 The max- d_{\min} precoder solution for 16-QAM modulation

Through two modulation schemes above, we can see that the complexity of max- d_{\min} precoder is exponential to the modulation level. With no exception, for 16-QAM modulation, its solution is obviously complicated [65]. In the Table 2.1, in each interval of channel angle, we provide the value of parameters for constructing the max- d_{\min} precoding given in (2.19).

Precoder	γ	ψ	ϕ	θ
\mathbf{F}_{r1}	(0, 5.128°)	0	$\text{atan} \frac{1}{6+\sqrt{3}}$	$\text{atan}(2 \sin \phi)$
\mathbf{F}_{T1}	(5.128°, 5.26°)	$\text{atan} \frac{5\sqrt{2}-7}{\tan \gamma}$	45°	45°
\mathbf{F}_{T2}	(5.26°, 8.40°)	$\arccos \frac{\alpha - \alpha \cos^2 \gamma}{\alpha - 2 \cos^2 \gamma}$ ($\alpha = 1 + \frac{6}{\sqrt{34}}$)	$\text{atan} \frac{3}{5}$	45°
\mathbf{F}_{T3}	(8.40°, 15.38°)	$\text{atan} \frac{\sqrt{10/\sqrt{14}-1}}{\tan \gamma \sqrt{10/\sqrt{14}+1}}$	$\text{atan} \frac{3}{5}$	$\frac{1}{2} \text{atan} \frac{\sqrt{10}}{2}$
\mathbf{F}_{T4}	(15.38°, 45°)	$\text{atan} \frac{\sqrt{2}-1}{\tan \gamma}$	45°	45°

Table 2.1: Parameter values for max- d_{\min} precoder in 16-QAM modulation

2.1.3.4 General expression of max- d_{\min} precoder for high QAM modulation levels

The optimal solutions of max- d_{\min} precoder propose heavier complexity for higher modulation levels. As seen in the previous subsection, the max- d_{\min} precoding matrix for 16-QAM carries out a sophisticated structure. Logically, for higher modulation levels such as 64-QAM or 128-QAM, the solution is hyper complicated. Aiming to propose a general solution that is suitable for every QAM modulation, whereas maintaining the simplicity, the authors in [62] provide the general expression of max- d_{\min} precoder.

Precoder \mathbf{F}_1 :

When the channel angle is in the interval $0 \leq \gamma \leq \gamma_0$, the max- d_{\min} precoder pours power only on the first virtual subchannel, it means that the angle $\psi = 0$. The precoding matrix is simplified as

$$\mathbf{F}_1 = \sqrt{E_s} \begin{pmatrix} \cos \theta & \sin \theta e^{i\phi} \\ 0 & 0 \end{pmatrix} \quad (2.23)$$

$$\text{where } \begin{cases} \phi = \arctan \frac{1}{2N+\sqrt{3}} \\ \theta = \arctan(2 \sin \phi) \end{cases} \quad (N = 2^k - 1)$$

Precoder \mathbf{F}_2 :

For the remaining values of γ the optimized max- d_{\min} solution for a 4^k -QAM modulation can be considered in the case with $\theta = \pi/4$, $\phi = \pi/4$. The precoding matrix is expressed as:

$$\mathbf{F}_2 = \frac{\sqrt{E_s}}{2} \begin{pmatrix} \cos \psi & 0 \\ 0 & \sin \psi \end{pmatrix} \begin{pmatrix} \sqrt{2} & 1+i \\ -\sqrt{2} & 1+i \end{pmatrix} \quad (2.24)$$

where $\psi = \arctan \frac{\sqrt{2}-1}{\tan \gamma}$.

Channel threshold γ_0 :

The general expression above is the simplified version of the max- d_{\min} precoder thus the threshold γ_0 corresponds to the modulation level, and it can be expressed as:

$$\tan \gamma_0 = \sqrt{\frac{\sqrt{2}-1}{\sqrt{2}N^2 + \sqrt{6}N + \sqrt{2}-1}}. \quad (2.25)$$

To point out the impressive performance of max- d_{\min} precoded with respect to the other precoders, we plot in Figure 2.3 the BER of four well-known precoding designs: max- d_{\min} , MMSE, beamforming, and waterfilling. As we can see, the max- d_{\min} precoder outperforms the others.

2.1.4 Feedback link requirement

Since it requires the CSI at the transmitter to design the corresponding precoder, the precoding MIMO is by nature a closed loop system. Generally, the CSI is estimated at the reception side, then fed back to transmitter. Usually, the receiver feeds channel matrix back to the transmitter which operates the remaining calculations to get the precoding. Meaning that the transmitter possesses a powerful enough processor to do all the computations to generate the precoding matrix. However, being in the context of WBAN, this method is inefficient in a node with small size and very limited power source. Therefore, the precoding matrix is computed at the reception and fed back to transmitter. On the other hand, the receiver should also know this matrix for the decoding process.

The hypothesis of a perfect CSI at the transmitter can not be real, since the channel estimation, quantification and feed back process always suffer from errors.

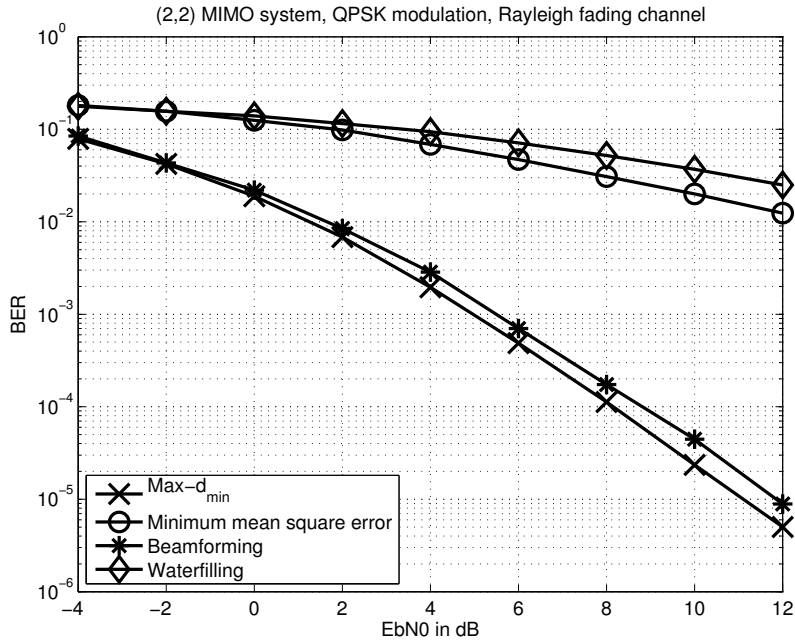


Figure 2.3: BER performance of different precoding designs

In reality, the number of feedback bits is finite, we must trade it off with the delay as well as energy consumption to ensure a highest transmission efficiency. A new approach in recent years, named "Limited Feedback" [52], creating a codebook in both transmission and reception sides allows to achieve a sufficient performance with several feedback bits. More specifically, after obtaining the channel knowledge, the reception chooses from codebook (pre-created for both the transmitter and receiver) a precoding matrix corresponding to its design. Afterwards, it feeds back the matrix index to the transmitter. By this way, the feedback process is more practical and economical since only the index of precoding matrix is sent back instead of the entire matrix as in the conventional methods.

In this Section, we present the feedback process according to the max- d_{\min} precoding system. Specifically, two methods will be studied. In the first one, we perform all operations at the reception then obtain the precoding matrix \mathbf{F} . We quantize directly this matrix, then feed back entry by entry to the transmitter. This work demands many bits for the quantization, because each entry is a complex number. In the second one, we pre-construct a codebook, choose a matrix in it following the

max- d_{\min} criterion and feed the index back. The performance of both methods will be compared and evaluated under Matlab simulations.

2.1.4.1 Direct feedback

The matrix \mathbf{F} that maximizes the Euclidean distance at the reception side will be completely quantized element by element. If taking 2 bits of quantization for each real part and imaginary part, it means we spend totally 16 bits for a 2×2 precoding matrix. But to obtain sufficient performance (compared to perfect CSIT system), we need at least 32 bits in total (see Figure 2.4). Feeding back the precoding matrix directly is a classical method. However as we can see the expense for a satisfactory performance is significant. For that reason, we consider the limited feed back [52, 53] that is able to reduce the number of feed back bits by using a codebook.

2.1.4.2 Limited feedback

To carry out the limited feedback, we create in both transmission and reception side, a codebook containing precoding matrices. Once the receiver obtains the channel information, it chooses, among matrices in the codebook, a precoding matrix that fits the predefined criteria. The index of this matrix is then fed back to the transmitter. This method requires memory in both the transmitter and receiver to store the codebook. In return, it reduces the power consumption, as well as the delay time for feedback process.

Herein, we describe the construction of the codebook for the precoding matrix \mathbf{F} and the selection at the receiver when the channel information is available [55]. The set of matrices \mathbf{F}_v is built, whose size depends on the number of bits fed back. For the reason that this matrix is used to singular-value-decompose the channel matrix \mathbf{H} , it must take into account the distribution of this channel matrix \mathbf{H} . Based on the study of Ghadir Madi in [55] and D. J. Love in [52], for a Rayleigh fading channel \mathbf{H} , the set \mathcal{F}_v for all values of \mathbf{F}_v is proposed as follows

$$\mathcal{F}_v = (\mathbf{F}_{DFT}, \Theta \mathbf{F}_{DFT}, \dots, \Theta^{N-1} \mathbf{F}_{DFT}), \quad (2.26)$$

where $N = 2^n$, n is the number of bits for codebook, \mathbf{F}_{DFT} and Θ are 2x2 matrices defined by

$$\begin{cases} \mathbf{F}_{DFT}(k, l) = (1/\sqrt{2})e^{j\pi kl} \\ \Theta = \begin{pmatrix} e^{j(2\pi/N)u_1} & 0 \\ 0 & e^{j(2\pi/N)u_2} \end{pmatrix} \end{cases}, \quad (2.27)$$

where vector $\mathbf{u} = [u_1, u_2]^T$ is integer vector that satisfies $0 \leq u_1, u_2 \leq N - 1$. They are chosen to maximize the minimum Chordal distance between the matrix \mathbf{F}_{DFT} and $\Theta^l \mathbf{F}_{DFT}$:

$$\mathbf{u} = \arg \max \left\{ \min_{1 \leq l \leq N-1} d(\mathbf{F}_{DFT}, \Theta^l \mathbf{F}_{DFT}) \right\}, \quad (2.28)$$

where the Chordal distance d is given by

$$d(A, B) = \frac{1}{\sqrt{2}} \|AA^* - BB^*\|_F, \quad (2.29)$$

where $\|\cdot\|_F$ denotes the Frobenius matrix norm.

For each matrix \mathbf{F}_{vi} in the dictionary $\mathcal{F}_v = (\mathbf{F}_{v1}, \mathbf{F}_{v2}, \dots, \mathbf{F}_{vN})$, $i = (1, \dots, N)$ which is already generated at the destination, the following steps are proposed to create the dictionary \mathcal{F}_d for the matrices \mathbf{F}_d :

1. A set of random MIMO Rayleigh channel matrices \mathbf{H} is generated.
2. For each matrix \mathbf{H} , we calculate the matrix \mathbf{F}_d through the max- d_{\min} optimization criterion mentioned in Appendix A. Then the following criterion is applied to find out the matrix \mathbf{F}_{di} corresponding to \mathbf{F}_{vi} :

$$\mathbf{F}_{di} = \arg \max_{(\mathbf{H}, \mathbf{F}_d) \in \Delta, (x_k, x_l) \in \mathcal{S}} \left(\min_{(\mathbf{H}, \mathbf{F}_d) \in \Delta, (x_k, x_l) \in \mathcal{S}} |\mathbf{H}\mathbf{F}_{vi}\mathbf{F}_d\mathbf{e}(x_k, x_l)|^2 \right), \quad (2.30)$$

where Δ is the set of matrices \mathbf{H} extracted and matrices \mathbf{F}_d associated.

In this method, the dictionary of \mathbf{F}_d is obtained according to the considered MIMO channel model, and has the same size as the dictionary \mathcal{F}_v :

$$\mathcal{F}_d = (\mathbf{F}_{d1}, \mathbf{F}_{d2}, \dots, \mathbf{F}_{dN}), \quad i = (1..N) \quad (2.31)$$

Afterwards, the codebook \mathcal{F} for the matrix $\mathbf{F} = \mathbf{F}_v \mathbf{F}_d$ will be built as follows:

$$\mathcal{F} = (\mathbf{F}_{v1}\mathbf{F}_{d1}, \mathbf{F}_{v2}\mathbf{F}_{d2}, \dots, \mathbf{F}_{vN}\mathbf{F}_{dN}) = (\mathbf{F}_1, \mathbf{F}_2, \dots, \mathbf{F}_N). \quad (2.32)$$

This codebook is created offline, and available at both the transmission and reception sides. During transmission, after obtaining the channel information, the destination will choose, from this codebook, a corresponding precoder matrix then send its index to the transmitter.

To determine which precoder in the codebook is optimal for a certain channel \mathbf{H} , the following criterion will be applied

$$\mathbf{F} = \arg \max \left\{ \min_{\mathbf{F}_i \in \mathcal{F}, (x_k, x_l) \in \mathcal{S}} |\mathbf{H}\mathbf{F}_i \mathbf{e}(x_k, x_l)|^2 \right\}. \quad (2.33)$$

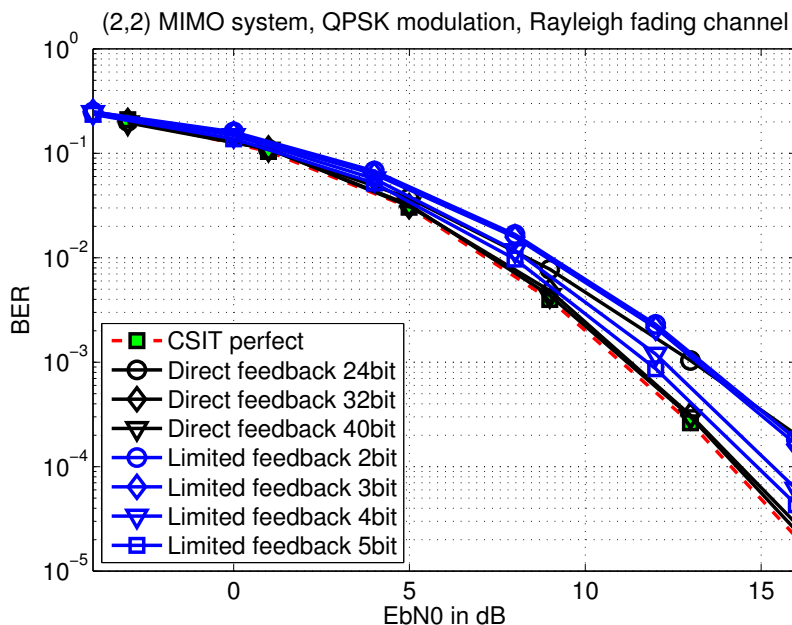


Figure 2.4: BER performance of direct feedback and limited feedback in comparison to a perfect CSIT system for $\max-d_{\min}$ precoder.

Figure 2.4 exhibits the performance of the direct feedback (i.e. the whole matrix \mathbf{F} , but quantized thanks to a finite number of bits) and the limited feedback (i.e. the codebook index), compared to the perfect CSIT. This simulation is carried over a 2×2 MIMO system, with a QPSK modulation, and Rayleigh fading channel. As we can see, to obtain a sufficient performance, a direct feedback system needs at least 32 bits in total to send back the precoding matrix. Instead, with only 5 bits the limited feedback proposes an approximate performance. However, the counterpart is that it

requires a flash memory at the transmitter and receiver to store the codebook. But this memory is totally feasible to be implemented for a codebook containing only 32 precoding matrices.

2.2 Distributed max- d_{\min} precoding (DMP)

As mentioned in the previous chapter, to tackle the power consumption issue in WSN (or in WBAN in particular), the cooperative technique is presented with two typical scenarios: cooperative relay and cooperative MIMO. However, with the advantages in exploiting the CSIT, we are exploring the potential of the MIMO precoding technique in WSN. Especially, the max- d_{\min} precoding, with the expense of more complicated precoder structure, is very promising in this point of view.

Although showing the promising interest to be applied to cooperative relay network, the existing studies on the distributed precoding are still very limited, especially in WSN. Most of distributed precoders are dedicated to cellular networks, and particularly the downlink via the coordination of multiple base stations. Some interesting structures can be cited such as weight sum rate maximization, leakage projected dirty paper coding, layered virtual SINR (signal to interference plus noise ratio) maximization [31] [15] [106]. Unlike WSN, where the energy efficiency is one of the most important constraints, in the cellular network the distributed precoding aims to increase the data rate in the downlink. Another fundamental difference is the insignificant space limitation at the base station in the downlink, where multiple antennas can be easily deployed. The base station collaboration then enhances the spectral efficiency.

The distributed precoding in WSN exists mostly in the form of distributed beamforming [6] [30]. This distributed scheme shows an impressive SNR gain but always suffers from the synchronization problem. Moreover, the survey on the energy efficiency issues have not been carefully investigated on the distributed beamforming for WSN. The authors in [56] have presented also a distributed approach for WSN by using the max- d_{\min} precoder and P-OSM (precoding for orthogonalized spatial multiplexing). But the investigations on the cooperation and forwarding is still lim-

ited. There is also the lack of a spectral-efficient representation due to the use of MIMO precoding (compared to other cooperative schemes).

Thanks to the outstanding BER performance of max- d_{\min} precoder, we introduce the distributed max- d_{\min} precoding as a cooperative scheme in WSN. Different to the study in [56], herein we propose to investigate different protocols using a cooperating node (Decode-Forward, Amplify-Forward). Regarding the local data exchange of a cooperative scheme, we propose the transmission of the precoded signal between the source and cooperative node aiming to enhance significantly the spectral efficiency. The energy efficiency is also studied with a global energy model containing the circuit and transmission consumption.

2.2.1 System model

We consider a simplified network, described in Figure 2.5, involving three nodes: a source, a cooperative node and a destination. The source and the cooperative nodes are sensor nodes, equipped with single antenna and constrained to low energy consumption to limit battery replacement. The destination is supposed to be an external AP without power constraint and neither stringent complexity constraint, comparatively to the sensor nodes. By allowing two antennas at the access point, the network is equivalent to a virtual 2×2 MIMO system. An error-free and delay-free feedback link provides the CSIT. Thanks to this CSIT, MIMO precoding techniques can be applied to the virtual MIMO system to deal with the channel impairments such as fading, antenna correlation, shadowing, path loss. We propose to apply the general max- d_{\min} precoder, described in details in Section 2.1.3.4, to this virtual MIMO system. Like for all cooperative techniques, two phases are needed:

- Local data exchange: the source node shares its data with the cooperative node via the SISO channel h .
- Precoding transmission: thanks to the spatial multiplexing properties of the precoder, the source and the cooperative node transmit the precoded signals simultaneously to the access point via the virtual MIMO channel matrix \mathbf{H} .

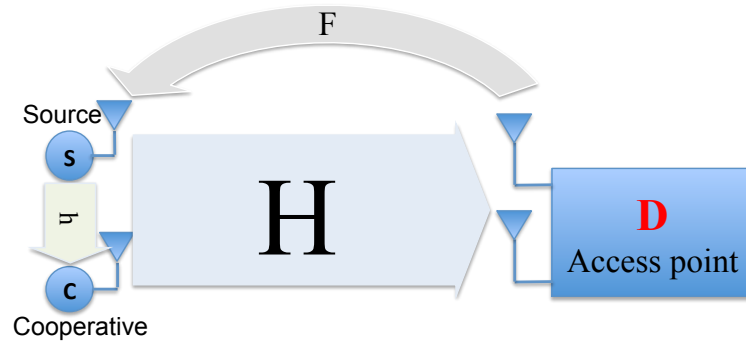


Figure 2.5: System model of a distributed precoded scheme

In the second phase, the general expression of the $\max-d_{\min}$ precoder, described in section 2.1.3.4, will be picked up. Even though this is not an optimal solution, it performs outstandingly with a huge reduction of complexity for all 4^k -QAM modulation. We assume that the signal in the transmit constellation is normalized. For 4^k -QAM modulation the transmitted symbol s belong to the set

$$S = \frac{1}{\sqrt{M}} \{a + bi; a - bi; -a + bi; -a - bi\}, \quad (2.34)$$

where $M = \frac{2}{3}(4^k - 1)$ and $a, b \in (1, 3, \dots, 2^k - 1)$, meaning $E\{ss^*\} = 1$. In our precoding system, a vector of two symbols will be transmitted. Equivalently, in a SISO transmission, the total energy for this vector is equal to 2. Whereas, in our precoding system, with the constraint $\text{trace}(\mathbf{F}\mathbf{F}^*) = 1$, the average total energy for 2 symbols $E[\text{trace}((\mathbf{F}\mathbf{s})(\mathbf{F}\mathbf{s})^*)] = 1$. Therefore, to make a fair comparison in energy consumption, the transmit signal in the precoding system is multiplied by a coefficient $\sqrt{2}$ such that $\mathbf{x} = \sqrt{2}\mathbf{F}\mathbf{s}$.

Power allocation in DMP :

In order to investigate the effects of the relay position on the cooperative schemes, we take into account the path loss explicitly in the transmission model. The distances $S \rightarrow D$, $S \rightarrow C$, $C \rightarrow D$ (Figure 2.5) are denoted by d_{SD} , d_{SC} , d_{CD} , respectively. Then the relative power gain of $S \rightarrow C$ and $C \rightarrow D$ links, with respect to $S \rightarrow D$ link, are given by $G_{SC} = (d_{SD}/d_{SC})^K$, $G_{CD} = (d_{SD}/d_{CD})^K$ [83], where K is a path loss exponent, varying from 1.6 to 6 in indoor wireless channel. Due to the fact that

two transmission phases are carried out in the DMP, an allocation strategy must be considered to pour reasonably the power between two phases. As an example, in the case of the local channel is good, we set lower power for the local exchange phase, in contrast we pour more power if this link goes worse. The aim is to always maintain the best performance given the channel knowledge. To have a fair comparison between various schemes, we assume the overall energy for each modulated symbol used in both local transmission (\mathcal{E}_L) and precoding transmission (\mathcal{E}_D) is \mathcal{E} . It means $\mathcal{E}_L = \beta\mathcal{E}, \mathcal{E}_D = (1 - \beta)\mathcal{E}$, where β denotes the power allocation parameter. This parameter can be optimized, based on various criterion such as: BER minimization [103], capacity maximization [40], outage minimization [54], network lifetime maximization, total transmit power minimization [34]...

2.2.2 Decode and Forward relaying (DMPDF)

The Decode and Forward scheme will transmit 2 symbols within 3 time slots. In the first and second time slots, the first transmission phase is performed. Two symbols s_0, s_1 are sent one by one through a SISO channel, represented by h . Hence, the cooperative node (also called relay node) receives

$$\mathbf{y}_c = h\sqrt{\mathcal{E}_L G_{SC}}[s_0 \quad s_1]^T + \mathbf{n}_c, \quad (2.35)$$

where \mathbf{n}_c denotes the AWGN noise vector at the cooperative node. The received signal is then decoded to \hat{s}_0 and \hat{s}_1 . With the presence of AWGN in this phase, errors always occur randomly on \hat{s}_0 and \hat{s}_1 .

Then the precoding signal is built as follows

$$\begin{cases} F_{11}s_0 + F_{12}s_1 & \text{at the source node} \\ F_{21}\hat{s}_0 + F_{22}\hat{s}_1 & \text{at the cooperative node} \end{cases}. \quad (2.36)$$

Due to a different distance to the destination, the relay has a gain G_{CD} in received energy, referenced to the source. If in a co-located precoding based system with 2 antennas on both receiver and transmitter, the energy received at the sink is $2\mathcal{E}_D$ [68]. In the considered distributed precoding system, this value is absolutely larger if the cooperative node is closer than the source node (with respect to the destination).

In addition, we have an objective of obtaining the same energy at the destination from both nodes. Supposing that source and cooperative nodes have the knowledge of all the distances (i.e they know the relative power gains). Let us define the \mathcal{E}_{D_S} and \mathcal{E}_{D_C} are respectively the transmit energy at the source and cooperative nodes. We assume the synchronization of two nodes is perfect, thus in the third time-slot, both nodes transmit this signal simultaneously. Therefore, we have constraints as

$$\begin{cases} \mathcal{E}_{D_S} + \mathcal{E}_{D_C} = 2\mathcal{E}_D \\ \mathcal{E}_{D_S} = \mathcal{E}_{D_C} G_{CD} \end{cases} \Leftrightarrow \begin{cases} \mathcal{E}_{D_S} = 2\frac{G_{CD}}{G_{CD}+1}\mathcal{E}_D \\ \mathcal{E}_{D_C} = 2\frac{1}{G_{CD}+1}\mathcal{E}_D \end{cases}. \quad (2.37)$$

By writing the aforementioned process in a matrix form, the received signal at the destination will be

$$\mathbf{y} = \sqrt{2}\mathbf{G}\mathbf{H} \begin{pmatrix} \sqrt{2\frac{G_{CD}}{G_{CD}+1}}\mathcal{E}_D(f_{11}s_0 + f_{12}s_1) \\ \sqrt{2\frac{1}{G_{CD}+1}}\mathcal{E}_D(f_{21}\hat{s}_0 + f_{22}\hat{s}_1)\sqrt{G_{CD}} \end{pmatrix} + \mathbf{G}\mathbf{n}. \quad (2.38)$$

The precoding matrix \mathbf{F} is designed only according to the channel \mathbf{H} so that $\mathbf{F} = \max\text{-}d_{\min}(\mathbf{H})$ [65] [16]. There is no need to estimate the SISO channel h at the destination.

2.2.3 Amplify and Forward relaying (DMPAF)

Instead of decoding the signal received from the source node, the cooperative node amplifies it with a designed factor and forwards it to the destination. Clearly, as in DMP-DF, both channels h and \mathbf{H} have a significant influence on the system performance. Therefore, we propose two schemes with different uses of matrix \mathbf{H} and h for the design of the precoding matrix and the amplifying factor at the cooperative node. The first scheme, called *factor multiplying*, constructs the matrix \mathbf{F} based on the channel \mathbf{H} . The effect of channel h will be taken into account at the cooperative node by the amplifying factor. The design of the second scheme, called *channel customizing*, is based on an equivalent representation of the received signal, bringing out a customized channel matrix containing both \mathbf{H} and h . This scheme assumes the knowledge of h and \mathbf{H} at the destination.

Regarding the local data exchange between the source and the cooperative node, two configurations can be carried out: 1) Local Successive Transmission (LST): the

transmission of the non precoded symbols on orthogonal channels, typically thanks to TDMA; 2) Local Precoded Transmission (LPT): the transmission of a part of the precoded signal, i.e. a linear combination of the symbols. For this configuration, the signal sent from the source during the local data exchange is not useful at the destination.

2.2.3.1 Factor multiplying

We design the precoding matrix according to the channel matrix \mathbf{H} such that $\mathbf{F} = \max\text{-}d_{\min}(\mathbf{H})$ and reduce the effect of channel h by multiplying the received signal with an amplifying factor.

- *Configuration 1: Local successive transmission:* s_0 and s_1 will be sent one by one to the cooperative node, according to TDMA. The cooperative node receives

$$\mathbf{y}_c = \begin{pmatrix} y_{c0} \\ y_{c1} \end{pmatrix} = \begin{pmatrix} h\sqrt{\mathcal{E}_L G_{SC}} s_0 + n_{c0} \\ h\sqrt{\mathcal{E}_L G_{SC}} s_1 + n_{c1} \end{pmatrix}. \quad (2.39)$$

At the cooperative node, the received signal is normalized by its energy, precoded, and retransmitted to the destination. At the same time, the source node also transmits its precoded signal to the destination. Then the received vector at destination is written as

$$\mathbf{y} = \mathbf{GH} \begin{pmatrix} \sqrt{2E_D}(F_{11}s_0 + F_{12}s_1) \\ g_1(F_{21}y_{c0} + F_{22}y_{c1}) \end{pmatrix} + \mathbf{Gn}, \quad (2.40)$$

where amplifying factor g_1 is chosen as

$$g_1 = \frac{h^*}{|h|} \sqrt{\frac{2\mathcal{E}_D G_{CD}}{\mathcal{E}_L G_{SC} |h|^2 + N_{n_c}}}, \quad (2.41)$$

where N_{n_c} is the noise variance at the cooperative node. The factor g_1 is aimed to reduce the effect of the AWGN noise and the channel h [47] and to prevent the power saturation at the cooperative node.

- *Configuration 2: Local precoded transmission :* Instead of transmitting symbol by symbol in the local exchange phase, the source sends s_0 and s_1 simultaneously, thanks to the linear combination $s_{pre} = F_{21}s_0 + F_{22}s_1$, to the cooperative

node. Then the cooperative node receives

$$y_{c_{pre}} = h\sqrt{2\mathcal{E}_L G_{SC}} s_{pre} + \mathbf{n}_c, \quad (2.42)$$

The remaining steps are similar to the local successive transmission. The destination then receives

$$\mathbf{y} = \mathbf{GH} \begin{pmatrix} \sqrt{2\mathcal{E}_D}(F_{11}s_0 + F_{12}s_1) \\ g_2 y_{c_{pre}} \end{pmatrix} + \mathbf{Gn}, \quad (2.43)$$

where $g_2 = \frac{h^*}{|h|} \sqrt{\frac{2\mathcal{E}_D G_{CD}}{2\mathcal{E}_L G_{SC}|h|^2 + N_{nc}}}$.

2.2.3.2 Channel customizing

In this scheme, we take the channel h into account by a customized channel via an equivalent transformation of the received constellation. Like in the factor multiplying scheme, two configurations will be studied regarding the local data exchange. The received signals during the precoding transmission for the two configurations are as follows.

- *Configuration 1: Local successive transmission* By replacing (2.39) into 2.40 we obtain

$$\begin{aligned} \mathbf{y} &= \mathbf{GH} \begin{pmatrix} \sqrt{2E_D} & 0 \\ 0 & \sqrt{2E_D} \sqrt{\frac{G_{CD}}{1 + \frac{N_0}{E_L G_{SC}|h|^2}}} \end{pmatrix} \mathbf{Fs} + \\ &+ \begin{pmatrix} H_{12}(g_1 F_{21} n_{c0} + g_1 F_{22} n_{c1}) \\ H_{22}(g_1 F_{21} n_{c0} + g_1 F_{22} n_{c1}) \end{pmatrix} + \mathbf{n}_v \\ &= \sqrt{2E_D} \mathbf{GH} \begin{pmatrix} 1 & 0 \\ 0 & w_1 \end{pmatrix} \mathbf{Fs} + \mathbf{n}'_c + \mathbf{n}_v, \end{aligned} \quad (2.44)$$

where $w_1 = \sqrt{\frac{G_{CD}}{1 + \frac{N_0}{E_L G_{SC}|h|^2}}}$,

$$\mathbf{n}'_c = \begin{pmatrix} H_{12}(g_1 F_{21} n_{c0} + g_1 F_{22} n_{c1}) \\ H_{22}(g_1 F_{21} n_{c0} + g_1 F_{22} n_{c1}) \end{pmatrix}.$$

- *Configuration 2: Local precoded transmission* Similarly, equation (2.43) is rewritten as

$$\mathbf{y} = \sqrt{2E_D} \mathbf{GH} \begin{pmatrix} 1 & 0 \\ 0 & w_2 \end{pmatrix} \mathbf{Fs} + \begin{pmatrix} H_{12} g_2 n_c \\ H_{22} g_2 n_c \end{pmatrix} + \mathbf{n}_v, \quad (2.45)$$

$$\text{where } w_2 = \sqrt{\frac{G_{CD} N_0}{1 + 2E_L G_{SC} |h|^2}}.$$

Therefore, the precoding matrix will be designed based on a customized channel matrix involving the contribution of both \mathbf{H} and h such as

$$\mathbf{F} = \text{max-}d_{\min} \left(\mathbf{H} \begin{pmatrix} 1 & 0 \\ 0 & w_i \end{pmatrix} \right), \quad i = 1, 2. \quad (2.46)$$

Regarding the complexity on the signal processing at the sensor nodes, thanks to limited feedback, the sensor nodes are absolved from the computation. Therefore, there is not any complexity difference in terms of signal processing at the sensor nodes between our distributed precoding and the cooperative STBC scheme. Like in other cooperative system, the main problem in our system is the asynchronous that may seriously affects the system performance [67], and the need of feedback link. The second term can be managed by using the limited feedback as mentioned in subsection 2.1.4. The effect of the asynchronous on the performance is crucially important in MIMO system. As reported, the max- d_{\min} precoding less degradation in terms of BER, compared to the other MIMO system.

2.2.4 Energy model

The total energy of a wireless system consists of two elements: transmission energy and circuit consumption energy. For a same BER target, a cooperative scheme requires less transmission energy; reversely it demands more power for cooperative data exchange and circuit consumption on cooperative nodes. Certainly, for short distances, the cooperative scheme will not offer a better energy efficiency than non cooperative transmission. For the long distances, where the transmission consumption dominates the total energy, we expect that cooperative systems provide high energy efficiency. In this section we describe the energy model used to estimate the energy consumption of both cooperative and non cooperative systems.

2.2.4.1 Circuit energy consumption model

In a wireless system, both the transmitter and the receiver possess radio frequency blocks such as filter, power amplifier, digital-to-analog converter, mixer... [20]. The

circuit power consumption for each transmitter and receiver is then given by

$$P_{Tx} = P_{DAC} + P_{mix} + P_{filt} + P_{syn}, \quad (2.47)$$

$$P_{Rx} = P_{LNA} + P_{mix} + P_{IFA} + P_{filr} + P_{ADC} + P_{syn}, \quad (2.48)$$

where P_{DAC} , P_{mix} , P_{filt} , P_{syn} , P_{LNA} , P_{IFA} , P_{filr} , P_{ADC} denote the power of digital-analog converter, mixer, filter at transmitter, synthesizer, low noise amplifier, intermediate frequency amplifier, filter at receiver and analog-digital converter, respectively. The amplifier power P_{pa} for emission relates directly to the transmission power $P_{pa} = (1 + \alpha)P_{trans}$, where $\alpha = \frac{\xi}{\eta} - 1$ with η is the drain efficiency of the RF power amplifier and ξ is the Peak-to-Average Ratio (PAR) which depends on the modulation scheme and the associated constellation size [20].

2.2.4.2 Transmission power consumption

We suppose the radio signal is impaired by a path loss following a K-law since the extra-BAN link is always considered. Therefore the required transmission power is given by

$$P_{trans}(d) = \hat{E}_b R_b \times \frac{(4\pi d)^K}{G_t G_r \lambda^2} M_l N_f, \quad (2.49)$$

where d denotes the transmission distance, \hat{E}_b denotes the needed energy per bit for a BER target, R_b is the bit rate, G_t and G_r are the antenna gains of transmission and reception sides, respectively. λ is the carrier wavelength, M_l is the link margin, N_f is the receiver noise figure defined as $N_f = M_n/N_0$ with $N_0 = -174 \text{ dBm/Hz}$ the single side thermal noise Power Spectral Density (PSD) and M_n denotes the PSD of the total effective noise at receiver input [20].

2.2.4.3 Spectral efficiency and bit rate

The total spectral efficiency with QPSK modulation is shown in the Table 2.2 for the different schemes, cooperative and non cooperative.

The bit rate in the wireless system relates directly to the spectral efficiency and the bandwidth. In addition, the bit rate R_b of each transmission phase affects the total energy consumption as follows

$$E_{total} = \frac{P_{cL} + P_{paL}}{R_{bL}} + \frac{P_{cD} + P_{paD}}{R_{bD}}, \quad (2.50)$$

Table 2.2: Spectral efficiency of different cooperative schemes with QPSK

	SISO	MRC	Distributed Alamouti	DMP DF	DMPAF LPT
$\eta_S(\text{b/s/Hz})$	2	2	1	1.5	2

where P_{c_L} , P_{pa_L} and P_{c_D} , P_{pa_D} denote the total circuit power consumption and amplifier power for local data exchange phase and precoding transmission phase, respectively. R_{b_L} and R_{b_D} are the bit rates of the local data exchange and the precoding transmission respectively. Normally, the bit rate in a precoding system will be twice the one of a SISO system because it transmits 2 symbols in 1 time slot instead of only 1 symbol. However, the DMP involves two phases with different bit rates according to the considered scheme. The Distributed Alamouti scheme is carried out by the Alamouti code in the virtual 2×2 MIMO system [66]. This scheme consumes 4 time slots for transmitting 2 symbols s_0, s_1 . In the local exchange phase, the Distributed Alamouti, the DMPDF, and the DMPAF-LST schemes achieve the same spectral efficiency as the SISO transmission. Whereas, with 2 modulated symbols transmitted in a precoded symbol, the DMPAF-LPT represents twice the bit rate of the others. In the second phase, corresponding to the precoding transmission, all DMP schemes transmit the signal twice as fast as the non cooperative schemes (SISO and SIMO), while the Distributed Alamouti scheme achieves the same bit rate as the SISO scheme.

2.2.5 Simulation results

We evaluate the schemes proposed in Section 2.2.2, and 2.2.3 by Monte Carlo simulations. In our system, we use the QPSK modulation, the channels h and \mathbf{H} are Rayleigh fading channels. We transmit 150 000 frames, each frame contains 100 bits. The channel is assumed to be stable for the transmission time of one frame. The distance d_{SC} is supposed to be 5% of d_{SD} .

In the power allocation problem, we need to minimize the BER with respect to

power allocation parameter β :

$$\begin{aligned} & \min_{\beta} \text{BER}(\beta) \\ & \text{subject to } \mathcal{E}_L + \mathcal{E}_D = \text{constant}. \end{aligned} \quad (2.51)$$

The BER approximation is not a simple issue in the max- d_{\min} precoding system and especially complicated in the distributed max- d_{\min} precoding system. In a first approximation, the power allocation parameter β will be found by a numerical search for the Optimal Power Allocation (OPA). For the Equal Power Allocation (EPA), $\beta = 0.5$. Thanks to the analytical derivation error problem in Chapters 3 and 4, we will be able to propose a less consuming computation resource for this power allocation.

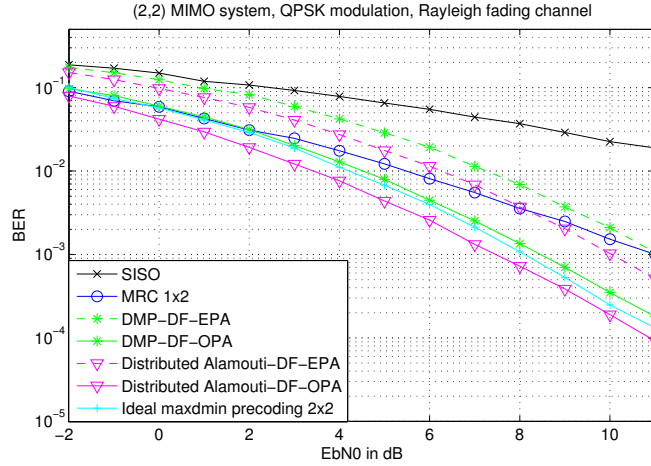


Figure 2.6: BER performance comparison: DMP vs. traditional schemes

For QPSK modulation, $E_b/N_0 = (\mathcal{E}/2)/N_0$. The BER performance comparison between various schemes is given in Figure 2.6. The DMPDF proposes a significant transmission power reduction β compared to the SISO transmission and the MRC 1×2 , for the same BER target. Comparing the distributed Alamouti and the DMPDF, a loss of 1 dB occurs at a BER equal to 10^{-3} . We recall that they operate at different spectral efficiencies (see Table 2.2). Figure 2.6 also shows the advantage of the optimal power allocation on the DMP performance, the OPA always provides a 3 dB gain compared to the EPA scheme. In Figure 2.7, the DMPDF and DMPAF schemes propose equivalent performance. In terms of BER, even though it saves 1

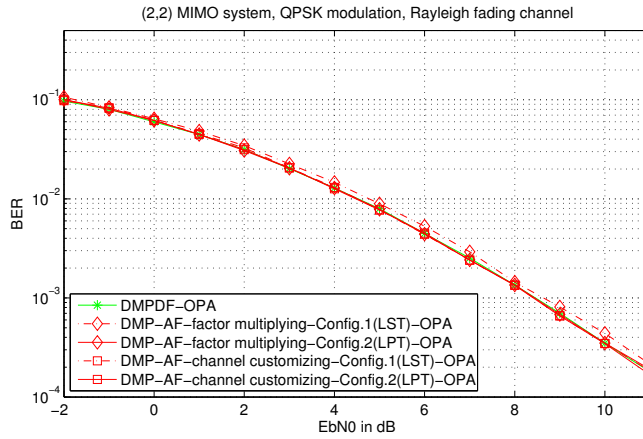


Figure 2.7: BER performance comparison of DMP schemes

time slot, the DMPAF-LPT schemes still has same performance as DMPAF-LST. Besides, there is no difference between the DMPAF with *amplifying factor* and the DMPAF with *customizing channel*.

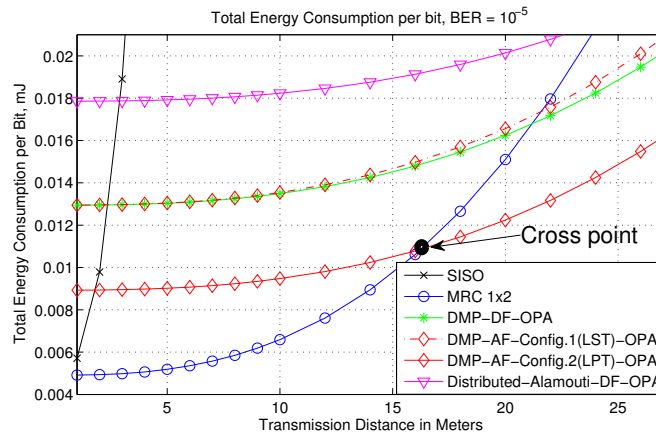


Figure 2.8: Total energy consumption vs. distance (10^{-5} BER)

Anyhow, our final objective is the energy optimization. Thus a complete investigation of all power aspects of a wireless system must be studied to have a comprehensive view on the energy performance. We consider the energy efficiency with the parameters given in Table 2.3. Particularly for our system, because the access point is a powerful computer plugged directly to the power source, then we do not take into account the power constraint of the destination. The required BER at the destination is supposed to be 10^{-5} and the path loss exponent is assumed

to be 2.6, for all schemes. Figure 2.8 shows the total energy consumption per bit for different schemes versus distances from 1 to 27 meters. There is no difference between the DMPAF-*factor multiplying* and DMPAF-*channel customizing* in terms of BER performance and spectral efficiency, consequently we homogenize them in the energy efficiency investigation in Figure 2.8. By reducing 1 time slot in the local exchange phase, the DMPAF-LPT always provides an improvement in energy efficiency compared to the DMPDF and DMPAF-LST. Moreover, regarding the distributed Alamouti scheme, even though it achieves an impressive BER performance, its low spectral efficiency makes it consuming more energy. On the other side, thanks to a good BER performance and higher spectral efficiency, the DMPAF-LPT always has the best energy efficiency compared to other DMPs. For a small distance, we only need a low transmission power to obtain the targeted performance, thus the circuit consumes most of energy. Therefore the more simple scheme will outperform the more complicated ones and the MRC 1×2 transmission takes the advantage in terms of energy efficiency. In contrast, when the distance increases, the transmission energy dominates the total energy consumption. Hence, optimizing transmission energy is more valuable. If the distance is longer than 16 meters, the DMPAF-LPT shows the best energy efficiency.

Table 2.3: Parameter values of the consumption model [20]

$f_c = 2,5GHz$	$P_{mix} = 30.3mW$	$\eta = 0.35$
$G_t G_r = 5dBi$	$P_{filt} = P_{filr} = 2.5mW$	
$B = 10kHz$	$P_{DAC} = 15.4mW$	$P_{syn} = 50mW$
$N_f = 10dB$	$T_s = \frac{1}{B}$	$M_l = 40dB$
$P_{ADC} = 6.7mW$	$\frac{N_0}{2} = -174dBm/Hz$	$P_{LNA} = 20mW$

The path loss exponent $K = 2.6$ is just an assumption. The environment can be more intricate: indoor, outdoor, crowded, or an echoic environment. Obviously, in each path loss environment our distributed scheme responds differently. For an overall view, in Figure 2.9 we investigate the crossing point for different path loss exponents. The *Crossing point* (Figure 2.8) represents the distance from which the

DMPAF-LPT outperforms the others. We observe that when the path loss goes heavier, the DMP takes the advantage for shorter distances.

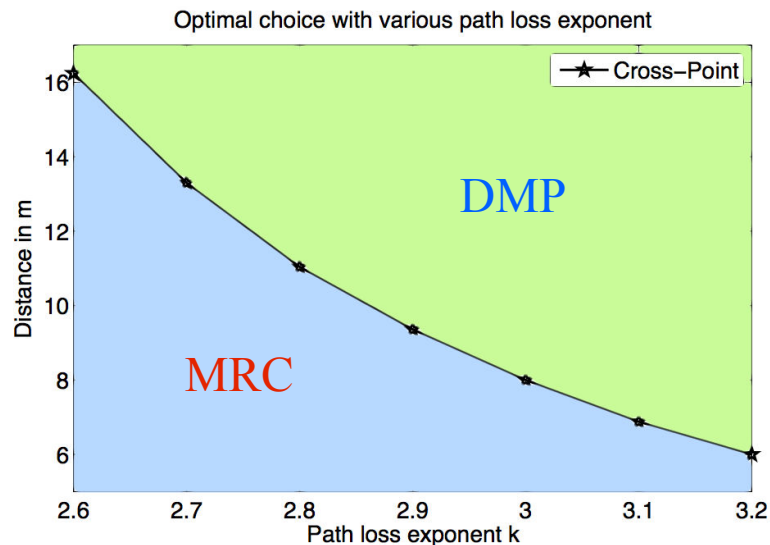


Figure 2.9: The *crossing points* for different path loss exponents

2.3 Conclusion

The cooperative technique is already well-investigated but is often presented in the form of distributed space-time block code, seen as an open-loop virtual MIMO system. In this chapter, we introduce the idea to adapt the closed-loop system to the cooperative system, named: the distributed precoding. The CSIT is exploited to design a precoding matrix according to a specific criterion. We select the $\max-d_{\min}$ precoding to go further since its outstanding performance is already demonstrated for point-to-point colocated MIMO system.

Aiming to achieve a high energy efficiency, we have proposed and investigated the distributed precoding schemes based on $\max-d_{\min}$ criterion. Two relaying types - Decode and Forward, Amplify and Forward - with different data exchanges (local successive transmission, local precoded transmission) have been defined and studied. Based on an overall energy model, we have derived their energy efficiency in WSN context. With respect to other cooperative techniques, the DMP proposes a high spectral efficiency, typically doubled compared to the Distributed Alamouti

one. Whatever the distance, the DMP always achieve a lower energy consumption than the Distributed Alamouti scheme. For a BER equal to 10^{-5} and a path loss exponent equal to 2.6, the DMPAF-LPT achieves a lower energy consumption than the MRC 1×2 scheme for a distance between the source to access point greater than 16 m. Moreover, when the path loss exponent increases, transmission energy becomes preponderant with respect to circuit energy and the DMP takes the advantage for smaller distances, typically few meters.

Furthermore, the obtained performance analysis will be used advantageously to allocate the transmit power between two phases of considered DMP. However, besides the numerical evaluation, the mathematical basis need is obvious to rigorously confirm the considered DMP performance. For this reason, the two next chapters provide the theoretical performance analysis for both forwarding type of the DMP: DF and AF. Due to different natures in forwarding the signal of relay, two separate approaches will be proposed. For the DMP-DF, we base on the decoding error probability at the cooperative node to derive the equivalent system model. The DMP-AF leads to a transformation of channel matrix and the total noise at the destination. To obtain the bit error probability, we investigate the statistical distribution of the minimum Euclidean distance between two received points.

Chapter 3

Distributed max- d_{\min} precoding: Decode-and-Forward

3.1 Introduction

In this chapter, we specifically consider the Decode-and-Forward structure (the Amplify-and-Forward will be targeted in next chapter). We address the performance analysis of the distributed precoding scheme, deploying the Euclidean distance based precoding via cooperative technique in a general WSN (described in subsection 2.2.2 of Chapter 2); the implementation into WBAN is totally similar. The decode-and-forward relaying is focused on the basic case with one single relay node, one source node and a destination which possesses two co-located antennas. The given methodology in this chapter is however obviously extendable for the larger systems. These extensions might be considered in the future works with more relay nodes and/or more antennas at the destination.

In addition, we propose to examine the possibility to use the information of the relay performance at the destination [8]. This information is adopted by calculating the log-likelihood ratio to detect more efficiently the symbol in the maximum likelihood (ML) decoder at the destination. A new maximum likelihood decoder is introduced, exploiting the decoding error probability of the relay to enhance the detection at the destination. In the light of the fact that the complexity of ML decoder augments severely in a full use of this information, we propose a suboptimal and less complex solution taking advantage of the max-log approximation.

Accordingly, our contributions in this chapter are listed as follows:

1. Without the relay decoding information at the destination
 - The performance analysis for the distributed max- d_{\min} precoder is proposed that takes into account the errors at the relay.
 - Based upon that, the power allocation is then derived to maximize the total system performance at the destination with a constant power.
2. With the knowledge of relay decoding information at the destination, we propose a new ML decoder for the distributed max- d_{\min} precoder that can improve the symbol detection.

The rest of this chapter is organized as follows: In Section 3.2, we introduce

the Decode and Forward scheme for the distributed max- d_{\min} precoding. In Section 3.3, the performance of this protocol is analyzed. The new ML decoder that takes advantage of the relay decoding information is described in Section 3.5. Section 4.5 concludes the chapter.

3.2 Decode and Forward for the distributed max- d_{\min} precoding

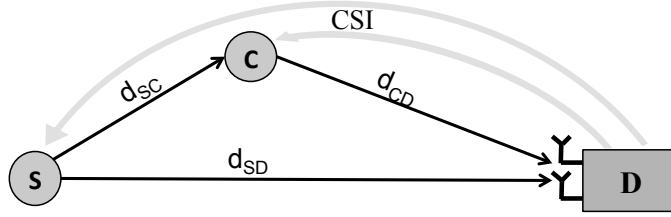
3.2.1 Distributed scheme description

We consider the cooperative relay network given in Figure 4.1a, involving a source S , a cooperative node (also called relay) C and a destination D . The destination is typically an access point, with no stringent constraints on size, energy consumption or signal processing. On the contrary, the source and the cooperative node are typically sensor nodes, with limited size and limited bulk of energy. To enhance transmission reliability, and potentially reduce the energy consumption, we would like to take profit of the CSI at the transmitter side thanks to MIMO precoding. However, as both source and cooperative nodes are equipped with a single antenna, due to their limited size, the precoding scheme is deployed in a distributed manner over S and C . The destination supports the implementation of two antennas so that the considered network can be seen as a virtual 2×2 MIMO system. The MIMO precoding consists in the multiplication of the 2×2 precoder matrix \mathbf{F} by the symbol vector to transmit $\mathbf{s} = [s_0 \ s_1]^T$, where $[\cdot]^T$ stands for matrix transpose. Thus, the cooperative MIMO scheme needs two transmission phases, illustrated in Figure 4.1b. The local phase corresponds to the transmission of \mathbf{s} from the source to the cooperative node, via a SISO (Single-Input Single-Output) channel h . Two time slots are thus needed. The precoding phase deploys the distributed precoding scheme over the source and the cooperative node, via a virtual MIMO channel \mathbf{H} , in one time slot.

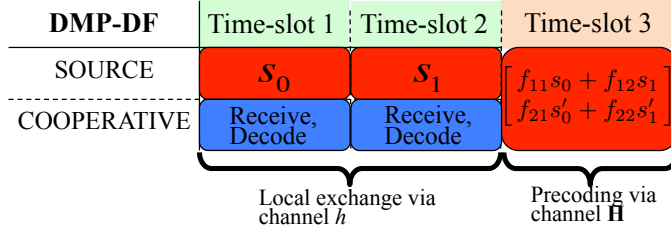
The different distances between S , C , and D are referred as d_{SC} , d_{CD} , and d_{SD} , for $S \rightarrow C$, $C \rightarrow D$, $S \rightarrow D$, respectively. We define the power gain relative to the

$S \rightarrow C$ distance and the $C \rightarrow D$ distance, by $G_{SC} = \left(\frac{d_{SD}}{d_{SC}}\right)^K$ and $G_{CD} = \left(\frac{d_{SD}}{d_{CD}}\right)^K$, respectively. K is the path loss exponent, varying from 1.6 to 6 according to the propagation environment.

In terms of energy, during the local transmission and the precoding transmission, the energy per symbol is equal to \mathcal{E}_L and \mathcal{E}_D , such that the energy constraint $\mathcal{E}_L + \mathcal{E}_D = \mathcal{E}$ is satisfied, where \mathcal{E} is the total energy to transmit one symbol. One of the parameters to optimize is the parameter β that allocates the power over the two phases, such that $\mathcal{E}_L = \beta\mathcal{E}$, and $\mathcal{E}_D = (1 - \beta)\mathcal{E}$.



(a) System model with involved distances.



(b) Time resource used in DMP-DF.

Figure 3.1: Distributed scheme description with a source node, a relay node and a destination.

3.2.2 System model

During the local phase, the cooperative node receives

$$\mathbf{y}_c = h\sqrt{\mathcal{E}_L}G_{SC}\mathbf{s} + \mathbf{n}_c, \quad (3.1)$$

where \mathbf{n}_c denotes a 2×1 vector containing the AWGN (Additive White Gaussian Noise) noise at C . The received signals are then decoded to $\hat{\mathbf{s}}$.

In the next phase, both S and C precode the signal \mathbf{s} and $\hat{\mathbf{s}}$, by the 2×2 matrix \mathbf{F} with the power constraint $\text{trace}(\mathbf{F}\mathbf{F}^*) = 1$ (defined as the sum of the

elements on the main diagonal). As \mathcal{E} is the total energy for one symbol, therefore $E[\text{trace}((\mathbf{F}\mathbf{s})(\mathbf{F}\mathbf{s})^H)] = \mathcal{E}$. That implies that the total energy in the precoding system for transmitting 2 symbols is only \mathcal{E} , whereas in a SISO system this value is $2\mathcal{E}$ ($E[\text{trace}(\mathbf{s}\mathbf{s}^*)] = 2\mathcal{E}$). Therefore, to make a fair comparison in energy consumption, the transmit signal in the precoding system is $\mathbf{x} = \sqrt{2}\mathbf{F}\mathbf{s}$, such that the consumed energy will be $\text{trace}(\mathbf{x}\mathbf{x}^*) = 2\mathcal{E}$. As a result, in the phase of precoding transmission of our distributed scheme, the transmit power is $2\mathcal{E}_D$.

As described in section 2.2.2, due to a different distance to the destination, the relay has a gain G_{CD} in received energy, referenced to the source. Supposing that source and cooperative nodes have the knowledge of all the distances, by writing the aforementioned process in a matrix form with the mentioned power statement, the received signal at the destination will be

$$\mathbf{y} = \sqrt{2}\mathbf{G}\mathbf{H} \begin{pmatrix} \sqrt{2\frac{G_{CD}}{G_{CD}+1}}\mathcal{E}_D(f_{11}s_0 + f_{12}s_1) \\ \sqrt{2\frac{1}{G_{CD}+1}}\mathcal{E}_D(f_{21}\hat{s}_0 + f_{22}\hat{s}_1)\sqrt{G_{CD}} \end{pmatrix} + \mathbf{G}\mathbf{n} \quad (3.2)$$

$$= 2\sqrt{\frac{G_{CD}}{G_{CD}+1}}\mathcal{E}_D\mathbf{G}\mathbf{H} \begin{pmatrix} \mathbf{f}_1\mathbf{s} \\ \mathbf{f}_2\hat{\mathbf{s}} \end{pmatrix} + \mathbf{G}\mathbf{n}, \quad (3.3)$$

where \mathbf{n} denotes the AWGN noise vector at the destination, $\mathbf{f}_1 = [f_{11} \ f_{12}]$ and $\mathbf{f}_2 = [f_{21} \ f_{22}]$ are row vectors of the designed precoding matrix \mathbf{F} accordingly to the MIMO channel matrix \mathbf{H} [65] based on the maximization of minimum Euclidean distance ($\max\text{-}d_{\min}$) between two points in the received constellation. This design process is described in details in section 3.2.3.

To obtain the precoding matrix, the CSI can be made available at the transmitter through a feedback link. However, instead of a full CSI feedback, we consider a limited feedback that reduces significantly the load on the feedback link, typically 3 or 4 bits for 2×2 MIMO system. The limited feedback approach relies on a codebook, created at both transmission and reception sides [52, 53, 60]. Before the precoded transmission occurs, the receiver estimates the channel via a training phase. Afterward, it chooses from the precoding codebook, generated offline, a matrix that maximizes the minimum Euclidean distance between the received vectors in the constellation. The precoding matrix index is then fed back to the transmitter. Besides the reduction of the feedback link rate, this method liberates the transmitter

from the computation of the precoding matrix and reduces the energy needed for the reception of feedback data at the transmitter.

3.2.3 Precoder design

In this study, we focus on the QPSK modulation that is very popular in WSN. Indeed, thanks to its low peak-to-average power ratio, the power amplifier can be more energy efficient and low cost. Therefore, the optimal solution of the precoding matrix for this modulation is provided in subsection 2.1.3.2 of chapter 2. However, interested readers would find the optimal solution of the max- d_{\min} criterion for other modulation schemes and numbers of data streams in [16, 65]. In higher level modulations, such as 16-QAM or 64-QAM, a general suboptimal solution can be proposed in a similar 2-matrix form [62].

3.2.4 Theoretical error probability

Because of the presence of two forms \mathbf{F}_{r1} and \mathbf{F}_{octa} in (2.21) and (2.22), the performance analysis of the max- d_{\min} precoder becomes very complicated. In this subsection, we discuss about the d_{\min} based performance analysis for the max- d_{\min} precoding system. Considering a colocated MIMO precoding system with the general expression of max- d_{\min} precoder given in subsection 2.1.3.4, the performance analysis was studied in [73] based on the distribution of minimum Euclidean distance (d_{\min}) between two points in the received constellation. The authors addressed out the probability density function (pdf) of d_{\min}^2 , then the average bit error probability was derived as

$$\tilde{P}_e \approx \int_{\mathcal{D}_{d_{\min}^2}} \frac{N_b N_n}{2b \log_2 M} \operatorname{erfc} \left(\sqrt{\frac{SNR \cdot x}{4}} \right) f_{d_{\min}^2}(x) \partial x, \quad (3.4)$$

where N_n denotes the average number of neighbors, N_b is the average of difference bits between two neighbors, and b is the number of transmit symbols (i.e number of data streams). $f_{d_{\min}^2}(x)$ denotes the pdf of d_{\min}^2 , where the distance d_{\min}^2 is calculated by

$$d_{\min}^2 = \min_{\mathbf{s}_k, \mathbf{s}_l \in \mathcal{S}} \|\mathbf{GHF}(\mathbf{s}_k - \mathbf{s}_l)\|^2, \quad (3.5)$$

Table 3.1: Value of N_b and N_n for QPSK and 16-QAM

	N_b QPSK	N_n QPSK	N_b 16-QAM	N_n 16-QAM
\mathbf{F}_{r1}	3.5	1.471	4.313	2.032
\mathbf{F}_{octa}	7	1.488	13.875	2.291

where \mathcal{S} denotes the modulated constellation [16]. Because the precoding matrix is given by two forms, its pdf is also expressed in two forms and the integral is splitted into two parts. The details for the derivation of equation (3.4) are given in [73]. With the same justification, N_b and N_n get two different values for the two cases \mathbf{F}_{r1} and \mathbf{F}_{octa} (see table 3.1).

In terms of performance analysis, the distributed scheme is more intricate compared to a colocated system. Indeed, the local transmission phase as well as the precoding phase have impacts on the total system performance. During the local transmission phase, decoding errors at the cooperative node occur. This information on decoding errors then could be used or not at the destination. In Section 3.3, the performance is analyzed without the decoding information of the cooperative node; knowing the error probability at the cooperative node, we propose to enhance the performance of the ML decoder in section 3.5.

3.3 Performance analysis

3.3.1 Definition of the different hypothesis

If the error probability at the cooperative node is unavailable at the destination, the ML decoder will detect the received signal as if the local transmission phase is error free, like in the colocated precoding system. Let us call ϵ the symbol error rate for the local transmission between the source and the relay. Hence, four hypothesis can be enumerated for a QPSK modulation, depending on the error event at the cooperative node.

1. Θ_0 : during the local transmission phase, both symbols are correctly decoded at the cooperative node. Consequently, the probability of this event is $P(\Theta_0) =$

$(1-\epsilon)^2$. This event corresponds to the colocated system case. In the precoding transmission, the symbol error probability is given by $P\{\tilde{\mathbf{s}} \neq \mathbf{s}|\Theta_0\}$.

2. Θ_1 and Θ_2 : for these two events we consider that, during the local transmission phase, one of the decoded symbol is wrong whereas the other one is correct. The event probability is equal to $P(\Theta_i) = (1-\epsilon)\epsilon$, $i = 1, 2$, and the error probability at the destination will be denoted as $P\{\tilde{\mathbf{s}} \neq \mathbf{s}|\Theta_i; i = 1, 2\}$.
3. Θ_3 : both symbols are decoded wrongly. Therefore $P(\Theta_3) = \epsilon^2$, and the error probability at the destination is denoted as $P\{\tilde{\mathbf{s}} \neq \mathbf{s}|\Theta_3\}$.

All channel in this paper is supposed to be normalized Rayleigh-fading. The source-relay is solely a SISO channel h , meaning the pdf of channel amplitude is written as

$$f_{|h|^2}(x) = e^{-x} \quad (3.6)$$

For a QPSK modulation, the bit error probability is given by $p = \mathcal{Q}(SNR_l)$ ($\mathcal{Q}(x) = \frac{1}{2\pi} \int_x^\infty e^{-\frac{u^2}{2}} \partial u$), where SNR_l denotes the signal-to-noise ratio for the considered channel. In our case $SNR_l = \mathcal{E}_L G_{SC} |h|^2$. We get the symbol error probability expressed as $p_s = 1 - (1-p)^2 = 2p - p^2$. Thus, the average symbol error probability for the local transmission phase can be written as

$$\epsilon = \int_0^\infty (2\mathcal{Q}(\mathcal{E}_L G_{SC} x) - \mathcal{Q}^2(\mathcal{E}_L G_{SC} x)) e^{-x} \partial x \quad (3.7)$$

$$= 1 - \varsigma - \frac{1}{2} \left(\frac{2}{\pi} \varsigma \arctan(\varsigma) - \varsigma + \frac{1}{2} \right), \quad (3.8)$$

where $\varsigma = \sqrt{\frac{\mathcal{E}_L G_{SC}}{\mathcal{E}_L G_{SC} + 2}} = \sqrt{\frac{\beta \mathcal{E} G_{SC}}{\beta \mathcal{E} G_{SC} + 2}}$.

Finally, the error probability at the destination is written as

$$P\{\tilde{\mathbf{s}} \neq \mathbf{s}\} = \sum_{i=1}^4 P(\Theta_i) P\{\tilde{\mathbf{s}} \neq \mathbf{s}|\Theta_i\} \quad (3.9)$$

3.3.2 Study of hypothesis Θ_0

Since there is no error at the relay, we fall into the case of a colocated system. By taking into account the energy received during the precoding phase, equation (2.10)

is slightly modified to get the received signal at the destination expressed as

$$\mathbf{y} = 2\sqrt{\frac{G_{CD}}{G_{CD} + 1}}\mathcal{E}_D\mathbf{G}\mathbf{H}\mathbf{F}\mathbf{s} + \mathbf{n}_v. \quad (3.10)$$

In this case, the error probability $P\{\hat{\mathbf{s}} \neq \mathbf{s}|\Theta_0\}$ at the destination is computed with the same methodology as given in Subsection 3.2.4.

3.3.3 Study of Hypothesis Θ_1 & Θ_2

Without loss of generality, we focus on the event Θ_2 . The analysis of the event Θ_1 will be trivially derived afterwards. The QPSK constellation is defined as $\mathcal{S} = \{1, j, -1, -j\}$. For the event Θ_2 , during the local transmission phase, the first symbol s_0 is decoded correctly whereas the second one s_1 is wrong. Whatever the transmitted symbol s_1 , the decoded symbol \hat{s}_1 belongs to $\{-s_1, js_1, -js_1\}$. Consequently, the signal transmitted from the source and the relay during the precoding phase is given by

$$\mathbf{x}(i) = \begin{pmatrix} f_{11}s_0 + f_{12}s_1 \\ f_{21}s_0 + f_{22}\hat{s}_1 \end{pmatrix} = \begin{pmatrix} f_{11} & f_{12} \\ f_{21} & a_i f_{22} \end{pmatrix} \mathbf{s}, \quad (3.11)$$

where $a_i = \{-1, j, -j\}$. The received signal at the destination is then

$$\mathbf{y}(i) = 2\sqrt{\frac{G_{CD}}{G_{CD} + 1}}\mathcal{E}_D\mathbf{G}\mathbf{H} \begin{pmatrix} f_{11} + f_{12} \\ f_{21} + a_i f_{22} \end{pmatrix} \mathbf{s} + \mathbf{n}_v \quad (3.12)$$

$$= 2\sqrt{\frac{G_{CD}}{G_{CD} + 1}}\mathcal{E}_D\mathbf{G}\mathbf{H} \left(\mathbf{F} + \begin{pmatrix} 0 & 0 \\ 0 & (a_i - 1)f_{22} \end{pmatrix} \right) \mathbf{s} + \mathbf{n}_v. \quad (3.13)$$

Since the ML decoder has no information about the error probability at the relay, a_i is not known at the destination. Consequently, the ML decoder considers that the precoding matrix utilized at the transmitter side is \mathbf{F} whereas the system model is correctly defined by equation (3.13), corresponding to an erroneous precoding matrix $\mathbf{F}_2(i)$ as below

$$\mathbf{F}_2(i) = \mathbf{F} + \begin{pmatrix} 0 & 0 \\ 0 & (a_i - 1)f_{22} \end{pmatrix}. \quad (3.14)$$

This equivalent precoding matrix accounts for the decoding errors at the relay. Equation (3.13) can be rewritten to bring out an interference term as follows

$$\mathbf{y}(i) = 2\sqrt{\frac{G_{CD}}{G_{CD} + 1}}\mathcal{E}_D\mathbf{G}\mathbf{H}\mathbf{F}\mathbf{s} + \underbrace{(a_i - 1)2\sqrt{\frac{G_{CD}}{G_{CD} + 1}}\mathcal{E}_D\mathbf{G}\mathbf{H}\begin{pmatrix} 0 & 0 \\ 0 & f_{22} \end{pmatrix}\mathbf{s}}_{\text{Interference}} + \mathbf{n}_v. \quad (3.15)$$

The interference term denoted by $\mathbf{I}_2(i)$ depends on the signal strength at the destination and the erroneous symbol detected by the relay, represented by the value of a_i .

We assume that all three events corresponding to the 3 values of a_i are equiprobable so that the symbol error probability at the destination for the event Θ_2 is expressed as

$$P\{\tilde{\mathbf{s}} \neq \mathbf{s}|\Theta_2\} = \frac{1}{3} \sum_1^3 P\{\tilde{\mathbf{s}} \neq \mathbf{s}|\Theta_2, a_i\}, \quad i = 1, 2, 3. \quad (3.16)$$

Similarly, for the event Θ_1 , the ML decoder utilizes the precoding matrix \mathbf{F} instead of the actual precoding matrix given by

$$\mathbf{F}_1(i) = \mathbf{F} + \begin{pmatrix} 0 & 0 \\ (a_i - 1)f_{21} & 0 \end{pmatrix}, \quad a_i \in \{-1, j, -j\}, \quad i = 1, 2, 3. \quad (3.17)$$

For the event Θ_1 , the interference term is expressed as

$$\mathbf{I}_1(i) = (a_i - 1)2\sqrt{\frac{G_{CD}}{G_{CD} + 1}}\mathcal{E}_D\mathbf{G}\mathbf{H}\begin{pmatrix} 0 & 0 \\ f_{21} & 0 \end{pmatrix}\mathbf{s}, \quad (3.18)$$

and the error probability is then written

$$P\{\tilde{\mathbf{s}} \neq \mathbf{s}|\Theta_1\} = \frac{1}{3} \sum_1^3 P\{\tilde{\mathbf{s}} \neq \mathbf{s}|\Theta_1, a_i\}. \quad (3.19)$$

Because of the interference term given in equations (3.15) and (3.18), the symbol error probability $P\{\tilde{\mathbf{s}} \neq \mathbf{s}|\Theta_\nu, a_i\}; \nu = 1, 2; i = 1, 2, 3$ is not trivially derived from the methodology presented in section 3.2.4. The section 3.3.5 will present the new methodology based on the approximation of the SINR (signal to interference and noise ratio).

3.3.4 Study of hypothesis Θ_3

If the relay wrongly decodes both symbols, the erroneous precoding matrix then becomes

$$\mathbf{F}_3(i, z) = \mathbf{F} + \begin{pmatrix} 0 & 0 \\ (a_i - 1)f_{21} & (a_z - 1)f_{22} \end{pmatrix}, \quad (3.20)$$

with $i, z = 1..3$; $a_{i,z} \in \{-1, j, -j\}$. According to the hypothesis 3, the interference could be expressed as

$$\mathbf{I}_3(i, z) = 2\sqrt{\frac{G_{CD}}{G_{CD} + 1}}\mathcal{E}_D\mathbf{GH} \begin{pmatrix} 0 & 0 \\ (a_i - 1)f_{21} & (a_z - 1)f_{22} \end{pmatrix} \mathbf{s}. \quad (3.21)$$

Subsequently, the symbol error probability for the event Θ_3 is written as

$$P\{\tilde{\mathbf{s}} \neq \mathbf{s}|\Theta_3\} = \frac{1}{9} \sum_1^9 P\{\tilde{\mathbf{s}} \neq \mathbf{s}|\Theta_3, a_{\{i,z\}}\}. \quad (3.22)$$

3.3.5 Interference investigation

In order to derive a closed-form of the bit error probability of our DMP-DF scheme we propose to investigate the interference terms in the system model obtained for the events Θ_1 , Θ_2 , and Θ_3 .

Taking into account the interference term, the bit error probability in the hypothesis Θ_ι ($\iota = 1..3$) is given as

$$P\{\Theta_\iota, a_i\} \approx \frac{N_b N_n}{2b \log_2 M} \operatorname{erfc}\left(\sqrt{\frac{SINR_\iota(i)d_{\min}^2}{4}}\right), \quad (3.23)$$

where the signal to interference plus noise ratio $SINR$ is calculated by

$$SINR_\iota(i) = \frac{(G_{CD} + 1)\mathcal{E}_D}{\|\mathbf{I}_\iota(i)\|^2 + N_0}, \quad (3.24)$$

with N_0 denoting the noise variance at the destination. The interferences defined in the previous section are the random variables. Moreover, there is no doubt that they vary dependently with the minimum Euclidean distance. At this point, we assign that

$$\|\mathbf{I}_\iota(i)\|^2 = r_\iota(i) \cdot d_{\min}^2, \quad (3.25)$$

where $r_\iota(i)$ is a random variable representing the dependence.

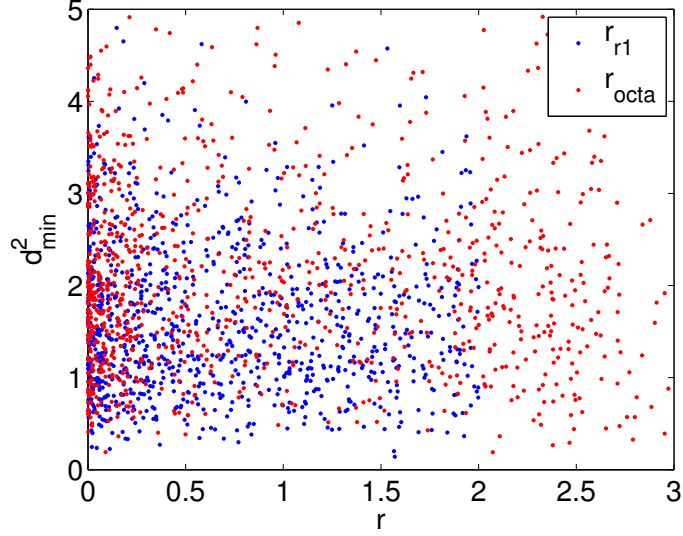


Figure 3.2: Illustration the correlation between d_{\min}^2 and r in the hypothesis 1 (similar results for both remaining hypothesis)

The theoretical study is now arduous and we consider the arbitrary simplifying hypothesis that $r_\iota(i)$ and d_{\min}^2 are independent. The figure 3.2 can illustrate this independence by plotting out the points determined by the large number of $r_\iota(i)$ and d_{\min}^2 , generated numerically. As can be seen in this figure, these two variables are almost uncorrelated. In addition, a numerical study reenforces this supposition with low co-variance values. As a result, the average error probability is rewritten as

$$\tilde{P}e\{\Theta_\iota, a_i\} \approx \int_0^\infty \int_0^\infty \frac{N_b N_n}{2b \log_2 M} \kappa(r_\iota(i), d_{\min}^2) f_{r_\iota(i)}(r_\iota(i)) f_{d_{\min}^2}(d_{\min}^2) \partial d_{\min}^2 \partial r_\iota(i), \quad (3.26)$$

where $\kappa(r_\iota(i), d_{\min}^2) = \operatorname{erfc} \left(\sqrt{\frac{(G_{CD}+1)\mathcal{E}_D}{(G_{CD}+1)\mathcal{E}_D r_\iota(i) d_{\min}^2 + N_0} \frac{d_{\min}^2}{4}} \right)$. If we consider the outer integral in (3.26) as an expectation with respect to $r_\iota(i)$, we obtain

$$\tilde{P}e\{\Theta_\iota, a_i\} \approx \int_0^\infty E_{r_\iota(i)} \{g(r_\iota(i), d_{\min}^2)\} f_{d_{\min}^2}(d_{\min}^2) \partial d_{\min}^2, \quad (3.27)$$

where

$$g(r_\iota(i), d_{\min}^2) = \frac{N_b N_n}{2b \log_2 M} \operatorname{erfc} \left(\sqrt{\frac{4 \frac{G_{CD}}{G_{CD+1}} \mathcal{E}_D}{4 \frac{G_{CD}}{G_{CD+1}} \mathcal{E}_D r_\iota(i) d_{\min}^2 + N_0} \cdot \frac{d_{\min}^2}{4}} \right). \quad (3.28)$$

The last hard point is the last mathematical expectation over $r_\iota(i)$ and we propose 2 methods to solve this problem in the next paragraphs.

3.3.6 Solution 1: Derive an upper-bound

The function $g(r_\iota(i), d_{\min}^2)$ is a concave function with respect to $r_\iota(i)$. Therefore, Jensen's inequality [37] allows to state:

$$\mathbb{E}_{r_\iota(i)} [g(r_\iota(i), d_{\min}^2)] \leq g(\mathbb{E}[r_\iota(i)], d_{\min}^2) \quad (3.29)$$

Without loss of generality, we study the ratio $r_1(j)$ in the event Θ_1 then derive similarly for Θ_2 and Θ_3 . As assumed above that $r_1(i)$ and d_{\min}^2 are independent, we obtain

$$\mathbb{E}[r_1(i)] \approx \frac{\mathbb{E}[|\mathbf{I}_1(i)|^2]}{\mathbb{E}[d_{\min}^2]}. \quad (3.30)$$

We can observe in the Figure 3.3 that the value of two sides in the equation (3.30) are always equivalent. This figure is obtained numerically by generating a huge number of data then analyzing statistically them.

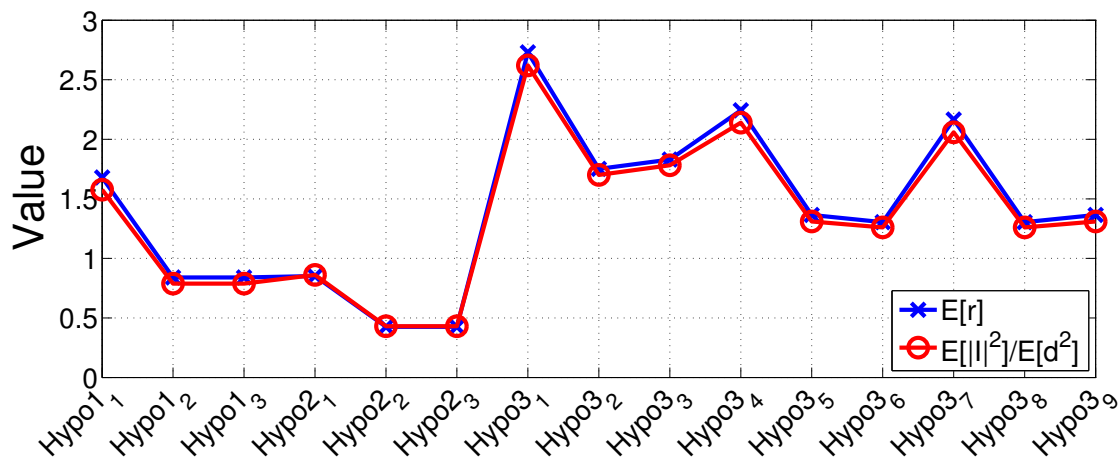


Figure 3.3: Close values of the expectations in different hypothesis.

Due to the fact that $\mathbf{G}^T \mathbf{G} = \mathbf{I}_2$, and $|s_0|^2 = |s_1|^2 = 1$, the ratio $r_1(i)$ becomes

$$\mathbb{E}[r_1(i)] \approx \frac{|a_i - 1|^2 \mathbb{E}[|f_{21}|^2 (|h_{12}|^2 + |h_{22}|^2)]}{\mathbb{E}[d_{\min}^2]}. \quad (3.31)$$

Applying the Cauchy-Schwarz inequality [94] for the numerator in the equation (3.32) leads to:

$$\mathbb{E}[r_1(i)] \leq \frac{|a_i - 1|^2 \sqrt{\mathbb{E}[|f_{21}|^4] \mathbb{E}[(|h_{12}|^2 + |h_{22}|^2)^2]}}{\mathbb{E}[d_{\min}^2]}. \quad (3.32)$$

Since, the channel is supposed to be Rayleigh fading, we can easily obtain the value $\mathbb{E}\{|h_{12}|^2 + |h_{22}|^2\} = 6$. Then the expectation value of $r_1(i)$ is bounded as

$$\mathbb{E}[r_1(i)] \leq \frac{|a_i - 1|^2 \sqrt{6 \mathbb{E}[|f_{21}|^4]}}{\mathbb{E}[d_{\min}^2]}. \quad (3.33)$$

Similarly, results for hypothesis Θ_2 and Θ_3 are respectively:

$$\mathbb{E}[r_2(i)] \leq \frac{|a_i - 1|^2 \sqrt{6 \mathbb{E}[|f_{22}|^4]}}{\mathbb{E}[d_{\min}^2]}, \quad (3.34)$$

$$\mathbb{E}[r_3(i, z)] \leq \frac{|a_i - 1|^2 \sqrt{6 \mathbb{E}[|f_{21}|^4]} + |a_z - 1|^2 \sqrt{6 \mathbb{E}[|f_{22}|^4]}}{\mathbb{E}[d_{\min}^2]}. \quad (3.35)$$

From the study in [73], the expectation value of d_{\min}^2 can be calculated theoretically. The value of $\mathbb{E}[|f_{21}|^4]$, $\mathbb{E}[|f_{22}|^4]$ is provided in the Appendix A, for both two forms of precoder.

Finally, the average probability of the max- d_{\min} and its two forms can be upper-bounded by:

$$\begin{aligned} \tilde{P}\{\Theta_\iota, a_i\} &\leq \int_0^\infty g(\mathbb{E}\{r_\iota^{r_1}(i)\}, d_{\min}^2) f_{d_{\min}^2}^{r_1}(d_{\min}^2) \partial d_{\min}^2 \\ &\quad + \int_0^\infty g(\mathbb{E}\{r_\iota^{octa}(i)\}, d_{\min}^2) f_{d_{\min}^2}^{octa}(d_{\min}^2) \partial d_{\min}^2. \end{aligned} \quad (3.36)$$

3.3.6.1 Solution 2: Estimate the pdf

The upper bound, mentioned above, dresses out the dependence of the interference on the d_{\min} by a constant. However, in practice, this dependence varies in a certain interval. Setting $r_\iota(i) = \frac{\|L_1(i)\|^2}{d_{\min}^2}$, we aim to investigate this ratio in three hypothesis, proposed in previous subsections.

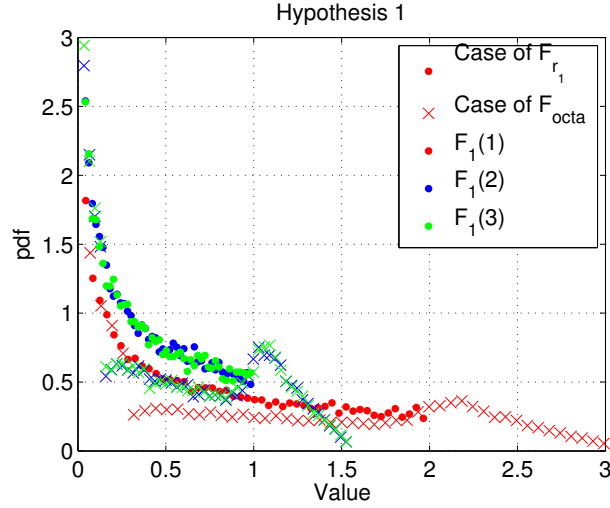


Figure 3.4: Distribution of $r_1(i)$ in Hypothesis 1: decoding erroneously the first symbol and correctly the second one

As we can see in figures 3.4, 3.5, 3.6, the values of r_i are not constant, they vary in all three hypothesis. Realizing that finding theoretically the distribution function of the ratio $r_l(i)$ is complicated, therefore we propose to discover the distribution of $r_l(i)$ by a numerical method. That means we generate a big number of data and channels, afterwards we collect all the value of $r_l(i)$ at each single time. With the help of Matlab, we can analyze the histogram of $r_l(i)$ as shown in the figures 3.4, 3.5, 3.6 for the case of hypothesis Θ_1 , Θ_2 , and Θ_3 , respectively. As shown by these figures, the distribution function of the ratio $r_l(i)$ is not simple, especially in the case of the precoder \mathbf{F}_{octa} . Therefore it is really difficult to describe them via a mathematical function. However, this problem can be solved numerically by Matlab.

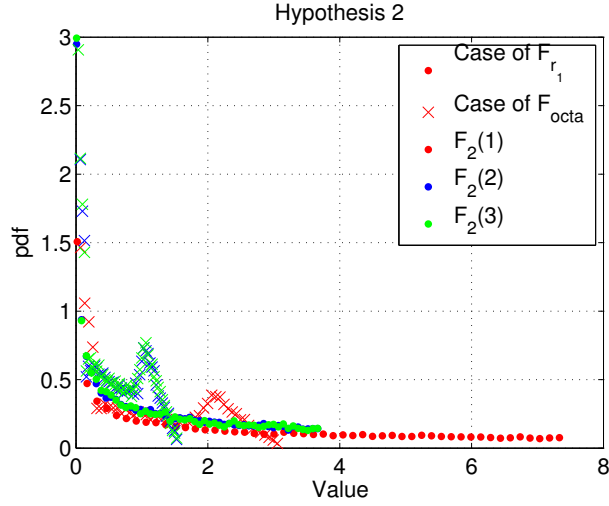


Figure 3.5: Distribution of $r_2(i)$ in Hypothesis 2: correctly decoding the first symbol and erroneously the second one

3.4 Results and discussions

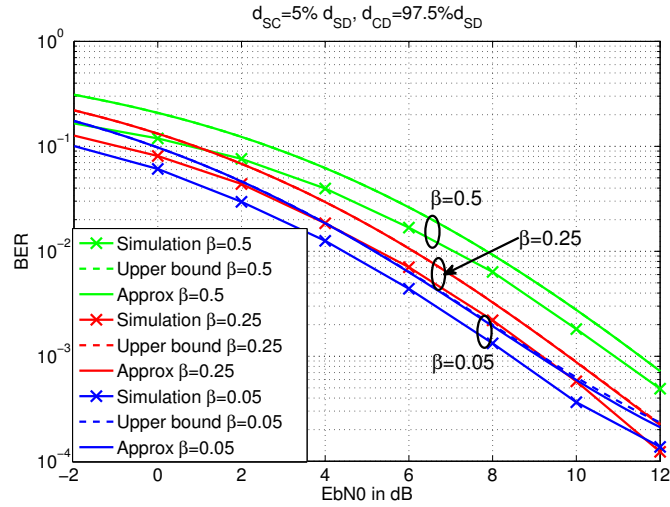


Figure 3.7: BER performance comparison between simulation result, upper bound and interfering estimation method in the configuration of $d_{SC} = 5\%d_{SD}, d_{CD} = 97.5\%d_{SD}$

From the upper bound in the equation (3.36) and the study on the pdf of d_{\min}^2 in [73], we derive the performance in BER of our distributed Decode-and-Forward precoding scheme. As a result, we plot below the performances in 3 configurations: $(d_{SC} = 5\%d_{SD}, d_{CD} = 97.5\%d_{SD})$, $(d_{SC} = 25\%d_{SD}, d_{CD} = 85\%d_{SD})$, and

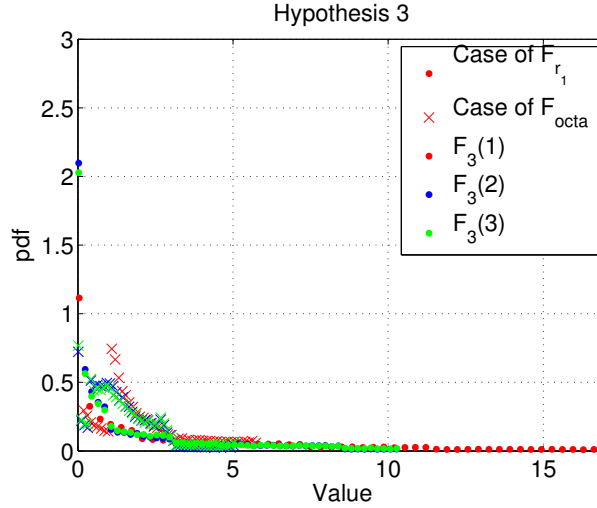


Figure 3.6: Distribution of $r_3(i)$ in Hypothesis 3: decoding erroneously both symbols

($d_{SC} = 50\%d_{SD}$, $d_{CD} = 60\%d_{SD}$) (Figure 3.7, 3.8, 3.9). For each configuration, we select three fixed values of β : 0.05, 0.25, 0.5 to exhibit the performance. In the figures, the curves *Approx* denote the performance using the numerical investigation in section 3.3.6.1 and the equation (3.26). As seen in the figures, in all cases there is always a gap between the closed-form error probability (and upper bound also) and simulation results. The reason that explains this gap could be addressed out from the approximation in [73] where there exists always the difference between the approximation and simulation, especially prominent in the case of 2×2 system. However, the variation in both approaches is totally the same. In other words, the upper bound in (3.23) proposes a good correspondence of the behavior to evaluate our distributed scheme.

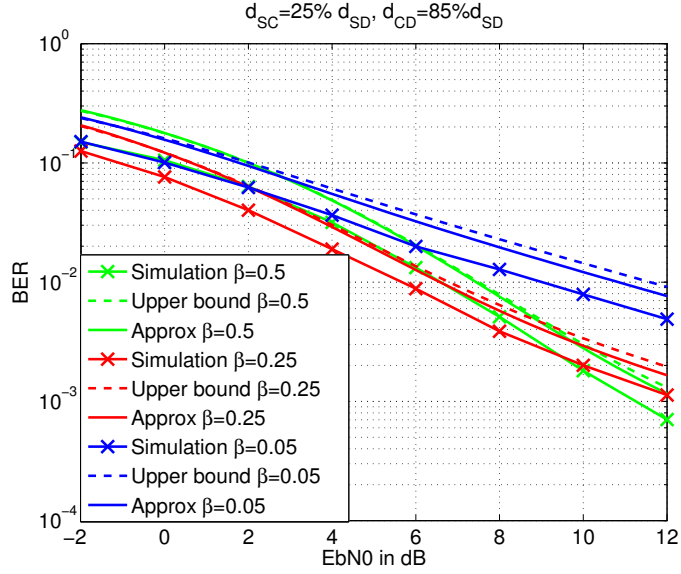


Figure 3.8: BER performance comparison between simulation result, upper bound and interfering estimation method in the configuration of $d_{SC} = 25\%d_{SD}, d_{CD} = 85\%d_{SD}$

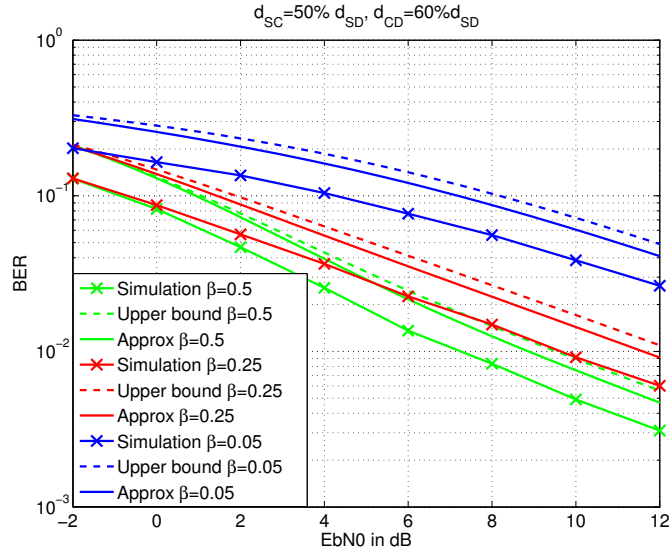


Figure 3.9: BER performance comparison between simulation result, upper bound and interfering estimation method in the configuration of $d_{SC} = 50\%d_{SD}, d_{CD} = 60\%d_{SD}$

Clearly, the performance of our distributed precoding is affected by both phases: local exchange and precoding transmission. Therein, the decoding error probability ϵ at the relay stands for the local exchange phase and the error probability $P\{\hat{\mathbf{s}} \neq$

$s|\Theta_i\}$ stands for for the precoding transmission phase. Our distributed deployment allows a power allocation that pours separately the power for each phase.

In [68], the authors proposed to optimize the power allocation upon a numerical search when a closed-form approximation was not available. For each E_b/N_0 , the simulation of BER for DMP Decode-and-Forward is carried out for many values of β , then we choose among them a value of β that offers the best BER. This work actually takes time and is unpractical if for each system configuration we have to process the numerical search. Subsequently, based on the analysis that we described in the previous section, we would like to optimally allocate the power for each transmission phase in our distributed scheme.

When the closed-form performance of our DMP Decode-and-Forward is derived approximately as above, we would like to optimize the power allocation by choosing the parameter β_0 that minimizes the BER performance. Using the upper bound in equation (3.23) for each hypothesis, we can obtain approximately the performance for every β . Consequently, the optimal power allocation will be easily and rapidly derived. In Figure 3.10, both β_0 obtained by simulation and by this approximation are plotted. As we can see that they are very close together and generally, the β_0 increases with E_b/N_0 . Conclusively, using the theoretical upper bound, derived in the previous section, the power is optimally allocated without difficulty.

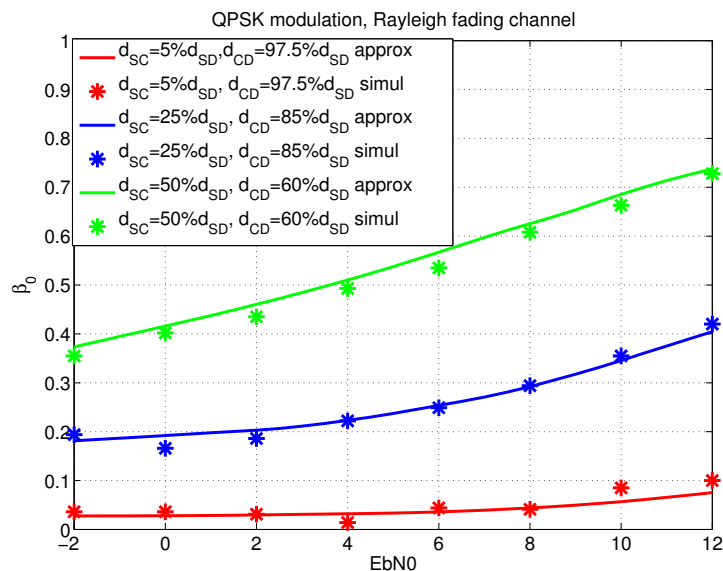


Figure 3.10: Power allocation parameter β_0 for best performance

After obtaining the best power allocation for our DMP-DF, in the Figure 3.11, we plot out the performance comparison between our DMP and conventional schemes such as SISO (Single-input Single-output), MRC (maximum ratio combining), and distributed Alamouti. In this Figure, we study two power allocations: 1) OPA (optimal power allocation) that provide best BER performance corresponding to each value β_0 at each E_b/N_0 ; 2) EPA (equal power allocation) that sets the same power for two phases, meaning $\beta = 0.5$. Comparing two power allocations, the OPA offers about 3 dB in gain with the EPA. In terms of BER, when the cooperative node is close to the source node ($(d_{SC} = 5\%d_{SD}, d_{CD} = 97.5\%d_{SD})$) the DMP with OPA outperforms significantly the SISO and MRC, and proposes a very slight degradation referenced to a colocated precoding system (multiple antennas on the transmitter). As a cooperative scheme, the distributed Alamouti OPA always offers better performance in the same configuration. However, it is important to notice that the spectral efficiency in schemes are different. To transmit 1 symbol, in SISO and MRC, we spend 1 time-slot; the DMP Decode-and-Forward takes 1.5 time-slots; whereas the distributed Alamouti takes 2 (see Figure 3.1b). In addition, on the study

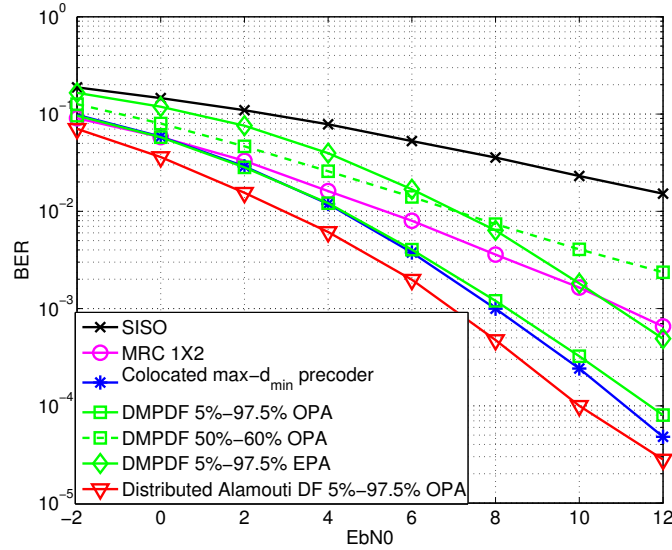


Figure 3.11: DMP vs. conventional schemes

of the relay position impact, we plot in the Figure 3.12, the BER performance in the three configurations above in the case of β_0 (OPA). The results show that closer

relays offer better benefits from the precoding.

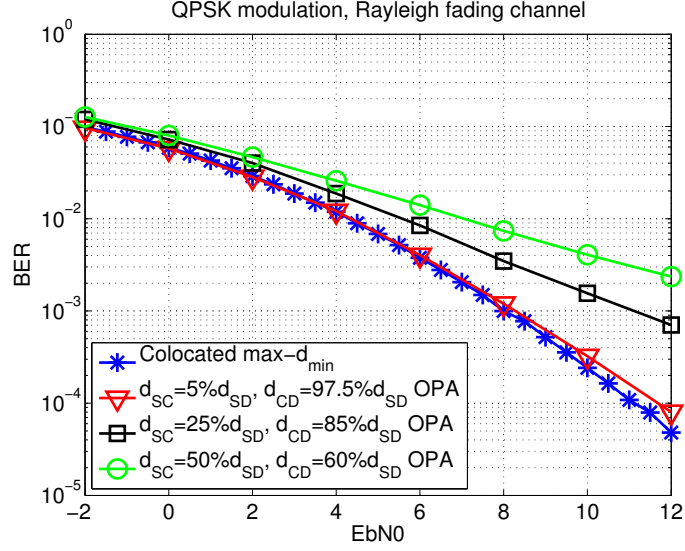


Figure 3.12: Relay position impact on DMP performance

3.5 Decoder design with the side information

If in the training phase between two nodes and the destination before effecting the transmission, the channel between the source and the relay nodes is obtained at the destination. Thereby, the error probability of decoding signal from source node at the relay ϵ could be calculated at the destination by equation (3.8). Since ϵ is available, the probability that we receive the value \mathbf{y} at the destination is decomposed into the four hypothesis mentioned in the previous section as follows

$$P_{\mathbf{y}|\mathbf{H},\epsilon,\mathbf{s}=\mathbf{s}_p} = (1 - \epsilon)^2 P_{\mathbf{y}|\mathbf{H},\epsilon,\Theta_0} + \epsilon(1 - \epsilon) P_{\mathbf{y}|\mathbf{H},\epsilon,\Theta_1} + \epsilon(1 - \epsilon) P_{\mathbf{y}|\mathbf{H},\epsilon,\Theta_2} + \epsilon^2 P_{\mathbf{y}|\mathbf{H},\epsilon,\Theta_3}. \quad (3.37)$$

Since \mathbf{y} is a 2-dimensional complex standard normal vector, the probability $P_{\mathbf{y}|\mathbf{H},\epsilon,\Theta_\iota}$ with $\iota = 0..3$ is derived as

$$P_{\mathbf{y}|\mathbf{H},\epsilon,\Theta_0} = \frac{1}{\pi^2 N_0} e^{-\frac{1}{N_0} |\mathbf{y} - \mathbf{H}_T \mathbf{F}_p \mathbf{s}_p|^2}, \quad (3.38)$$

$$P_{\mathbf{y}|\mathbf{H},\epsilon,\Theta_1} = \frac{1}{\pi^2 N_0 (M - 1)} \sum_{i=1}^{M-1} e^{-\frac{1}{N_0} |\mathbf{y} - \mathbf{H}_T \mathbf{F}_1^{(i)} \mathbf{s}_p|^2}, \quad (3.39)$$

$$P_{\mathbf{y}|\mathbf{H},\epsilon,\Theta_2} = \frac{1}{\pi^2 N_0 (M-1)} \sum_{i=1}^{M-1} e^{-\frac{1}{N_0} |\mathbf{y} - \mathbf{H}_T \mathbf{F}_2(i) \mathbf{s}_p|^2}, \quad (3.40)$$

$$P_{\mathbf{y}|\mathbf{H},\epsilon,\Theta_3} = \frac{1}{\pi^2 N_0 (M-1)^2} \sum_{i=1}^{(M-1)^2} e^{-\frac{1}{N_0} |\mathbf{y} - \mathbf{H}_T \mathbf{F}_3(i,z) \mathbf{s}_p|^2}, \quad (3.41)$$

where $M = 4$ for QPSK modulation. The probability $P_{\mathbf{y}|\mathbf{H},\mathbf{s}=\mathbf{s}_q}$ is derived similarly when we replace \mathbf{s}_p in the equations (3.37), (3.39), (3.40), (3.41) by \mathbf{s}_q . At the destination, a maximum likelihood decoder is utilized to detect the received signal. This means the log-likelihood ratio must be calculated in pairs to determine which point in the constellation is more likely to be transmitted. The LLR is expressed as follows

$$\Lambda_{p,q}^\epsilon = \ln \left(\frac{P_{\mathbf{y}|\mathbf{H},\epsilon,\mathbf{s}=\mathbf{s}_p}}{P_{\mathbf{y}|\mathbf{H},\epsilon,\mathbf{s}=\mathbf{s}_q}} \right) \quad (3.42)$$

$$= \ln \left(\frac{(1-\epsilon)^2 P_{\mathbf{y}|\mathbf{H},\epsilon,\Theta_0} + \epsilon(1-\epsilon)(P_{\mathbf{y}|\mathbf{H},\epsilon,\Theta_1} + P_{\mathbf{y}|\mathbf{H},\epsilon,\Theta_2}) + \epsilon^2 P_{\mathbf{y}|\mathbf{H},\epsilon,\Theta_3}}{(1-\epsilon)^2 P_{\mathbf{y}|\mathbf{H},\epsilon,\Theta_0} + \epsilon(1-\epsilon)(P_{\mathbf{y}|\mathbf{H},\epsilon,\Theta_1} + P_{\mathbf{y}|\mathbf{H},\epsilon,\Theta_2}) + \epsilon^2 P_{\mathbf{y}|\mathbf{H},\epsilon,\Theta_3}} \right). \quad (3.43)$$

Observation: With the consideration of ϵ in equation (3.37), the LLR obtained in (3.43) takes more advantage than the conventional ML for decoding the signal. The performance therefore is surely enhanced. In contrast, as seen in the equation (3.43), the computational complexity is clearly augmented, referencing to a conventional ML. Regarding the significance of the terms in (3.37) we see that in general cases, the value of ϵ is small enough to make the term of $\epsilon^2 P_{\mathbf{y}|\mathbf{H},\epsilon,\mathbf{s}_0 \neq \mathbf{s}_{p0}, \mathbf{s}_1 \neq \mathbf{s}_{p1}}$ insignificant to the others in $P_{\mathbf{y}|\mathbf{H},\mathbf{s}=\mathbf{s}_p}$ of equation (3.37). The proposed decoder now steps to a huge complexity reduction as

$$\Lambda_{p,q}^\epsilon \approx \ln \left(\frac{(1-\epsilon)^2 e^{-\frac{|\mathbf{y} - \mathbf{H}_T \mathbf{F}_p \mathbf{s}_p|^2}{N_0}} + \frac{\epsilon(1-\epsilon)}{M-1} \sum_{i=1}^{M-1} (e^{-\frac{|\mathbf{y} - \mathbf{H}_T \mathbf{F}_1^i \mathbf{s}_p|^2}{N_0}} + e^{-\frac{|\mathbf{y} - \mathbf{H}_T \mathbf{F}_2^i \mathbf{s}_p|^2}{N_0}})}{(1-\epsilon)^2 e^{-\frac{|\mathbf{y} - \mathbf{H}_T \mathbf{F}_p \mathbf{s}_q|^2}{N_0}} + \frac{\epsilon(1-\epsilon)}{M-1} \sum_{i=1}^{M-1} (e^{-\frac{|\mathbf{y} - \mathbf{H}_T \mathbf{F}_1^i \mathbf{s}_q|^2}{N_0}} + e^{-\frac{|\mathbf{y} - \mathbf{H}_T \mathbf{F}_2^i \mathbf{s}_q|^2}{N_0}})} \right). \quad (3.44)$$

Even though (3.44) still seems to be very complicated compared to the conventional ML. In the literature, the max-log approximation is widely used thanks to its substantial simplicity but still maintaining an impressive accuracy [42], [32], [17]:

$$\ln \left(\sum_{i=1}^K \exp(a_i) \right) \approx \max_{i \in \{1,2,\dots,K\}} (a_i). \quad (3.45)$$

Based upon that we can have a simplified ML as below:

$$\Lambda_{p,q}^\epsilon \approx \max_{a_p \in \vartheta_p} (a_p) - \max_{a_q \in \vartheta_q} (a_q), \quad (3.46)$$

where ϑ_p contains $\{\ln(1-\epsilon)^2 - \frac{1}{N_0}|\mathbf{y} - \mathbf{H}_T \mathbf{F} \mathbf{s}_p|^2, \ln(\frac{\epsilon(1-\epsilon)}{M-1}) - \frac{1}{N_0}|\mathbf{y} - \mathbf{H}_T \mathbf{F}_j^i \mathbf{s}_p|^2\}$, with $i = 1, 2, 3$ and $j = 1, 2$. Similarly, we obtain the ϑ_q by replacing \mathbf{s}_q for \mathbf{s}_p .

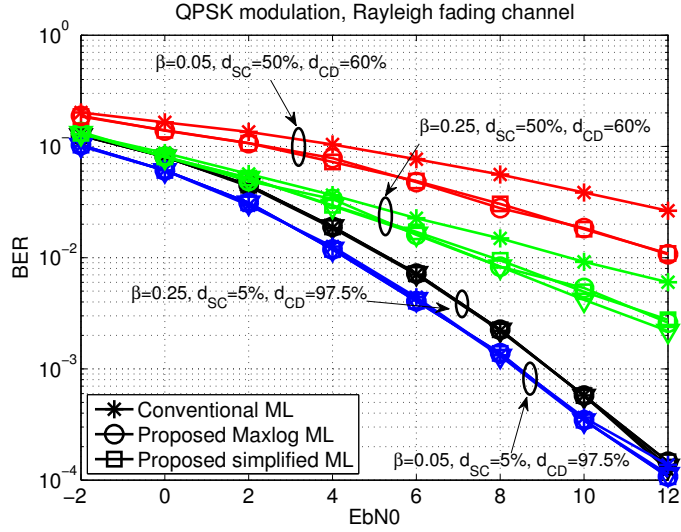


Figure 3.13: Performance comparison between different ML decoders for different values of β

We carry out a DMP Decode and Forward system with two configurations: $d_{SC} = 50\%d_{SD}$, $d_{CD} = 60\%d_{SD}$ and $d_{SC} = 5\%d_{SD}$, $d_{CD} = 97.5\%d_{SD}$. With the use of ϵ in the ML decoder, the performance analysis issue becomes very complicated, thus the closed-form of the error probability is not available for our proposed ML decoder and its simplifications. Therefore, we compare the performance of conventional ML with proposed ML in (3.43) and simplified ML in (3.44) under 2 values of β : 0.05 and 0.25 in Figure 3.13 by simulations. The illustration shows that our proposed MLs only take the advantage when the link between the source and cooperative nodes is weak. In that case, the use of ϵ affects more significantly the detection at the destination. However, our proposed MLs offer a significant improvement as the expense of higher complexity as shown in the Table 3.2. Comparing the proposed full ML and two simplified MLs, there is only a tiny degradation in terms of performance, meanwhile the complexity is reduced notably.

Table 3.2: Complexity comparison between different ML decoder

Numerical computations	Summation	Multiplication	Exponential	Logarithm
Conventional ML	1808	1824	16	15
Full proposed ML	29200	29312	256	15
Simplified ML	12784	12848	112	15
Max-log simplified ML	12658	12883	0	2

3.6 Conclusion

To optimize the life time of a WSN or WBAN, it is always necessary to bring out an energy-efficient transmission strategy. The DMP could be a good candidate which benefits the advantages from the max- d_{\min} precoding. Aiming to confirm the numerical results of DMP-DF claimed in the previous chapter, a theoretical basis is proposed. The performance analysis is not a simple issue in a MIMO precoding system in general, and especially in the distributed system. Our analysis is basically based on the minimum distance evaluation [73], combined with the approximate interfering transformation. From this basis, we derive analytically the upper bound of the error probability then perform the optimal power allocation that provides the best performance of a DMP scenario, managing the power between transmission phases. Moreover, we propose the use of the decoding error information of the relay to enhance the detection performance at the destination. A new ML decoder, which fully exploits this information significantly improves the decoding error rate but suffers from the hyper complexity. Consequently, we simplify it by eliminating some minor terms in the ML detection expression; or by an approximated function. This complexity issue might be solved in the future with an application of a sphere decoder by zoning a group of constellation points around the received point. At

the expense of a higher complexity, the use of our proposed ML decoder takes the advantage for the cases where the separating distance of two nodes is significant.

Besides the decode-and-forward relaying, we mentioned also the amplify-and-forward scheme which provides more flexibility in signal processing as well as more benefit of spectral efficiency. The performance analysis for this structure would be different to the methodology that is studied in this chapter. The next chapter will tackle with this issue.

Chapter 4

Distributed max- d_{\min} precoding: Amplify-and-Forward

4.1 Introduction

In section 2.2.5, the simulations show that the DMP apparently offers the advantage of precoding technique, using the CSIT to enhance the transmission quality. With two possibilities of processing data at the cooperative node: DF and AF, the DF is investigated in the previous chapter. The DMP-AF is already introduced and evaluated numerically in chapter 2. Various scenarios have been considered with different local transmission phases as well as different methods of constructing the precoding matrix (whether taking the local channel into account or not). In terms of performance and energy efficiency, the DMP-AF *Local Precoded Transmission* is the best candidate among them (see figures 2.6, 2.8). In this scheme the spectral efficiency is improved thanks to the transmission of a precoded signal in the local exchange phase. In addition, a custom channel matrix, based on an equivalent transformation of system model, is considered to design the precoding matrix.

Besides the numerical performance evaluation provided in the chapter 2, this chapter presents the performance analysis of the DMP Amplify-and-Forward protocol. The *Local precoded transmission* with the channel customizing scheme is selected due to its higher spectral efficiency and performance. The theoretical performance analysis on the channel capacity and outage probability are carried out, based upon the statistical distribution of minimum Euclidean distance between two received vectors. We also address out the power allocation strategy, defining the power applied to the two phases of the DMP-AF protocol that offers the best channel capacity performance.

Accordingly, we propose the following contributions:

- The probability density function (pdf) of minimum Euclidean distance between two received vectors (d_{\min}) in a DMP Amplify-and-Forward is carried out.
- Thanks to the pdf of d_{\min} we obtain the channel capacity and outage probability analytically.
- The power allocation strategy that maximizes the channel capacity or the outage probability is established.

The rest of this chapter is organized as follows: In Section 4.2, we introduce the distributed precoding in a WBAN. Then the Amplify and Forward scheme is described using the distributed max- d_{\min} precoding. Section 4.3 analyzes the distribution of d_{\min}^2 and based on that, in Section 4.4, the performance analysis on the channel capacity and outage probability is given. Afterward, the power allocation is derived based on the maximization of channel capacity. Section 4.5 concludes the chapter.

4.2 System description

The system is proposed similarly to the DF scheme where the virtual MIMO system is established allowing the precoding to be deployed. The system model is illustrated in Figure 4.1a with a source node, a cooperative node (both equipped with one single antenna) and a station (equipped with two or more antennas). The virtual MIMO system is then formed and the considered distributed precoding is deployed via the cooperative protocol by two transmission phases: local data exchange and precoding transmission as in section 2.2.3 of chapter 2.

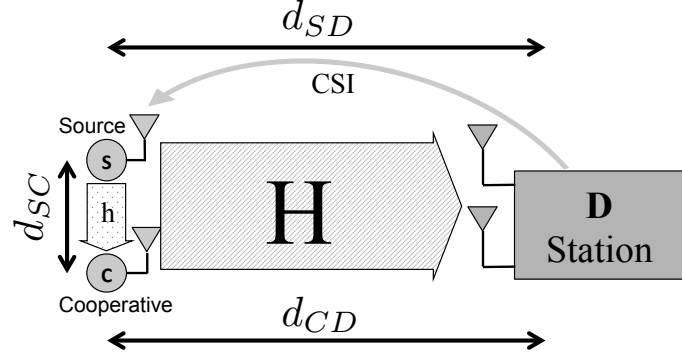
The max- d_{\min} precoding solution is already described in the subsection 3.2.3, and the DMP-AF uses the same principle to design the precoder as the DMP-DF. The difference in the AF scheme is that the system model can be transformed equivalently to obtain a customizing channel matrix containing the local channel. The precoding design will take into account this new channel to generate the precoding matrix.

Let us consider the signal processing in the Amplify-and-Forward scheme. After receiving the signal from the source node, the cooperative node amplifies it with a designed factor and forwards it to the destination. Supposing that $\mathbf{s} = [s_0 \ s_1]^T$ is the vector of symbols from the source node. Since the cooperative node does not decode the incoming signal, a precoded data that combines two symbols can be expressed as

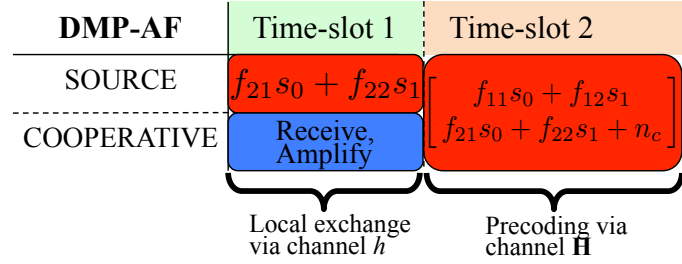
$$s_{pre} = f_{21}s_0 + f_{22}s_1. \quad (4.1)$$

Then the cooperative node receives

$$y_c = h\sqrt{2\mathcal{E}_L G_{SC}}s_{pre} + n_c, \quad (4.2)$$



(a) System model with involved distances.



(b) Time resource used in DMP-AF.

Figure 4.1: Distributed scheme description with a source node, a relay node and a destination.

where h and n_c denote the channel between two nodes and the AWGN noise at the cooperative node, respectively. As we can see, thanks to the precoded signal, we save one time slot with respect to the transmission of symbol by symbol. Also for maximizing the spectral efficiency, the system with only one relay is chosen. Actually, the system with more relays can be deployed, however we lose one more time slot for each added relay. This expense diminishes the spectral efficiency, and also means that the energy efficiency is decreased. There is no doubt that with additional relays the error probability is decreased due to the diversity increment. However, more relays mean the consuming energy is increased for the electronic circuit and signal processing. In addition, the network topology will suffer from high complexity when multiple relays exist. Therefore, the system with one relay offers the best compromise of low energy consumption, high spectral efficiency and performance in the WBAN context.

Satisfying the power constraint at the cooperative node, the received signal is

normalized by its power, then re-transmitted to the destination as

$$\begin{aligned} x_c &= \frac{h^*}{|h|^2} \frac{\sqrt{2\mathcal{E}_D G_{CD}}}{\sqrt{2\mathcal{E}_L G_{SC} + N_0}} y_c \\ &= \frac{h^*}{|h|^2} \frac{\sqrt{2\mathcal{E}_D G_{CD}}}{\sqrt{2\mathcal{E}_L G_{SC} + N_{c_0}}} (h\sqrt{2\mathcal{E}_L G_{SC}} s_{pre} + n_c), \end{aligned} \quad (4.3)$$

where N_{c_0} is the noise variance at the cooperative node. If we ignore the synchronization issue, simultaneously the source node transmits:

$$x_s = \sqrt{2\mathcal{E}_D} (f_{11}s_0 + f_{12}s_1). \quad (4.4)$$

Then the destination receives

$$\mathbf{y} = \mathbf{GH} \begin{pmatrix} x_s \\ x_c \end{pmatrix} + \mathbf{Gn}, \quad (4.5)$$

where \mathbf{n} denotes the AWGN vector at the destination. We already assumed in the previous section that the destination is a powerful access point, which is able to embed two or more antennas. Therefore, the channel matrix $\mathbf{H} \in \mathcal{C}^{n_R \times 2}$ is given by

$$\mathbf{H} = \begin{pmatrix} h_{11} & h_{12} \\ h_{21} & h_{22} \\ \dots & \dots \\ h_{n_R 1} & h_{n_R 2} \end{pmatrix}, \text{ where } n_R \text{ is the number of antennas at the destination. The}$$

received signal in (4.5) can be rewritten as

$$\begin{aligned} \mathbf{y} &= \mathbf{GH} \begin{pmatrix} \sqrt{2\mathcal{E}_D} (f_{11}s_0 + f_{12}s_1) \\ gh\sqrt{2\mathcal{E}_L G_{SC}} s_{pre} \end{pmatrix} + \mathbf{G} \begin{pmatrix} h_{12}gn_c \\ h_{22}gn_c \\ \dots \\ h_{n_R 2}gn_c \end{pmatrix} + \mathbf{Gn}, \\ &= \sqrt{2\mathcal{E}_D} \mathbf{GH} \begin{pmatrix} 1 & 0 \\ 0 & w \end{pmatrix} \mathbf{Fs} + \mathbf{G} \begin{pmatrix} h_{12}gn_c \\ h_{22}gn_c \\ \dots \\ h_{n_R 2}gn_c \end{pmatrix} + \mathbf{Gn}. \end{aligned} \quad (4.6)$$

where

$$g = \frac{h^*}{|h|^2} \frac{\sqrt{2\mathcal{E}_D G_{CD}}}{\sqrt{2\mathcal{E}_L G_{SC} + N_{c_0}}}, \quad (4.7)$$

$$w = \sqrt{\frac{2\mathcal{E}_L G_{SC} G_{CD}}{2\mathcal{E}_L G_{SC} + N_0}}. \quad (4.8)$$

In this scheme, we take the channel h into account by a customized channel via an equivalent transformation of the received constellation as above. Then the precoding matrix is designed based on a customized channel matrix involving the contribution of both \mathbf{H} and h as below

$$\mathbf{F} = \max\text{-}d_{\min} \left(\mathbf{H} \begin{pmatrix} 1 & 0 \\ 0 & w \end{pmatrix} \right). \quad (4.9)$$

As mentioned in the chapter 2, the limited feedback is a suitable solution to obtain this precoding matrix at the transmission side.

As mentioned in section 2.2.5, the simulations point out the advantage in BER performance of this distributed scheme in comparison with the conventional point-to-point system (SISO, MRC). Additionally, with respect to DMP-DF and the DMP-AF *Local successive transmission*, it reduces the transmission time by one time slot by allowing the transmission of two symbols simultaneously, but still proposes the same performance. Subsequently, it achieves the best energy efficiency among the DMPs. Obviously, the theoretical basis is indispensable besides this numerical result. Thus, the performance analysis will be mentioned in the next section.

4.3 Euclidean distance distribution analysis

In general, the performance analysis for a precoding system is not a simple issue. Particularly for the considered max- d_{\min} precoding, the complication comes from two forms of precoder \mathbf{F}_{r1} and \mathbf{F}_{octa} that are present in its design. Moreover, because of its distributed version, the appearance of an alternative local phase sophisticates the theoretical study on the performance substantially. In the detection's point of view, the d_{\min} shows out how far the received points are separated in the constellation. Hence, once the statistical property of d_{\min} is achieved, the system performance can be derived afterwards. To tackle with this issue, the study on the minimum Euclidean distance (d_{\min}) is proposed to be investigated [73]. In this section, we aim to derive the probability density function of d_{\min} and based upon that some

evaluations such as ergodic capacity, outage probability could be established. We continue with the equivalent system model given in (4.6):

$$\mathbf{y} = \sqrt{2\mathcal{E}_D}\mathbf{H}_v\mathbf{F}_d\mathbf{s} + \mathbf{G} \left(\begin{pmatrix} h_{12}gn_c \\ h_{22}gn_c \\ \dots \\ h_{n_R2}gn_c \end{pmatrix} + \mathbf{n} \right), \quad (4.10)$$

where $\mathbf{H}_v = \mathbf{G}_v\mathbf{H} \begin{pmatrix} 1 & 0 \\ 0 & w \end{pmatrix} \mathbf{F}_v = \text{diag}(\sigma_1, \sigma_2)$, and σ_1, σ_2 are the eigenvalues in decreasing order of the equivalent channel matrix $\mathbf{H}_{eq} = \mathbf{H} \begin{pmatrix} 1 & 0 \\ 0 & w \end{pmatrix}$, and $\mathbf{F} = \mathbf{F}_v\mathbf{F}_d$. They can be rewritten as

$$\begin{cases} \sigma_1 = \rho \cos \gamma \\ \sigma_2 = \rho \sin \gamma \end{cases} \leftrightarrow \begin{cases} \gamma = \text{atan}(\frac{\sigma_2}{\sigma_1}) \\ \rho = \sqrt{\sigma_1^2 + \sigma_2^2} \end{cases} \quad (4.11)$$

The minimum Euclidean distance between signal points at the reception side is defined as

$$d_{\min}^2(\mathbf{F}_d) = \min_{\mathbf{s}_k, \mathbf{s}_l \in \mathcal{S}, \mathbf{s}_k \neq \mathbf{s}_l} \|\mathbf{H}_v\mathbf{F}_d(\mathbf{s}_k - \mathbf{s}_l)\|^2, \quad (4.12)$$

where \mathcal{S} denotes the constellation of the transmitted vectors. From [16], d_{\min} can be derived for the Amplify and Forward as

$$\begin{cases} d_{\min}^2(\mathbf{F}_{r1}) = \frac{4}{\sqrt{3+3}}\mathcal{E}_D\rho^2 \cos^2 \gamma \\ d_{\min}^2(\mathbf{F}_{octa}) = 4(2 - \sqrt{2})\mathcal{E}_D\rho^2 \frac{\cos^2 \gamma \sin^2 \gamma}{1+(2-2\sqrt{2})\cos^2 \gamma} \end{cases} \quad (4.13)$$

We propose the variable substitution:

$$\begin{cases} \Gamma = \lambda_1 + \lambda_2 = \rho^2 \\ \Omega = \frac{\lambda_1 - \lambda_2}{\lambda_1 + \lambda_2} = \cos 2\gamma \end{cases}, \quad (4.14)$$

where $\lambda_1 = \sigma_1^2, \lambda_2 = \sigma_2^2$ are the eigenvalues of the matrix $\mathbf{Z} = \left(\mathbf{H} \begin{pmatrix} 1 & 0 \\ 0 & w \end{pmatrix} \right)^\dagger \times \mathbf{H} \begin{pmatrix} 1 & 0 \\ 0 & w \end{pmatrix}$. The shortened square distance then is expressed as

$$d_{\min}^2 = \alpha\Gamma\delta(\Omega), \quad (4.15)$$

where

$$\begin{cases} \alpha = \alpha_{r_1} = \frac{\mathcal{E}_D}{\sqrt{3+3}}, & \delta(\Omega) = \delta_{r_1}(\Omega) = 1 + \Omega & \text{for } \mathbf{F}_{r_1}, \\ \alpha = \alpha_{octa} = \mathcal{E}_D, & \delta(\Omega) = \delta_{octa}(\Omega) = \frac{1-\Omega^2}{2-\sqrt{2}\Omega} & \text{for } \mathbf{F}_{octa}. \end{cases} \quad (4.16)$$

Our analysis obviously requires the joint pdf of Γ and Ω to derive the pdf of d_{\min}^2 . However, at first we need to find out the joint pdf of the eigenvalues λ_1, λ_2 of the customized matrix \mathbf{Z} . Since \mathbf{H} is supposed to be an uncorrelated normalized Rayleigh fading channel, its entries are the complex normal distribution random variables $\mathcal{CN}(0, 1)$. We consider the equivalent channel $\mathbf{H}_{eq} = \mathbf{H} \begin{pmatrix} 1 & 0 \\ 0 & w \end{pmatrix}$ as a correlated channel at the reception side. As a result, the joint pdf of the eigenvalues $\lambda = [\lambda_1, \lambda_2]$ of $\mathbf{Z} = \mathbf{H}_{eq}^\dagger \mathbf{H}_{eq}$ is derived as [14]:

$$f_{\lambda_1, \lambda_2}(\lambda) = K(w) \cdot |U(\lambda, w)| \cdot |V(\lambda)| \cdot \prod_{i=1}^2 \lambda_i^{n_R-2}, \quad (4.17)$$

where

$$K = \frac{w^{-2n_R+2}}{(w^2-1)(n_R-1)!(n_R-2)!}, \quad (4.18)$$

$$U(\lambda, w) = \begin{pmatrix} e^{-\lambda_1} & e^{-\lambda_2} \\ \frac{e^{-\lambda_1}}{w^2} & \frac{e^{-\lambda_2}}{w^2} \end{pmatrix}, \quad (4.19)$$

$$V(\lambda) = \begin{pmatrix} 1 & 1 \\ \lambda_1 & \lambda_2 \end{pmatrix}. \quad (4.20)$$

Then the joint pdf of the two eigenvalues is written as

$$f_{\lambda_1, \lambda_2}(\lambda_1, \lambda_2) = \frac{w^{-2n_R+2}(\lambda_1 - \lambda_2)\lambda_1^{n_R-2}\lambda_2^{n_R-2}}{(w^2-1)(n_R-1)!(n_R-2)!} \left(e^{-(\lambda_2 + \frac{\lambda_1}{w^2})} - e^{-(\lambda_1 + \frac{\lambda_2}{w^2})} \right). \quad (4.21)$$

Since the joint pdf of λ_1 and λ_2 is available, we apply the change of variable rule

$$\begin{cases} \lambda_1 = \Gamma \frac{1+\Omega}{2} \\ \lambda_2 = \Gamma \frac{1-\Omega}{2} \end{cases}, \quad (4.22)$$

to find out the joint pdf of Γ and Ω as

$$f_{\Gamma, \Omega}(\Gamma, \Omega) = f_{\lambda_1, \lambda_2} \left(\Gamma \frac{1+\Omega}{2}, \Gamma \frac{1-\Omega}{2} \right) \times \frac{\Gamma}{2} = \frac{w^{-2n_R+2} \Gamma^{2n_R-2} \Omega (1-\Omega^2)^{n_R-2}}{2^{2n_R-3} (w^2-1)(n_R-1)!(n_R-2)!} \times \left(e^{-\frac{\Gamma}{2} \frac{(1-\Omega)w^2+1+\Omega}{w^2}} - e^{-\frac{\Gamma}{2} \frac{(1+\Omega)w^2+1-\Omega}{w^2}} \right). \quad (4.23)$$

Afterward, it is necessary to derive the pdf of d_{\min}^2 by applying the substitution in (4.15):

$$\Gamma = \frac{d_{\min}^2}{\alpha\delta(\Omega)}, \quad (4.24)$$

then obtaining

$$f_{d_{\min}^2, \Omega}(d_{\min}^2, \Omega) = \Upsilon(\Omega, \mathcal{E}_D, w, n_R, d_{\min}^2) \times \left(e^{-\frac{d_{\min}^2}{2\alpha\delta(\Omega)} \frac{(1-\Omega)w^2+1+\Omega}{w^2}} - e^{-\frac{d_{\min}^2}{2\alpha\delta(\Omega)} \frac{(1+\Omega)w^2+1-\Omega}{w^2}} \right). \quad (4.25)$$

where

$$\Upsilon(\Omega, \mathcal{E}_D, w, n_R, d_{\min}^2) = \frac{w^{-2n_R+2}\Omega(1-\Omega^2)^{n_R-2}(d_{\min}^2)^{2n_R-2}}{2^{2n_R-3}(w^2-1)(n_R-1)!(n_R-2)!(\alpha\delta(\Omega))^{2n_R-1}} \quad (4.26)$$

Notice that our precoding scheme proceeds two structures \mathbf{F}_{r_1} and \mathbf{F}_{octa} corresponding to two intervals of Ω , therefore the pdf function in (4.25) must be studied separately for the two cases.

From (4.25), the pdf of d_{\min}^2 is expressed as

$$f_{d_{\min}^2}(d_{\min}^2) = \int_{\mathcal{D}_\Omega} f_{d_{\min}^2, \Omega}(d_{\min}^2, \Omega) d\Omega, \quad (4.27)$$

where \mathcal{D}_Ω denotes the integrating domain of Ω for each precoder. The threshold Ω_0 that separates two domains has to be determined. Thus, based on the threshold γ_0 and the equation (4.14): Ω_0 is equal to $\cos(2\gamma_0)$, the precoder \mathbf{F}_{r_1} takes $\Omega_0 \leq \Omega \leq 1$ and the precoder \mathbf{F}_{octa} takes $0 \leq \Omega \leq \Omega_0$. The pdf of d_{\min}^2 is finally expressed as

$$f_{d_{\min}^2}(d_{\min}^2) = \int_0^{\Omega_0} f_{d_{\min}^2, \Omega}(d_{\min}^2, \delta_{octa}(\Omega), \alpha_{octa}) d\Omega + \int_{\Omega_0}^1 f_{d_{\min}^2, \Omega}(d_{\min}^2, \delta_{r_1}(\Omega), \alpha_{r_1}) d\Omega. \quad (4.28)$$

In order to derive the final expression of the pdf of d_{\min}^2 , it is necessary to integrate of the function $f_{d_{\min}^2, \Omega}$ with respect to Ω in each interval corresponding to each precoder \mathbf{F}_{r_1} or \mathbf{F}_{octa} . The expression of $f_{d_{\min}^2, \Omega}$ is effectively different for the two precoders \mathbf{F}_{r_1} and \mathbf{F}_{octa} due to the difference of $\delta(\Omega)$ and α in each precoder. We propose to resolve the integrals separately.

4.3.1 The case of \mathbf{F}_{r_1}

According to (4.16), $\alpha_{r_1} = \frac{\mathcal{E}_D}{\sqrt{3+3}}$, $\delta_{r_1}(\Omega) = 1 + \Omega$. Then the joint pdf of d_{\min}^2 and Ω for \mathbf{F}_{r_1} is rewritten as

$$f_{d_{\min}^2, \Omega}^{r_1}(d_{\min}^2, \Omega) = A \frac{(d_{\min}^2)^{2n_R-2} \Omega (1 - \Omega^2)^{n_R-2}}{\alpha_{r_1}^{2n_R-1} (1 + \Omega)^{2n_R-1}} \times \left(e^{-\frac{d_{\min}^2}{2\alpha_{r_1} w^2} \frac{(1-\Omega)w^2+1+\Omega}{1+\Omega}} - e^{-\frac{d_{\min}^2}{2\alpha_{r_1} w^2} \frac{(1+\Omega)w^2+1-\Omega}{1+\Omega}} \right), \quad (4.29)$$

where $A = \frac{w^{-2n_R+2}}{2^{2n_R-3}(w^2-1)(n_R-1)!(n_R-2)!}$. Then the pdf of d_{\min}^2 is calculated by:

$$f_{d_{\min}^2}^{r_1}(d_{\min}^2) = \int_{\Omega_0}^1 A \frac{(d_{\min}^2)^{2n_R-2} \Omega (1 - \Omega^2)^{n_R-2}}{\alpha_{r_1}^{2n_R-1} (1 + \Omega)^{2n_R-1}} \times \left(e^{-\frac{d_{\min}^2}{2\alpha_{r_1} w^2} \frac{1-\Omega}{1+\Omega} w^2} e^{-\frac{d_{\min}^2}{2\alpha_{r_1} w^2}} - e^{-\frac{d_{\min}^2}{2\alpha_{r_1} w^2} \frac{1-\Omega}{1+\Omega}} e^{-\frac{d_{\min}^2 w^2}{2\alpha_{r_1} w^2}} \right) d\Omega. \quad (4.30)$$

We substitute

$$\begin{cases} t = \frac{1-\Omega}{1+\Omega} \Rightarrow \Omega = \frac{1-t}{1+t} \Rightarrow d\Omega = -\frac{2}{(1+t)^2} dt \\ A_{r_1} = A \frac{(d_{\min}^2)^{2n_R-2}}{\alpha_{r_1}^{2n_R-1}} \\ B_{r_1} = \frac{d_{\min}^2}{2\alpha_{r_1} w^2} \end{cases}. \quad (4.31)$$

The equation (4.30) is rewritten as

$$\begin{aligned} f_{d_{\min}^2}^{r_1}(d_{\min}^2) &= \frac{A_{r_1}}{4} \int_{t_0}^0 t^{n_R-2} (t-1) \left(e^{-B_{r_1} w^2 t} e^{-B_{r_1}} - e^{-B_{r_1} t} e^{-B_{r_1} w^2} \right) dt \\ &= \frac{A_{r_1}}{4} \left(\frac{e^{-B_{r_1}}}{(B_{r_1} w^2)^{n_R-1}} \gamma_{\text{inc}}(n_R-1, B_{r_1} w^2 t_0) \right. \\ &\quad - \frac{e^{-B_{r_1} w^2}}{B_{r_1}^{n_R-1}} \gamma_{\text{inc}}(n_R-1, B_{r_1} t_0) \\ &\quad - \frac{e^{-B_{r_1}}}{(B_{r_1} w^2)^{n_R}} \gamma_{\text{inc}}(n_R, B_{r_1} w^2 t_0) \\ &\quad \left. + \frac{e^{-B_{r_1} w^2}}{B_{r_1}^{n_R}} \gamma_{\text{inc}}(n_R, B_{r_1} t_0) \right), \end{aligned} \quad (4.32)$$

where $t_0 = \frac{1-\Omega_0}{1+\Omega_0}$ and $\gamma_{\text{inc}}(a, x) = \int_0^x t^{a-1} e^{-t} dt$ is the lower incomplete gamma function.

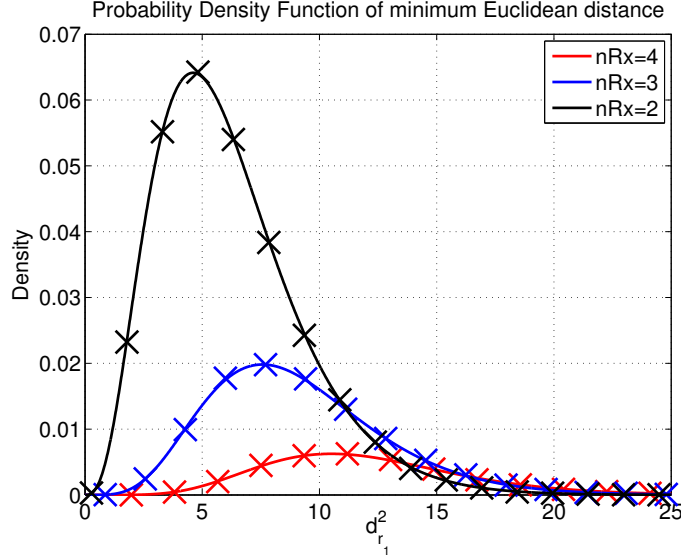


Figure 4.2: The pdf of d_{\min}^2 for \mathbf{F}_{r1} simulation approach vs. theoretical approach. The network is set as $d_{SD} = d_{CD}$, $d_{SC} = 5\%d_{SD}$; $E_b/N_0 = 0dB$; and $\beta = 0.05$. The solid line denotes for theoretical results, the cross mark denotes for simulations

The result in the equation (4.32) would be computed and then compared to the simulation in the figure 4.2. The network configuration is determined as: $d_{SD} = d_{CD}$, and $d_{SC} = 5\%d_{SD}$. The path loss exponent is supposed to be 2.6, and the noise is always normalized (noise variances N_0 and N_{c0} are equal to 1). The power allocation parameter in this evaluation is set to be 0.05. We plot the distribution of d_{\min}^2 in the case of \mathbf{F}_{r1} . The data is taken from two approaches: simulation and analysis (equation (4.32)). As shown in the figure, the theoretical result is totally matching the numerical result in all scenarios of receiver ($nR = 2, 3, 4$).

4.3.2 The case of \mathbf{F}_{octa}

Using the same methodology, we obtain the pdf of d_{\min}^2 of the precoder \mathbf{F}_{octa} by taking substitutions as follows

$$\begin{cases} \alpha_{octa} = \mathcal{E}_D \\ \delta_{octa}(\Omega) = \frac{1-\Omega^2}{2-\sqrt{2}\Omega} \\ A_{octa} = A \frac{(d_{\min}^2)^{2n_R-2}}{\alpha_{octa}^{2n_R-1}} \\ B_{octa} = \frac{d_{\min}^2}{2\alpha_{octa}w^2} \end{cases} \quad (4.33)$$

Hence,

$$f_{d_{\min}^2}^{octa}(d_{\min}^2) = A_{octa} \int_0^{\Omega_0} \frac{\Omega(2 - \sqrt{2}\Omega)^{2n_R-1}}{(1 - \Omega^2)^{n_R+1}} \times \left(e^{-B_{octa} w^2 \frac{2-\sqrt{2}\Omega}{1+\Omega}} - B_{octa} \frac{2-\sqrt{2}\Omega}{1-\Omega} - e^{-B_{octa} w^2 \frac{2-\sqrt{2}\Omega}{1-\Omega}} - B_{octa} \frac{2-\sqrt{2}\Omega}{1+\Omega} \right) d\Omega. \quad (4.34)$$

The solution of the integral in (4.34) is provided in the Appendix B. Accordingly, the matching of the numerical and theoretical result is illustrated in the Figure 4.3. The configuration parameters are set similarly as in the previous case. Furthermore, figures 4.2 and 4.3 also point out the benefit of a larger number of antennas at the receiver to improve d_{\min}^2 , and thus the BER performance

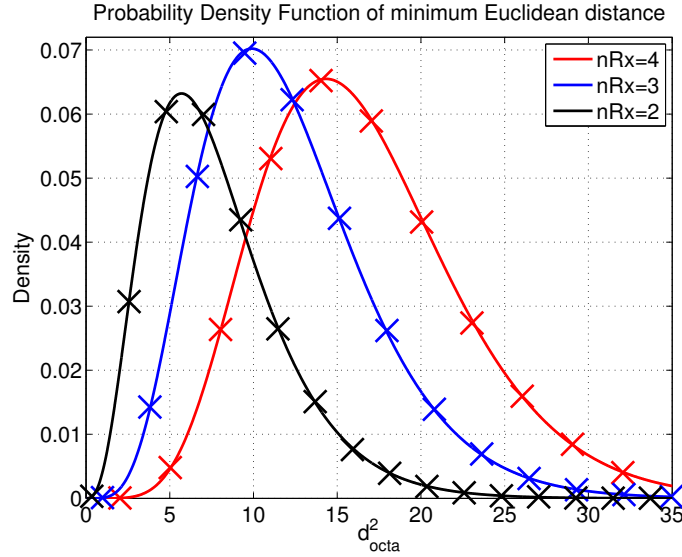


Figure 4.3: The pdf of d_{octa}^2 : simulation vs. theoretical approach. The network is set as $d_{SD} = d_{CD}$, $d_{SC} = 5\%d_{SD}$; $E_b/N_0 = 0dB$; and $\beta = 0.05$. The solid line denotes for approximations, the cross mark denotes for simulations

4.3.3 The complete form of d_{\min}^2

Combining the two forms mentioned in the section 4.3.2 and 4.3.1, the total pdf of d_{\min}^2 in (4.28) is finally calculated as

$$f_{d_{\min}^2}(d_{\min}^2) = f_{d_{\min}^2}^{r1}(d_{\min}^2) + f_{d_{\min}^2}^{octa}(d_{\min}^2). \quad (4.35)$$

In order to confirm the precision of our analysis, we establish a WBAN, described in section 4.2, supposing $d_{SC} = 0.05d_{CD}$, $d_{CD} = d_{SD}$. We compute the pdf of d_{\min}^2 with

multiple values of power allocation parameter β ($\beta = [0.05, 0.25, 0.5]$). Afterwards, the simulations with the same parameters are deployed. We plot in Figures 4.4, 4.5, 4.6 the distribution of d_{\min}^2 obtained by numerical approach and theoretical computation. These figures demonstrate the validity of the theoretical analysis. In addition, with respect to the power allocation, it seems that d_{\min}^2 distributes more beneficially when the parameter β is close to the value $\frac{d_{SC}}{d_{CD}} = 0.05$.

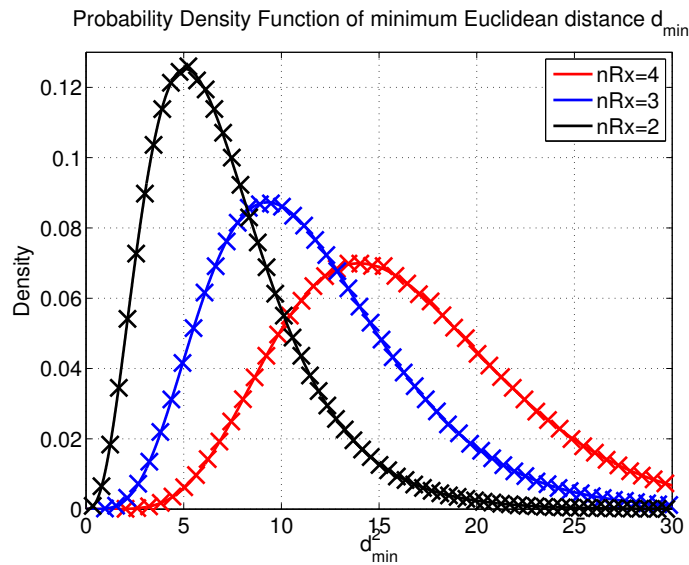


Figure 4.4: The pdf of d_{\min}^2 : theoretical vs. simulation approach. The network is set as $d_{SD} = d_{CD}$, $d_{SC} = 5\%d_{SD}$; $E_b/N_0 = 0dB$; and $\beta = 0.05$. The solid line denotes for approximations, the cross mark denotes for simulations

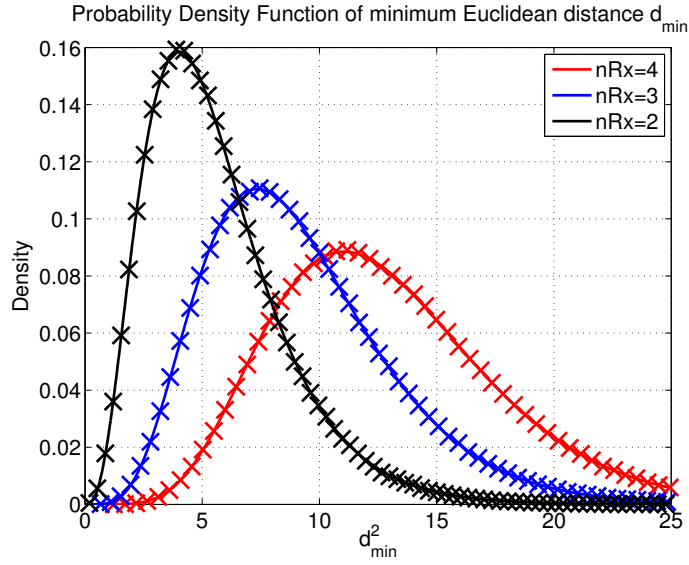


Figure 4.5: The pdf of d_{\min}^2 : theoretical vs. simulation approach. The network is set as $d_{SD} = d_{CD}$, $d_{SC} = 5\%d_{SD}$; $E_b/N_0 = 0dB$; and $\beta = 0.25$. The solid line denotes for approximations, the cross mark denotes for simulations

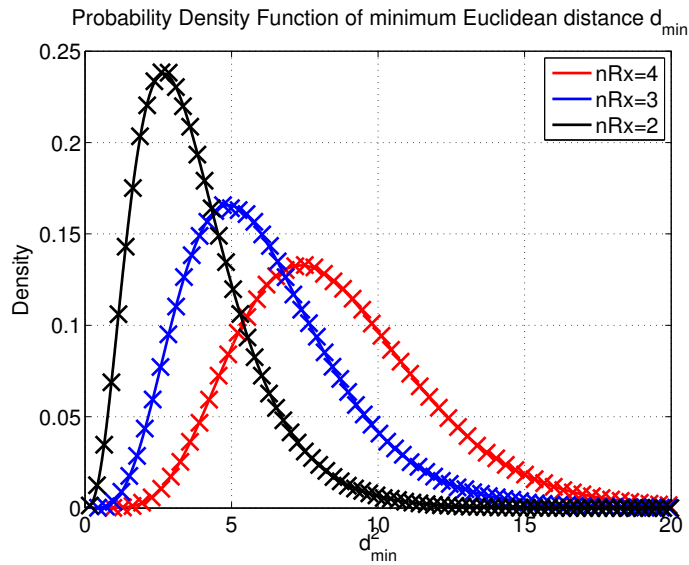


Figure 4.6: The pdf of d_{\min}^2 : theoretical vs. simulation approach. The network is set as $d_{SD} = d_{CD}$, $d_{SC} = 5\%d_{SD}$; $E_b/N_0 = 0dB$; and $\beta = 0.5$. The solid line denotes for approximations, the cross mark denotes for simulations

4.4 Euclidean distance based evaluation

Regardless the noise at the destination, the d_{\min}^2 represents the condition of the received signal, the greater d_{\min}^2 corresponds the better condition. That means when the points in the received constellation are farther apart, the probability of detecting erroneously is lower. Therefore, from the analysis of the distribution of Euclidean distance in the considered distributed scheme, the performance evaluation could be derived. Herein, we propose to apply it on evaluating the ergodic capacity and outage probability. Afterward, a power allocation strategy will be carried out based on the maximization of system ergodic capacity.

4.4.1 Ergodic capacity and power allocation strategy

By separating the points of the received constellation, the goal of the max- d_{\min} precoder is to enhance the system quality, and thereby decrease the power consumption. However, in a distributed scheme, the system model is obviously changed; and in accordance with that, a modified noise appears (see equation (4.6)). Therefore, the system performance is affected by both d_{\min} and modified noise, compared to a collocated system. In this subsection, the ergodic capacity will be studied in function of these both factors. From (4.6), we express the total noise at the destination as

$$\mathbf{n}_{total} = \mathbf{G}_v \left(\begin{pmatrix} h_{12}gn_c \\ h_{22}gn_c \\ \dots \\ h_{n_R2}gn_c \end{pmatrix} + \mathbf{n} \right). \quad (4.36)$$

According to the power constraint, the decoding matrix \mathbf{G}_v must satisfy $\mathbf{G}_v \mathbf{G}_v^H = I_2$ and its entries's norm distributes uniformly [16]. The effective noise becomes more complicated as it is a correlated noise with the covariance matrix expressed as

$$\Sigma_{\mathbf{n}_{total}} = \mathbf{G}_v \left(\begin{array}{cccc} |h_{12}|^2|g|^2 + N_0 & h_{12}h_{22}^*|g|^2 & \dots & h_{12}h_{n_R2}^*|g|^2 \\ h_{12}^*h_{22}|g|^2 & |h_{22}|^2|g|^2 + N_0 & \dots & h_{22}h_{n_R2}^*|g|^2 \\ \dots & \dots & \dots & \dots \\ h_{12}^*h_{n_R2}|g|^2 & h_{22}^*h_{n_R2}|g|^2 & \dots & |h_{n_R2}|^2|g|^2 + N_0 \end{array} \right) \mathbf{G}_v^H. \quad (4.37)$$

Defined as the maximum mutual information, the instantaneous ergodic capacity can be expressed as [45, 87]

$$C = \log_2 \left\| \mathbf{I}_2 + \frac{2\mathcal{E}_D}{n_t} \Sigma_{\mathbf{n}_{total}}^{-1} (\mathbf{H}_v \mathbf{F}_d)^H \mathbf{H}_v \mathbf{F}_d \right\|, \quad (4.38)$$

where n_t denotes the number of transmit antenna, and $\|\cdot\|$ denotes the determinant operation. Applying an eigenvalue decomposition to $\Sigma_{\mathbf{n}_{total}}^{-1}$ and $(\mathbf{H}_v \mathbf{F}_d)^H \mathbf{H}_v \mathbf{F}_d$, the average ergodic capacity can be then derived as

$$\tilde{C} = E[C] = E \left[\log_2 \prod_{i=1}^2 \left(1 + \frac{2\mathcal{E}_D}{n_t} \tau_i v_i \right) \right], \quad (4.39)$$

where τ_i and v_i denote the eigenvalues of $\Sigma_{\mathbf{n}_{total}}^{-1}$ and $(\mathbf{H}_v \mathbf{F}_d)^H \mathbf{H}_v \mathbf{F}_d$ in the decreased order, respectively. In order to finalize the calculation in (4.39), v_i and τ_i are required. Therefore, in the next subsection we compute successively them.

4.4.1.1 The values of v_i

The eigenvalues v_i of $(\mathbf{H}_v \mathbf{F}_d)^H \mathbf{H}_v \mathbf{F}_d$ are different for the two precoders: \mathbf{F}_{r1} and \mathbf{F}_{octa} . Thus, they will be provided separately as follows.

The case of \mathbf{F}_{r1}

We now have

$$\mathbf{H}_v \mathbf{F}_d = \begin{pmatrix} \sigma_1 & 0 \\ 0 & \sigma_2 \end{pmatrix} \begin{pmatrix} \sqrt{\frac{3+\sqrt{3}}{6}} & \sqrt{\frac{3-\sqrt{3}}{6}} e^{i\frac{\pi}{12}} \\ 0 & 0 \end{pmatrix}. \quad (4.40)$$

As a result, the two eigenvalues of matrix $(\mathbf{H}_v \mathbf{F}_d)^H \mathbf{H}_v \mathbf{F}_d$ are expressed in the decreasing order as

$$\begin{cases} v_1 = \sigma_1^2, \\ v_2 = 0 \end{cases}. \quad (4.41)$$

The case of \mathbf{F}_{octa}

The precoding matrix in this case is

$$\mathbf{F}_d = \mathbf{F}_{octa} = \frac{1}{\sqrt{2}} \begin{pmatrix} \cos\psi & 0 \\ 0 & \sin\psi \end{pmatrix} \begin{pmatrix} 1 & e^{i\frac{\pi}{4}} \\ -1 & e^{i\frac{\pi}{4}} \end{pmatrix} \quad (4.42)$$

Consequently, we obtain the two decreasing eigenvalues of $(\mathbf{H}_v \mathbf{F}_d)^H \mathbf{H}_v \mathbf{F}_d$ as

$$\begin{cases} v_1 = \sigma_1^2 \cos^2 \psi, \\ v_2 = \sigma_2^2 \sin^2 \psi \end{cases}. \quad (4.43)$$

4.4.1.2 The values of τ_i

The problem of determining the eigenvalues of matrix $\Sigma_{\mathbf{n}_{total}}^{-1}$ is not a simple question. For instant, we do not have the solution for the general case of n_R . However, in the simplest case, when the destination possesses two antennas (i.e $n_R = 2$), the noise covariance matrix is simply becoming

$$\Sigma_{\mathbf{n}_{total}}^{2 \times 2} = \mathbf{G}_v \begin{pmatrix} |h_{12}|^2 |g|^2 + N_0 & h_{12} h_{22}^* |g|^2 \\ h_{12}^* h_{22} |g|^2 & |h_{22}|^2 |g|^2 + N_0 2 \end{pmatrix} \mathbf{G}_v^H. \quad (4.44)$$

Thus, the eigenvalues of $\Sigma_{\mathbf{n}_{total}}^{-1}$ could be easily determined as

$$\begin{cases} \tau_1 = 1, \\ \tau_2 = \frac{1}{|h_{12}|^2 |g|^2 + |h_{22}|^2 |g|^2 + N_0} \end{cases}. \quad (4.45)$$

After all, the final purpose is to express the capacity in function of d_{\min}^2 then to derive the analytical result of ergodic capacity thanks to the pdf of d_{\min}^2 . Because the values of τ_i are available for the case $n_R = 2$ till now, we propose to study the ergodic capacity for this particular case. The generalization problem will be suggested for the future work. In next parts, we present separately the derivation for the precoder forms, then combine them to obtain the total ergodic capacity.

4.4.1.3 The average ergodic capacity

The case of \mathbf{F}_{r1}

From (4.41) and (4.45) the instantaneous capacity in this case will be derived as follow

$$C_{r1} = \log_2 \left(1 + \frac{2\mathcal{E}_D}{n_t} \sigma_1^2 \right) = \log_2 \left(1 + \frac{\sqrt{3} + 3}{2n_t} d_{\min}^2 \right). \quad (4.46)$$

The case of \mathbf{F}_{octa}

The instantaneous capacity will be derived based on (4.43) and (4.45) as

$$\begin{aligned}
C_{octa} &= \log_2 \left(1 + \frac{2\mathcal{E}_D}{n_t} \sigma_1^2 \cos^2 \psi \right) \left(1 + \frac{2\mathcal{E}_D}{n_t} \frac{\sigma_2^2 \sin^2 \psi}{\Psi} \right) \\
&= \log_2 \left(1 + \frac{2\mathcal{E}_D}{n_t} \left(\sigma_1^2 \cos^2 \psi + \frac{\sigma_2^2 \sin^2 \psi}{\Psi} \right) \right. \\
&\quad \left. + \frac{(2\mathcal{E}_D)^2}{(n_t)^2} \frac{\sigma_1^2 \cos^2 \psi \sigma_2^2 \sin^2 \psi}{\Psi} \right), \tag{4.47}
\end{aligned}$$

where $\Psi = |h_{12}|^2 |g|^2 + |h_{22}|^2 |g|^2 + N_0$. With $\psi = \text{atan}\left(\frac{\sqrt{2}-1}{\tan \gamma}\right)$, we have $\tan \psi = \frac{\sqrt{2}-1}{\tan \gamma}$. Then, we can obtain easily:

$$\begin{cases} \cos^2 \psi = \frac{\tan^2 \gamma}{\tan^2 \gamma + 3 - 2\sqrt{2}} \\ \sin^2 \psi = \frac{3 - 2\sqrt{2}}{\tan^2 \gamma + 3 - 2\sqrt{2}} \end{cases}. \tag{4.48}$$

Hence, the equation (4.47) is rewritten as

$$\begin{aligned}
C_{octa} &= \log_2 \left(1 + \frac{2\mathcal{E}_D}{n_t} \frac{\rho^2 \sin^2 \gamma}{\tan^2 \gamma + 3 - 2\sqrt{2}} \left(1 + \frac{3 - 2\sqrt{2}}{\Psi} \right) \right. \\
&\quad \left. + \left(\frac{2\mathcal{E}_D}{n_t} \frac{\rho^2 \sin^2 \gamma}{\tan^2 \gamma + 3 - 2\sqrt{2}} \right)^2 \frac{3 - 2\sqrt{2}}{\Psi} \right). \tag{4.49}
\end{aligned}$$

And finally, the instantaneous capacity is given by

$$C_{octa} = \log_2 \left(1 + \frac{d_{\min octa}^2}{n_t} \left(\frac{3 - 2\sqrt{2}}{(4 - 2\sqrt{2})\Psi} + \frac{1}{4 - 2\sqrt{2}} \right) + \frac{d_{\min octa}^4}{8n_t^2 \Psi} \right). \tag{4.50}$$

In (4.50), besides the random variable d_{\min}^2 , there is additionally Ψ that varies. Regarding the context of WBAN, where the distance between the two local nodes is effectively small compared to the distance to the external access point, and for an indoor path loss environment then $G_{SC} \gg G_{CD}$. Moreover, all channels are assumed to follow the Rayleigh distribution. Consequently, the variable Ψ in (4.47) could be approximated as a constant as

$$\Psi = |h_{12}|^2 |g|^2 + |h_{22}|^2 |g|^2 + N_0 \approx 2 \frac{2\mathcal{E}_D G_{CD}}{2\mathcal{E}_L G_{SC} + N_{c_0}} + N_0. \tag{4.51}$$

The complete form of ergodic capacity will take into account the two partial capacities above given in (4.46) and (4.50). Finally, the average ergodic capacity

is obtained by integrating the ergodic capacity with respect to the pdf of d_{\min}^2 , representing the statistical channel variations.

$$\begin{aligned} \tilde{C} = & \int_0^\infty \log_2 \left(1 + \frac{\sqrt{3}+3}{2n_t} x \right) f_{d_{\min}^2}^{r1}(x) \partial x + \\ & \int_0^\infty \log_2 \left(1 + \frac{x}{n_t} \left(\frac{3-2\sqrt{2}}{(4-2\sqrt{2})\Psi} + \frac{1}{4-2\sqrt{2}} \right) + \frac{x^2}{8n_t^2\Psi} \right) f_{d_{\min}^2}^{octa}(x) \partial x. \end{aligned} \quad (4.52)$$

4.4.2 Outage probability

In this subsection, we aim to analyze the outage event and the outage probability proposed in [74]. The outage event is defined as the mutual information falls under a predefined rate R , meaning $C < R$. Based on the capacity analysis above, we could derive the outage event separately for the two forms of precoder. Afterwards, the outage probability is established and computed in function of the pdf of d_{\min}^2 .

4.4.2.1 The case of \mathbf{F}_{r1}

The outage event for the spectral efficiency R is defined as

$$C_{r1} = \log_2 \left(1 + \frac{\sqrt{3}+3}{2n_t} d_{\min}^2 \right) < R. \quad (4.53)$$

$$\Leftrightarrow d_{\min}^2 < (2^R - 1) \frac{2n_t}{\sqrt{3}+3}. \quad (4.54)$$

Meaning that the outage probability in this case will be

$$P_{out}^{r1} = P \left\{ d_{\min}^2 < (2^R - 1) \frac{2n_t}{\sqrt{3}+3} \right\} = \int_0^{(2^R-1)\frac{2n_t}{\sqrt{3}+3}} f_{d_{\min}^2}^{r1}(x) \partial x. \quad (4.55)$$

4.4.2.2 The case of \mathbf{F}_{octa}

With the same definition of outage event, we obtain

$$C_{octa} = \log_2 \left(1 + \frac{d_{\min}^2}{n_t} \left(\frac{3-2\sqrt{2}}{(4-2\sqrt{2})\Psi} + \frac{1}{4-2\sqrt{2}} \right) + \frac{d_{\min}^4}{8n_t^2\Psi} \right) < R \quad (4.56)$$

$$\Leftrightarrow a_c d_{\min}^4 + b_c d_{\min}^2 + c_c < 0, \quad (4.57)$$

where

$$\begin{cases} a_c = \frac{1}{8n_t^2\Psi} \\ b_c = \frac{1}{n_t} \left(\frac{3-2\sqrt{2}}{(4-2\sqrt{2})\Psi} + \frac{1}{4-2\sqrt{2}} \right) \\ c_c = 1 - 2^R. \end{cases} \quad (4.58)$$

After resolving the inequality in (4.57), we obtain $d_{\min}^2 < \frac{-b_c + \sqrt{b_c^2 - 4a_c c_c}}{2a_c}$. As a result, the outage probability for this precoder is written as

$$P_{out}^{octa} = P\left\{d_{\min}^2 < \frac{-b_c + \sqrt{b_c^2 - 4a_c c_c}}{2a_c}\right\} = \int_0^{\frac{-b_c + \sqrt{b_c^2 - 4a_c c_c}}{2a_c}} f_{d_{\min}^2}^{octa}(x) \partial x. \quad (4.59)$$

The integrals in (4.55) and (4.59) can be trivially computed since the pdf $f_{d_{\min}^2}^{r1}$ and $f_{d_{\min}^2}^{octa}$ is already provided in the equations (4.32) and (4.34). The total outage probability in a DMP amplify and forward system therefore could be derived as

$$P_{out} = P_{out}^{r1} + P_{out}^{octa}. \quad (4.60)$$

In the considered distributed scheme, the theoretical results do not only evaluate the system performance, but they also help to achieve an efficient power allocation. As mentioned in the chapter 2, the power allocation can be derived by numerical search. In other words, the simulation is carried out for many values of power allocation parameter β then we choose among them the β_0 value that proposes the best system performance, in terms of BER. Herein, since the analytical ergodic capacity and outage probability are now available, we are able to allocate the power w.r.t. these theoretical figures of merit in the next subsection.

4.4.3 Power allocation

The power allocation strategy is aiming to optimize the system performance with respect to a pertinent criterion by dividing the power between the two transmission phases. That means the transmission power could be adapted to the system configuration. For example, when the cooperative node moves closer to the source node, the local phase should be poured less energy, and vice versa. The criterion could be diverse depending on the desired performance such as minimizing of total transmit power, maximizing the network lifetime, maximizing the channel capacity, minimizing the error rate [34, 40, 54, 96, 103]...

4.4.3.1 Capacity based power allocation

In this study, we introduce the power allocation with the objective of obtaining maximum capacity for a certain total transmit power. At this point, the problem

statement can be described as

$$\begin{aligned} & \max_{\beta_0^C} \tilde{C} \\ & \text{subject to } \mathcal{E} = \mathcal{E}_L + \mathcal{E}_D = \text{constant}. \end{aligned} \quad (4.61)$$

The theoretical capacity result given in subsection 4.4.1.3 is used to evaluate the performance of the considered system efficiently, for many values of β from 0 to 1. Then the optimal power allocation β_0^C offering the maximum ergodic capacity is selected.

4.4.3.2 Outage based power allocation

Similarly, this approach optimizes the outage probability, based on the analytical result given in subsection 4.4.2, as follows

$$\begin{aligned} & \min_{\beta_0^{P_{out}}} P_{out} \\ & \text{subject to } \mathcal{E} = \mathcal{E}_L + \mathcal{E}_D = \text{constant}. \end{aligned} \quad (4.62)$$

The $\beta_0^{P_{out}}$ is obtained by choosing, among many values of β , the one that achieves the minimum outage probability, evaluated according to 4.60.

4.4.3.3 Simulation results

In the figure 4.7, we plot the ergodic capacity for the considered DMP-AF. From the analysis of the pdf of d_{\min}^2 in section 4.3, the integral in (4.52) could be numerically computed. For equal power allocation (i.e EPA), the parameter β is equal to 0.5 as defined in section 2.2.1.

In this figure, the comparison between the numerical and theoretical approach is demonstrated. We can see there is only a slight difference between the theoretical ergodic capacity and the simulation result. This slight difference is due to the approximation in the equation (4.51). In addition, we illustrate how beneficial the capacity based optimal power allocation is w.r.t. the EPA case. As we can see, 3 dB of transmit power can be reduced when OPA is carried out.

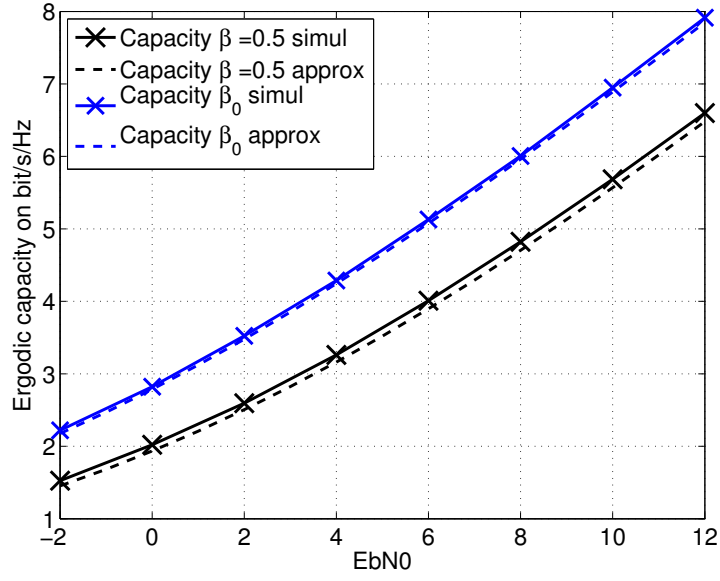


Figure 4.7: The ergodic capacity performances: comparison between the equal and optimal power allocation, $d_{SD} = d_{CD}$, $d_{SC} = 5\%d_{SD}$

We define two rates: $R = 1$ and $R = 2$ then illustrate the outage probability behavior in the Figure 4.8. Herein, we consider also two power allocations: EPA with $\beta = 0.5$ and OPA $\beta_0^{P_{out}}$. As we can see, the outage probability results for the two approaches are totally matching. In addition, this figure points out how benefit the power allocation provides in terms of outage probability. Regarding the OPA, 3 dB is gained w.r.t. EPA to obtain the same outage performance.

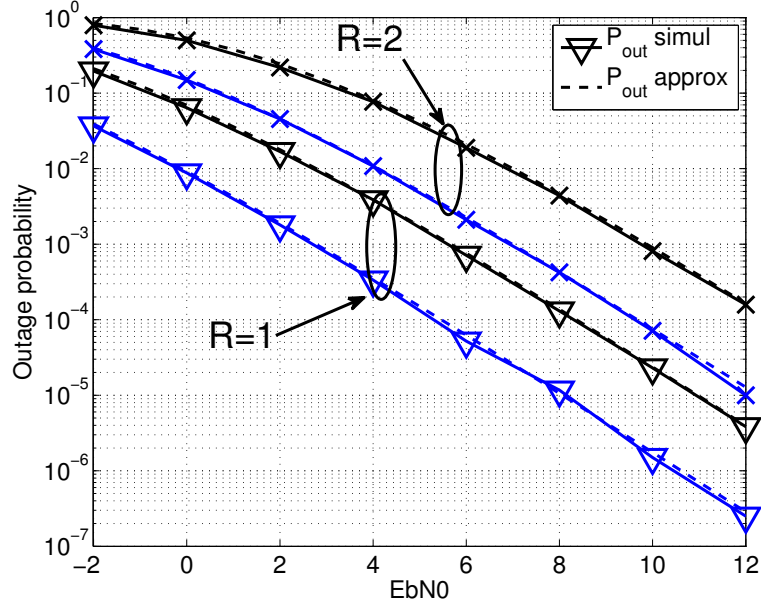


Figure 4.8: The outage probability for simulation and theoretical approximation with $\beta = 0.5$ and two values of threshold $R=1; 2$ bit/s/Hz; the network is set as $d_{SD} = d_{CD}$, $d_{SC} = 5\%d_{SD}$; blue and black color denote for the OPA and EPA, respectively; the solid line with mark denotes the simulation result, and the dash line denotes the theoretical result.

Using the close form of the average capacity in (4.52), and the outage probability in (4.60), the optimization problem can be established rapidly to address out the value of β_0^C , and $\beta_0^{p_{out}}$. In figure 4.9, we plot these values obtained thanks to simulation and theoretical approaches, such that the capacity is maximized and the outage probability is minimized. As seen in this figure, the theoretical results of the optimal power allocation parameter are totally identical in both approaches. However, there is a small difference with the simulated results.

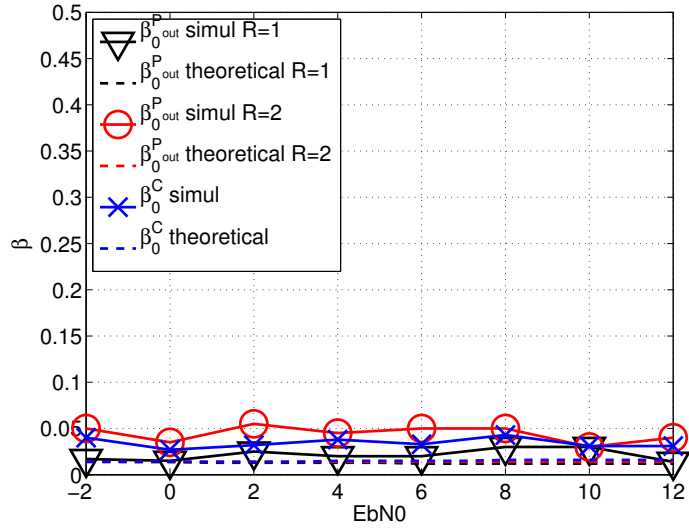


Figure 4.9: Values of β_0 versus E_b/N_0 to obtain the maximum capacity in the context of WBAN: $d_{SD} = d_{CD}$, $d_{SC} = 5\%d_{SD}$

4.5 Conclusion

Thanks to the amplify and forward protocol, the transmitted signal on the local transmission is directly a precoded signal, which is a liner combination of two symbols. By this way, one time slot is reduced, improving the spectral and energy efficiency. In addition, the precoding design is performed thanks to an equivalent transformation of the system model and the local channel is thus taken into account in the precoding matrix. The performance results pointed out the advantage of the DMP-AF in terms of spectral efficiency, and energy consumption with respect to the DMP-DF.

In chapter 2, we evaluated the BER performance of the considered DMP-AF by numerical method. Afterward based on that, the power allocation is computed numerically. To complement the performance evaluation, we propose in this chapter the theoretical study of the performance analysis. We investigate the statistical distribution of the minimum Euclidean distance on the equivalent system model. Based upon that, the ergodic capacity and the outage probability are derived analytically. The results show the judiciousness of our methodology. Considering the

power allocation strategy, we can adopt either the maximum ergodic capacity based approach or the outage probability. The result is that we gain 3 dB in comparison with an equal power allocation system.

Conclusions and future works

The development of high-tech medical health-care and the modernization of personal devices are leading to the intensive growth of WBAN, where the energy constraint is very important. Low-power wireless systems do not only enable long term operation, but also ensure the safety of body tissues. On the other side, the micro electronic technology is more and more reaching a new level, which offers miniature sizes for ultra low power devices. Since the energy consumption on electrical circuit can be coped with, the wireless transmission consumption becomes the most crucial issue to obtain an ultra-low-power system.

Distributed scheme proposition

This thesis takes place within the BoWI project, whose aim is to develop a new generation of WBAN. The wireless communication among the sensor nodes in BoWI is focused, and the most important objective is the design of an ultra-low power consumption system. In such a context, the wireless communication can be decomposed into two categories: intra-BAN and extra-BAN. As far as the extra-BAN is concerned, we proposed the DMP scheme by adopting the minimum Euclidean distance based precoding into the WBAN via cooperation. Two forwarding schemes were considered: Decode-and-Forward and Amplify-and-Forward. Regarding the DMP-AF, we also investigated various configurations based on different local exchanges as well as precoding design. By simulations, we pointed out the out-performance of both DF and AF DMP in terms of error rate. Besides, thanks to the exploitation of spatial multiplexing in the precoding transmission phase, the DMP was shown to offer a gain in spectral efficiency with respect to the cooperative relay or STBC. Especially with the DMP-AF, we even reached the data rate of a non-cooperative transmission.

Energy efficiency investigation

In terms of energy efficiency, we addressed out the comparison among various possibilities including SISO, SIMO, and distributed STBC. Considering the energy consumption, two elements were taken into account: the circuit consumption and the transmit consumption. The transmit consumption is affected firstly by the performance of the considered system, then by the distance separating the source and

destination. Differently, the circuit consumption is determined by the complexity of transmission protocol. For that reason, the SISO transmission takes the advantage according to the highest simplicity. However, assuming a powerful data station without energy constraint at the destination, we also considered the SIMO transmission with the same circuit consumption as SISO transmission. Another factor that affects the consumption is the data rate of the considered scheme, or in other words the spectral efficiency, which defines how fast the data is transmitted for a given scenario. Due to the nature of a point-to-point system, the SISO and SIMO achieve the highest spectral efficiency, whereas this parameter is divided by two in the distributed STBC owing to the two transmission phases. To summarize, the SIMO transmission is the best choice for small distances where the circuit consumption is dominating, meanwhile for medium and slightly high distances, the DMP takes the advantage. For very long distances, where the system requires ultimately a lot of power for the wireless transmission. The distributed STBC, with very good BER performance, consumes less power transmission than the remaining schemes, thereby might be selected.

Performance analysis

We also carried out the performance analysis for both DMP-DF and DMP-AF schemes, and different approaches were adopted for each forwarding technique. For the DMP-DF, we transformed the system to an equivalent interfering system, where the interference appears due to the decoding error event at the cooperative node. Based on that, the error probability at the destination was analyzed according to the distribution of Euclidean distance. However, the interference is the obstacle that prevented us obtaining a closed form for error probability. For this reason, we derived an upper bound which proposes the same behavior as the system BER. This upper bound is mandatory and sufficient not only to evaluate the considered DMP system but also to perform the power allocation, i.e. minimize the error rate by reasonably pouring power among both local exchange phase and precoding transmission phase.

For the DMP-AF, the system model was expressed according to an equivalent

model, incorporating the effects of the local exchange phase. Consequently, the effective channel was established, before the statistical pdf of d_{\min} was computed. Through this analysis, we carry out d_{\min} -based performance evaluations such as ergodic capacity and outage probability. These performance criteria were expressed in function of d_{\min} , then derived theoretically thanks to the available pdf. Another purpose of this work is again to optimally allocate the power resource in the distributed scheme. Herein, we carried out the power allocation strategy based on the capacity maximization and outage probability minimization. The results highlighted the outstanding performance of the optimal power allocation compared to the equal one.

New maximum likelihood decoder with side information

We considered an evolution for the decode-and-forward relaying when side information, namely the probability of erroneously decoding the signal at the cooperative node, is available. This decoding information can be used at the destination in our new ML decoder, where the computation of log-likelihood ratio allows to detect the income signal with less failure probability. However, a full use of this side information affects crucially the receiver complexity. Therefore, a simplification was obviously necessary to obtain a reasonable trade-off between complexity and performance. We suggested two simplifications: neglecting insignificant terms and max-log approximation. The comparisons in terms of BER showed that the side information offers a significant advantage only when the distance between the source and the cooperative node is large enough. Moreover, the max-log ML decoder was shown to achieve performance close to the full proposed ML decoder, while substantially reducing complexity.

Future works

Extension of the DMP

This thesis was proposed in the context of BoWI project, focusing on the cooperative communications for WBAN. If the suggested DMP scheme was therefore investigated

in this context, in our point of view the DMP is a promising cooperative technique for large-scale WSN as well as other communication systems. In a general WSN, we would probably need to study the extension of a DMP system with a larger number of nodes participating at both transmission and reception sides. The system model will undoubtedly be more complex regarding the total channel and noise at the destination. In terms of energy consumption, the circuit consumption will be augmented due to multiple nodes operating. Moreover, the spectral efficiency is also an important factor that one needs to set an eye on. Regarding the DMP-AF, the multiple relays will disable the advantage of *Local Precoded Transmission*, because the precoded signal for each relay is different. Thus, we cannot gain the spectral efficiency when the number of relay is larger than 1.

On the other hand, the extension about the modulation level can be established. Thereby, the performance analysis of DMP-DF will become more complex due to diverse possibilities of error decoding at the relays. However, we can consider fixing the modulation for the local phase as QPSK, and the remaining phase can be adjusted to higher modulation level.

As we can see in both DMP-AF and DMP-DF, after transforming equivalently the system model, we obtain the new noise (DMP-AF) or new interference plus noise (DMP-DF). But in the considered system, these factors were not taken into account for the precoder design. If in the noise whitening step during the design, we take into account the effective noise plus interference, the system performance may be enhanced.

Perspectives on DMP-DF

Regarding the new ML decoder proposed in the context of DMP-DF, the sphere decoding algorithm can be considered as a sub-optimal solution. Unlike the proposed simplifications, this method reduces the complexity by searching inside a sphere covering the received point (Figure 4.10). The trade-off between complexity and performance can be flexibly obtained depending on the considered sphere radius unlike the static one proposed in section 3.5.

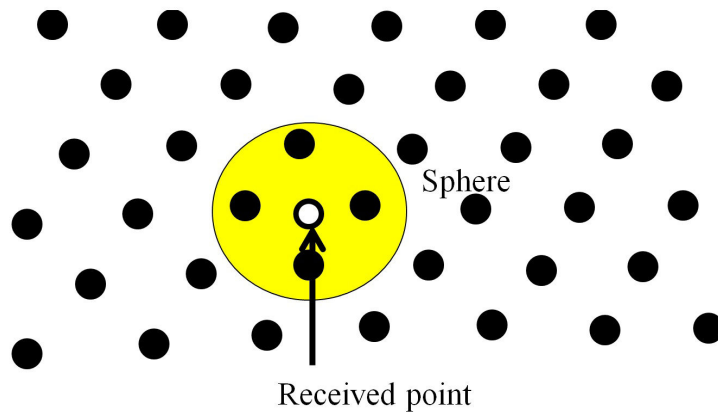


Figure 4.10: Sphere decoding principle

Intra-BAN communication

The intra-BAN communication is not a simple issue due to the channel model of body area network and the body movements that make the network changing randomly. As mentioned in the Chapter 1, some techniques such as intra-body communication, power control, RSSI-based scheduling, etc, can be listed as candidates for enhancing the performance, thereby reducing the energy consumption. In recent years, wake-up radio solutions were achieved and may become the future for the communication in many domains such as WSN, Internet of Things, wearable devices... The main idea is to avoid wasting energy by using a receiver dedicated to sense a wake-up command from the co-ordinator (see Figure 4.11). In WBAN context, the authors in [81], [57] designed a Wake-Up Receiver (WUR) that is capable to trigger the main radio transceiver with a specific address. Besides the constraint on the ultra-low power, the WUR is required to reject false wake up signal (meaning to detect correctly the wake up signal or non wake up signal). The addressing capability is also considered as an important need to obtain the efficiency and flexibility.

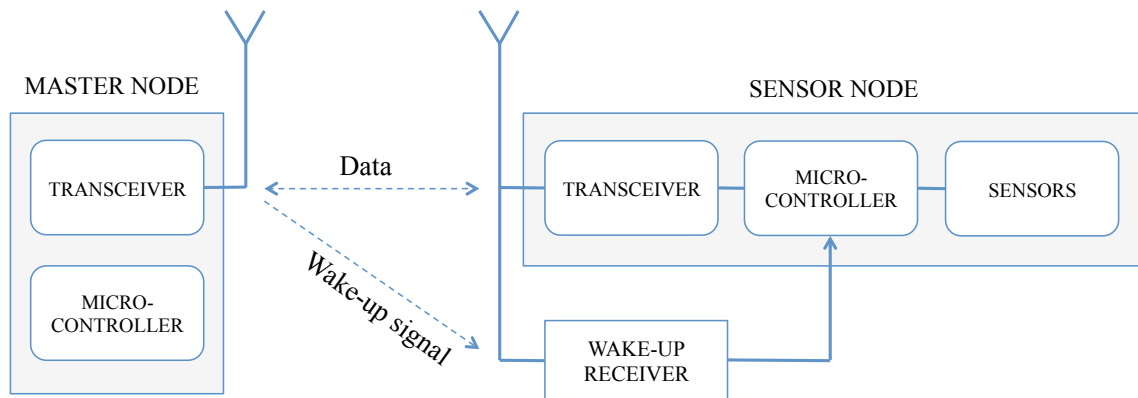


Figure 4.11: Wake Up Radio overview

Regarding the Zyggie prototype (proposed in BoWI project), there are many operating phases: RSSI phase, measuring phase, communicating phase. The prospective wake up radio module would probably wake up not only the main transceiver, but also the other modules such as sensors, RSSI module, Ultra Wideband distance measuring module... Thanks to the WUR, the communication can be performed when the RSSI/LQI reach an advantageous value. The comparison between this work and other energy efficient MAC protocol needs to be investigated in the future.

Appendices

Appendix A

Calculation of $E\{|f_{21}|^4\}$ and $E\{|f_{22}|^4\}$

In order to derive the bound in the equations (3.33), (3.34), (3.35), this appendix carries out the calculation of $E\{|f_{21}|^4\}$ and $E\{|f_{22}|^4\}$ for the two cases of precoder \mathbf{F}_{r_1} and \mathbf{F}_{octa} .

A.1 The case of \mathbf{F}_{r_1}

$$\mathbf{F} = \mathbf{F}_v \mathbf{F}_{r_1} = \begin{pmatrix} f_{v_{11}} & f_{v_{12}} \\ f_{v_{21}} & f_{v_{22}} \end{pmatrix} \begin{pmatrix} \sqrt{\frac{3+\sqrt{3}}{6}} & \sqrt{\frac{3-\sqrt{3}}{6}} e^{i\frac{\pi}{12}} \\ 0 & 0 \end{pmatrix} = \begin{pmatrix} \sqrt{\frac{3+\sqrt{3}}{6}} f_{v_{11}} & \sqrt{\frac{3-\sqrt{3}}{6}} e^{i\frac{\pi}{12}} f_{v_{11}} \\ \sqrt{\frac{3+\sqrt{3}}{6}} f_{v_{21}} & \sqrt{\frac{3-\sqrt{3}}{6}} e^{i\frac{\pi}{12}} f_{v_{21}} \end{pmatrix}. \quad (\text{A.1})$$

Thus, we obtain

$$\begin{cases} f_{21} = \sqrt{\frac{3+\sqrt{3}}{6}} f_{v_{21}} \Rightarrow |f_{21}| = \sqrt{\frac{3+\sqrt{3}}{6}} |f_{v_{21}}| \\ f_{22} = \sqrt{\frac{3-\sqrt{3}}{6}} e^{i\frac{\pi}{12}} f_{v_{21}} \Rightarrow |f_{22}| = \sqrt{\frac{3-\sqrt{3}}{6}} |f_{v_{21}}| \end{cases}. \quad (\text{A.2})$$

To calculate $E_{r_1}\{|f_{21}|^4\}$ and $E_{r_1}\{|f_{22}|^4\}$, it is sufficient to establish the expectation of $|f_{v_{21}}|^4$. Due to the fact that the norm of the entries of \mathbf{F}_v distributes uniformly in $[0, 1]$, the pdf of $|f_{v_{ij}}|^2$ can be expressed as

$$f_{|f_{v_{ij}}|^2}(x) = \begin{cases} 1 & \text{if } 0 \leq x \leq 1 \\ 0 & \text{otherwise.} \end{cases} \quad (\text{A.3})$$

Then the calculation is derived as

$$E\{|f_{v_{ij}}|^4\} = \int_0^1 x^2 \partial x = \frac{x^3}{3} \Big|_0^1 = \frac{1}{3}. \quad (\text{A.4})$$

Finally, the expectation of $E_{r_1}\{|f_{21}|^4\}$ and $E_{r_1}\{|f_{22}|^4\}$ are written as follows

$$\begin{cases} E_{r_1}\{|f_{21}|^4\} = \left(\frac{3+\sqrt{3}}{6}\right)^2 \frac{1}{3} = \frac{2+\sqrt{3}}{18} \\ E_{r_1}\{|f_{22}|^4\} = \left(\frac{3-\sqrt{3}}{6}\right)^2 \frac{1}{3} = \frac{2-\sqrt{3}}{18} \end{cases}. \quad (\text{A.5})$$

A.2 The case of \mathbf{F}_{octa}

$$\begin{aligned} \mathbf{F} &= \mathbf{F}_v \mathbf{F}_{octa} = \frac{1}{\sqrt{2}} \begin{pmatrix} f v_{11} & f v_{12} \\ f v_{21} & f v_{22} \end{pmatrix} \begin{pmatrix} \cos \psi & \cos \psi e^{i\frac{\pi}{4}} \\ -\sin \psi & \sin \psi e^{i\frac{\pi}{4}} \end{pmatrix} \\ &= \frac{1}{\sqrt{2}} \begin{pmatrix} f v_{11} \cos \psi - f v_{12} \sin \psi & f v_{11} \cos \psi e^{i\frac{\pi}{4}} + f v_{12} \sin \psi e^{i\frac{\pi}{4}} \\ f v_{21} \cos \psi - f v_{22} \sin \psi & f v_{21} \cos \psi e^{i\frac{\pi}{4}} + f v_{22} \sin \psi e^{i\frac{\pi}{4}} \end{pmatrix}. \end{aligned} \quad (\text{A.6})$$

In this case, $f_{21} = \frac{1}{\sqrt{2}}(f v_{21} \cos \psi - f v_{22} \sin \psi)$ and $f_{22} = \frac{1}{\sqrt{2}}(f v_{21} \cos \psi e^{i\frac{\pi}{4}} + f v_{22} \sin \psi e^{i\frac{\pi}{4}})$, thus

$$\begin{aligned} |f v_{21}|^2 &= \frac{1}{2} (|f v_{21}|^2 \cos^2 \psi + |f v_{22}|^2 \sin^2 \psi - \sin \psi \cos \psi (f v_{21}^* f v_{22} + f v_{21} f v_{22}^*)) \\ |f v_{22}|^2 &= \frac{1}{2} (|f v_{21}|^2 \cos^2 \psi + |f v_{22}|^2 \sin^2 \psi + \sin \psi \cos \psi (f v_{21}^* f v_{22} + f v_{21} f v_{22}^*)) \end{aligned} \quad (\text{A.7})$$

then we obtain

$$\begin{aligned} |f v_{21}|^4 &= \\ \frac{1}{4} & \left((|f v_{21}|^2 \cos^2 \psi + |f v_{22}|^2 \sin^2 \psi)^2 + \sin^2 \psi \cos^2 \psi (f v_{21}^* f v_{22} + f v_{21} f v_{22}^*)^2 \right. \\ & \left. - 2 \sin \psi \cos \psi (f v_{21}^* f v_{22} + f v_{21} f v_{22}^*) (|f v_{21}|^2 \cos^2 \psi + |f v_{22}|^2 \sin^2 \psi) \right) \\ |f v_{22}|^4 &= \\ \frac{1}{4} & \left((|f v_{21}|^2 \cos^2 \psi + |f v_{22}|^2 \sin^2 \psi)^2 + \sin^2 \psi \cos^2 \psi (f v_{21}^* f v_{22} + f v_{21} f v_{22}^*)^2 \right. \\ & \left. + 2 \sin \psi \cos \psi (f v_{21}^* f v_{22} + f v_{21} f v_{22}^*) (|f v_{21}|^2 \cos^2 \psi + |f v_{22}|^2 \sin^2 \psi) \right). \end{aligned} \quad (\text{A.8})$$

Since the entries of matrix \mathbf{F}_v are independent, therefore $E\{f v_{21}^* f v_{22}\} = E\{f v_{21} f v_{22}^*\} = 0$. Then, the expectation of $|f v_{21}|^4$ is equal to the expectation of $|f v_{22}|^4$ and is ex-

pressed as

$$\begin{aligned}
E_{octa}\{|f_{21}|^4\} &= \frac{1}{4}E\{|fv_{21}|^4 \cos^4 \psi + |fv_{22}|^4 \sin^4 \psi + 2 \sin^2 \psi \cos^2 \psi |fv_{21}|^2 |fv_{22}|^2 \\
&\quad + \sin^2 \psi \cos^2 \psi ((fv_{21}^* fv_{22})^2 + (fv_{21} fv_{22}^*)^2 + 2|fv_{21} fv_{22}|^2)\} \\
&= \frac{1}{4}E\{|fv_{21}|^4 \cos^4 \psi + |fv_{22}|^4 \sin^4 \psi + 4 \sin^2 \psi \cos^2 \psi |fv_{21}|^2 |fv_{22}|^2\}.
\end{aligned} \tag{A.9}$$

The expectation of $|fv_{ij}|^2$ is derived easily as

$$E\{|fv_{ij}|^2\} = \int_0^1 x \partial x = \frac{x^2}{2} \Big|_0^1 = \frac{1}{2}. \tag{A.10}$$

Therefore, the equation (A.9) becomes

$$\begin{aligned}
E_{octa}\{|f_{21}|^4\} &= \frac{1}{4}E\left\{\cos^4 \psi \frac{1}{3} + \sin^4 \psi \frac{1}{3} + 4 \sin^2 \psi \cos^2 \psi \frac{1}{2} \frac{1}{2}\right\} \\
&= \frac{1}{4}E\left\{\frac{1}{3}(\sin^2 \psi + \cos^2 \psi)^2 + \frac{1}{3} \sin^2 \psi \cos^2 \psi\right\} = \frac{1}{12}(1 + E\{\sin^2 \psi \cos^2 \psi\}).
\end{aligned} \tag{A.11}$$

In the next step, we provide the method to calculate the expectation of $\sin^2 \psi \cos^2 \psi$.

Firstly, we have

$$\tan \psi = \frac{\sqrt{2} - 1}{\tan \gamma} \Leftrightarrow \frac{\sin^2 \psi}{\cos^2 \psi} = \frac{3 - 2\sqrt{2}}{\tan^2 \gamma}. \tag{A.12}$$

Easily, we can derive

$$\begin{cases} \cos^2 \psi = \frac{\sin^2 \gamma}{(2-2\sqrt{2}) \cos^2 \gamma + 1} \\ \sin^2 \psi = \frac{(3-2\sqrt{2}) \cos^2 \gamma}{(2-2\sqrt{2}) \cos^2 \gamma + 1} \end{cases}. \tag{A.13}$$

Afterward, the product $\sin^2 \psi \cos^2 \psi$ is determined as

$$\sin^2 \psi \cos^2 \psi = \frac{(3 - 2\sqrt{2}) \sin^2 \gamma \cos^2 \gamma}{((2 - 2\sqrt{2}) \cos^2 \gamma + 1)^2} = \frac{3 - 2\sqrt{2}}{4} \frac{1 - \cos^2 2\gamma}{((1 - \sqrt{2}) \cos 2\gamma + 2 - \sqrt{2})^2} \tag{A.14}$$

$$= \frac{1}{4} \frac{1 - \cos^2 2\gamma}{(\cos 2\gamma - \sqrt{2})^2} \tag{A.15}$$

By definition, we have

$$\begin{cases} \lambda_1 = \rho^2 \cos^2 \gamma \\ \lambda_2 = \rho^2 \sin^2 \gamma, \end{cases} \tag{A.16}$$

where λ_1 and λ_2 are two eigenvalues of matrix $\mathbf{H}\mathbf{H}^\dagger$. Due to this fact, the joint pdf of λ_1 and λ_2 is provided as [36]

$$f_{\lambda_1, \lambda_2}(\lambda_1, \lambda_2) = e^{-(\lambda_1 + \lambda_2)} (\lambda_1 - \lambda_2)^2. \tag{A.17}$$

As shown in the equation (A.15), to derive the expectation of $\sin^2 \psi \cos^2 \psi$ our objective is to determine the distribution law of $\cos 2\gamma$. For this reason, we take the variable substitution as

$$\begin{cases} \Gamma = \lambda_1 + \lambda_2 = \rho^2 \\ \Omega = \frac{\lambda_1 + \lambda_2}{\lambda_1 - \lambda_2} = \cos 2\gamma \end{cases}. \quad (\text{A.18})$$

As a result, we set the joint pdf of Γ and Ω as follows

$$f_{\Gamma, \Omega}(\Gamma, \Omega) = f_{\lambda_1, \lambda_2} \left(\frac{\Gamma}{2}(1 + \Omega), \frac{\Gamma}{2}(1 - \Omega) \right) \times \frac{\Gamma}{2} = \frac{1}{2} \Omega^2 \Gamma^3 e^{-\Gamma}. \quad (\text{A.19})$$

Thus, the probability density function of $\Omega = \cos 2\gamma$ is derived as

$$f_{\Omega}(\Omega) = \int_0^{\infty} \frac{1}{2} \Omega^2 \Gamma^3 e^{-\Gamma} \partial \Gamma = 3\Omega^2. \quad (\text{A.20})$$

We notice that, because $0 \leq \gamma \leq \frac{\pi}{4}$, Ω distributes in the interval $[0 \ 1]$. However, for the case of \mathbf{F}_{octa} , when $\gamma_0 \leq \gamma \leq \frac{\pi}{4}$, therefore $0 \leq \Omega \leq \Omega_0 = \cos 2\gamma_0$ ($\gamma_0 = \text{atan} \left(\sqrt{\frac{\sqrt{2}-1}{\sqrt{2}N^2 + \sqrt{6}N + \sqrt{2}-1}} \right)$, $N = 2^k - 1$). As a result, the density function of Ω particularly in the case of \mathbf{F}_{octa} becomes

$$f_{\Omega_{octa}}(\Omega) = \frac{3\Omega^2}{\int_0^{\Omega_0} 3\Omega^2 \partial \Omega} = \frac{3}{\Omega_0^3} \Omega^2. \quad (\text{A.21})$$

Then the expectation of $\sin^2 \psi \cos^2 \psi$ in the equation (A.15) is expressed as

$$E\{\sin^2 \psi \cos^2 \psi\} = \int_0^{\Omega_0} \frac{1}{4} \frac{1 - \Omega^2}{(\Omega - \sqrt{2})^2} \frac{3\Omega^2}{\Omega_0^3} \partial \Omega. \quad (\text{A.22})$$

Finally, we obtain

$$E_{octa}\{|f_{21}|^4\} = \frac{1}{12} \left(1 + \int_0^{\Omega_0} \frac{1}{4} \frac{1 - \Omega^2}{(\Omega - \sqrt{2})^2} \frac{3\Omega^2}{\Omega_0^3} \partial \Omega \right) = E_{octa}\{|f_{22}|^4\}. \quad (\text{A.23})$$

Appendix B

Proof of pdf of d_{\min}^2 for precoder \mathbf{F}_{octa}

We take the change of variables for the integral in (4.34) as below

$$t = \frac{1 - \Omega}{1 + \Omega} \Rightarrow \Omega = \frac{1 - t}{1 + t} \Rightarrow d\Omega = -\frac{2}{(1 + t)^2} dt, \quad (\text{B.1})$$

we have

$$\begin{cases} \frac{2 - \sqrt{2}\Omega}{1 - \Omega} = \frac{2 - \sqrt{2} + (2 + \sqrt{2})t}{2t} \\ \frac{2 - \sqrt{2}\Omega}{1 + \Omega} = \frac{2 - \sqrt{2} + (2 + \sqrt{2})t}{2} \end{cases}. \quad (\text{B.2})$$

Then, the equation (4.34) can be rewritten as

$$\begin{aligned} f_{d_{\min}^2}^{octa}(d_{\min}^2) = & A_{octa} \int_1^{t_0} \frac{2(t-1)(2 - \sqrt{2} + (2 + \sqrt{2})t)^{2n_R-1}}{(4t)^{n_R+1}} \times \\ & \left(e^{-B(w^2 \frac{2-\sqrt{2}}{2} + \frac{2+\sqrt{2}}{2})} e^{-B(w^2 \frac{2+\sqrt{2}}{2} t + \frac{2-\sqrt{2}}{2t})} \right. \\ & \left. - e^{-B(\frac{2-\sqrt{2}}{2} + w^2 \frac{2+\sqrt{2}}{2})} e^{-B(\frac{2+\sqrt{2}}{2} t + w^2 \frac{2-\sqrt{2}}{2t})} \right) dt. \end{aligned} \quad (\text{B.3})$$

As a result, we can rewrite the pdf of d_{\min}^2 in the case of \mathbf{F}_{octa} as

$$f_{d_{\min}^2}^{octa}(d_{\min}^2) = \frac{2A_{octa}}{4^{n_R+1}} \int_{t_0}^1 \sum_l \mu_l t^l \left(\xi_1 e^{-(a_1 t + \frac{b_1}{t})} - \xi_2 e^{-(a_2 t + \frac{b_2}{t})} \right) dt, \quad (\text{B.4})$$

where

$$\left\{ \begin{array}{l} \sum_l \mu_l t^l = \frac{(t-1)(2-\sqrt{2}+(2+\sqrt{2})t)^{2n_R-1}}{t^{n_R+1}}, \\ \xi_1 = e^{-B(\frac{2-\sqrt{2}}{2}+w^2\frac{2+\sqrt{2}}{2})}, \\ a_1 = B_{\text{octa}}\frac{2+\sqrt{2}}{2}, \\ b_1 = B_{\text{octa}}w^2\frac{2-\sqrt{2}}{2}, \\ \xi_2 = e^{-B_{\text{octa}}(w^2\frac{2-\sqrt{2}}{2}+\frac{2+\sqrt{2}}{2})}, \\ a_2 = B_{\text{octa}}w^2\frac{2+\sqrt{2}}{2}, \\ b_2 = B_{\text{octa}}\frac{2-\sqrt{2}}{2}. \end{array} \right. \quad (\text{B.5})$$

Observing in equation (B.4) that we have the integral form

$$I = \int_{t_0}^1 \sum_l \mu_l t^l e^{-(at+\frac{b}{t})} dt, \quad (\text{B.6})$$

solved in [73], the solution is expressed as

$$\begin{aligned} \int_{t_0}^1 \sum_{-n_R-1}^{n_R-1} \mu_l t^l e^{-(at+\frac{b}{t})} dt &= \left[\sum_{-n_R+1}^{n_R-1} \omega_l t^l e^{-(at+\frac{b}{t})} \right]_{t_0}^1 + \\ &\beta_{K_0} \int_{t_0}^1 e^{-(at+\frac{b}{t})} \frac{1}{t} dt + \beta_{K_1} \int_{t_0}^1 e^{-(at+\frac{b}{t})} \frac{(t^2-1)^2}{4t^3} dt \\ &= \left[\sum_{-n_R+13}^{n_R-1} \omega_l t^l e^{-(at+\frac{b}{t})} \right]_{t_0}^1 + \beta_{K_0} \mathcal{A}_0 + \beta_{K_1} \mathcal{A}_1, \end{aligned} \quad (\text{B.7})$$

where $\mathcal{A}_0 = \int_{t_0}^1 e^{-(at+\frac{b}{t})} \frac{1}{t} dt$, $\mathcal{A}_1 = \int_{t_0}^1 e^{-(at+\frac{b}{t})} \frac{(t^2-1)^2}{4t^3} dt$ are of similar form than zero and first order modified Bessel function of second kind, respectively; and the coefficients ω_l , β_{K_0} , β_{K_1} are determined in [73] as follows:

$$\left\{ \begin{array}{l} \omega_l = \frac{1}{a}(-\mu_l + (l+1)\omega_{l+1} + b\omega_{l+2}) \text{ for } (n_R-1) \geq l \geq 2 \\ \omega_l = \frac{1}{b}(\mu_{l-2} + a\omega_{l-2} - (l-1)\omega_{l-1}) \text{ for } (-n_R-1) \leq l \leq -2 \end{array} \right. \quad \omega_{-1} = \frac{b\tau_a - a^2\tau_b - ba\tau_d - b\tau_e}{a^2+b^2}$$

$$\omega_0 = \frac{\tau_a + b\tau_b - a\tau_d - \tau_e}{a^2+b^2}$$

$$\omega_1 = \frac{a\tau_a + ab\tau_b + b^2\tau_d - a\tau_e}{a^2+b^2}$$

$$\beta_{K_0} = \frac{2a^2 - (b-a)^2 a\tau_b - (b-a)^2 b\tau_d + 2b^2\tau_e}{a^2+b^2} + \tau_c$$

$$\beta_{K_1} = \frac{2a^2\tau_a + 2ba^2\tau_b + 2b^2a\tau_d + 2b^2\tau_e}{a^2+b^2}, \quad (\text{B.8})$$

where $\tau_a = \mu_{-3} + 2\omega_{-2} + a\omega_{-3}$, $\tau_b = \mu_{-2} + a\omega_{-2}$, $\tau_c = \mu_{-1}$, $\tau_d = \mu_0 - b\omega_2$, $\tau_e = \mu_1 - 2\omega_2 - b\omega_3$.

In the next step, we need to calculate the integral

$$\mathcal{A}_0 = \int_{t_0}^1 e^{-(at+\frac{b}{t})} \frac{1}{t} dt = \int_{t_0\sqrt{\frac{a}{b}}}^{\sqrt{\frac{a}{b}}} e^{-\sqrt{ab}(\tau+\frac{1}{\tau})} \frac{1}{\tau} d\tau \quad (\text{B.9})$$

Obviously, this form is the same as $K_0(x)$, the zero order modified Bessel function of the second kind. On the other hand, $t_0\sqrt{\frac{a}{b}} < 1$, therefore:

$$\mathcal{A}_0 = 2K_0(2\sqrt{ab}) - \tilde{\mathcal{K}}_{-1}\left(\frac{1}{t_0\sqrt{\frac{a}{b}}}, \sqrt{ab}\right) - \tilde{\mathcal{K}}_{-1}\left(\sqrt{\frac{a}{b}}, \sqrt{ab}\right), \quad (\text{B.10})$$

where $\tilde{\mathcal{K}}_d(c, u)$ denotes the approximation:

$$\tilde{\mathcal{K}}_d(c, u) \approx e^{-\frac{u}{c}} \sum_{k=0}^N \Xi_N(k, \frac{u}{c}) \frac{\Gamma_{inc}(d+1-k, uc)}{k!u^{d+1-2k}}, \quad (\text{B.11})$$

where N is the development order, $\Gamma_{inc}(a, x) = \int_x^\infty t^{a-1} e^{-t} dt$ is the upper incomplete Gamma function and

$$\Xi_N(k, v) = (-1)^k \sum_{l=0}^k \frac{v^l}{l!} \quad (\text{B.12})$$

Let us now consider the integral

$$\begin{aligned} \mathcal{A}_1 &= \int_{t_0}^1 e^{-(at+\frac{b}{t})} \frac{(t^2-1)^2}{4t^3} dt \\ &= \int_{t_0\sqrt{\frac{a}{b}}}^{\sqrt{\frac{a}{b}}} e^{-\sqrt{ab}(\tau+\frac{1}{\tau})} \frac{(\frac{b}{a}\tau^2-1)^2}{4\frac{b}{a}\tau^3} d\tau. \end{aligned} \quad (\text{B.13})$$

Applying a similar method as for \mathcal{A}_0 in deriving the close form of \mathcal{A}_1 , we get

$$\begin{aligned} \mathcal{A}_1 &= \frac{1}{2a} \left(2\sqrt{\frac{b}{a}} K_1(2\sqrt{ab}) \right. \\ &\quad \left. - \sqrt{\frac{b}{a}} \left(\tilde{k}_1\left(\frac{1}{t_0\sqrt{\frac{a}{b}}}, \sqrt{ab}\right) + \tilde{k}_1\left(\frac{a}{b}, \sqrt{ab}\right) \right) \right. \\ &\quad \left. + b \left(\tilde{k}_2\left(t_0\sqrt{\frac{a}{b}}, \sqrt{ab}\right) - \tilde{k}_2\left(\sqrt{\frac{a}{b}}, \sqrt{ab}\right) \right) \right), \end{aligned} \quad (\text{B.14})$$

where $K_1(x)$ denotes the first order modified Bessel function of the second kind and

$$\tilde{k}_1(c, u) = u \left(\tilde{\mathcal{K}}_1(c, u) + \tilde{\mathcal{K}}_{-3}(c, u) - 2\tilde{\mathcal{K}}_{-1}(c, u) \right) \quad (\text{B.15})$$

$$\tilde{k}_2(c, u) = \left(1 - \frac{a}{b}\right) \tilde{\mathcal{K}}_{-1}(c, u) - \left(1 - \left(\frac{a}{b}\right)^2\right) \tilde{\mathcal{K}}_{-3}(c, u) \quad (\text{B.16})$$

Publications

[a] Viet-Hoa Nguyen, Olivier Berder, and Pascal Scalart. "On the efficiency of sphere decoding for linearly precoded MIMO systems." *IEEE Wireless Communications and Networking Conference (WCNC)*, pp. 4021-4025, 2013.

[b] Viet-Hoa Nguyen, Olivier Berder, Charlotte Langlais, and Baptiste Vrigneau. "Distributed minimum euclidean distance based precoding for wireless sensor network." *IEEE International Conference on In Computing, Networking and Communications (ICNC)*, pp. 918-923 , 2015.

[c] Viet-Hoa Nguyen, O. Berder, C. Langlais, and B. Vrigneau. Précodage distribué basé sur la distance euclidienne pour les réseaux de capteurs sans fil. *In GRETSI*, 2015.

[d] V. H. Nguyen, B. Vrigneau, M. Bhatnagar, O. Berder, and C. Langlais. Distributed Precoding for Decode-and-Forward Protocol Based Wireless Sensor Networks. To be submitted to *IEEE Transaction on Wireless Communication*.

[e] V. H. Nguyen, B. Vrigneau, O. Berder, and C. Langlais. On the performance of distributed precoding Amplify-and-Forward in Wireless Body Area Sensor Network. To be submitted to *IEEE International Conference on Communications (ICC)*, 2016.

Bibliography

- [1] “BoWI: Body World Interaction,” <http://www.bowi.cominlabs.ueb.eu/>.
- [2] “General minimum euclidean distance-based precoder for mimo wireless systems,” *EURASIP Journal on Advances in Signal Processing*, vol. 2013, no. 1, 2013.
- [3] H. Akaike, “Information theory and an extension of the maximum likelihood principle,” *Selected Papers of Hirotugu Akaike*, pp. 199–213, 1998.
- [4] I. F. Akyildiz, W. Su, Y. Sankarasubramaniam, and E. Cayirci, “A survey on sensor networks,” *IEEE Communications magazine*, vol. 40, no. 8, pp. 102–114, 2002.
- [5] P. Anghel, G. Leu, M. Kaveh *et al.*, “Multi-user space-time coding in cooperative networks,” *Proceedings IEEE International Conference on Acoustics, Speech, and Signal Processing (ICASSP)*, vol. 4, pp. IV–73, 2003.
- [6] G. Barriac, R. Mudumbai, and U. Madhow, “Distributed beamforming for information transfer in sensor networks,” *Third International Symposium on Information Processing in Sensor Networks (IPSN)*, pp. 81–88, 2004.
- [7] E. Beres and R. Adve, “Selection cooperation in multi-source cooperative networks,” *IEEE Transactions on Wireless Communications*, vol. 7, no. 1, pp. 118–127, 2008.
- [8] M. R. Bhatnagar and A. Hjørungnes, “ML decoder for decode-and-forward based cooperative communication system,” *IEEE Transactions on Wireless Communications*, vol. 10, no. 12, pp. 4080–4090, 2011.

- [9] A. Bletsas, A. Khisti, D. P. Reed, and A. Lippman, “A simple cooperative diversity method based on network path selection,” *IEEE Journal on Selected Areas in Communications*, vol. 24, no. 3, pp. 659–672, 2006.
- [10] A. Bletsas, A. Khisti, and M. Z. Win, “Opportunistic cooperative diversity with feedback and cheap radios,” *IEEE Transactions on Wireless Communications*, vol. 7, no. 5, pp. 1823–1827, 2008.
- [11] B. Braem, B. Latre, I. Moerman, C. Blondia, E. Reusens, W. Joseph, L. Martens, and P. Demeester, “The need for cooperation and relaying in short-range high path loss sensor networks,” *International Conference on Sensor Technologies and Applications (SensorComm)*, pp. 566–571, 2007.
- [12] D. Brennan, “Linear diversity combining techniques,” *Proceedings of the IRE*, vol. 47, no. 6, pp. 1075–1102, 1959.
- [13] Y. Chen, G. Yu, P. Qiu, and Z. Zhang, “Power-aware cooperative relay selection strategies in wireless ad hoc networks,” *IEEE 17th International Symposium on Personal, Indoor and Mobile Radio Communications*, pp. 1–5, 2006.
- [14] M. Chiani, M. Z. Win, and A. Zanella, “On the capacity of spatially correlated mimo rayleigh-fading channels,” *IEEE Transactions on Information Theory*, vol. 49, no. 10, pp. 2363–2371, 2003.
- [15] H.-J. Choi, S.-H. Park, S.-R. Lee, and I. Lee, “Distributed precoding techniques for weighted sum rate maximization in MIMO interfering broadcast channels,” *IEEE Vehicular Technology Conference (VTC Fall)*, pp. 1–5, 2012.
- [16] L. Collin, O. Berder, P. Rostaing, and G. Burel, “Optimal minimum distance-based precoder for MIMO spatial multiplexing systems,” *IEEE Transactions on Signal Processing*, vol. 52, no. 3, pp. 617–627, 2004.
- [17] D. Costello and S. Lin, *Error control coding*, 2004.
- [18] S. L. Cotton and W. G. Scanlon, “A statistical analysis of indoor multipath fading for a narrowband wireless body area network,” *IEEE 17th International*

- Symposium on Personal, Indoor and Mobile Radio Communications*, pp. 1–5, 2006.
- [19] T. M. Cover and A. E. Gamal, “Capacity theorems for the relay channel,” *IEEE Transactions on Information Theory*, vol. 25, no. 5, pp. 572–584, 1979.
- [20] S. Cui, A. J. Goldsmith, and A. Bahai, “Energy-efficiency of MIMO and cooperative MIMO techniques in sensor networks,” *IEEE Journal on Selected Areas in Communications*, vol. 22, no. 6, pp. 1089–1098, 2004.
- [21] E. Farella, A. Pieracci, L. Benini, and A. Acquaviva, “A wireless body area sensor network for posture detection,” *Proceedings 11th IEEE Symposium on Computers and Communications (ISCC)*, pp. 454–459, 2006.
- [22] A. Fort, C. Desset, P. Wambacq, and L. Biesen, “Indoor body-area channel model for narrowband communications,” *IET microwaves, antennas & propagation*, vol. 1, no. 6, pp. 1197–1203, 2007.
- [23] K. Fujii, K. Ito, and S. Tajima, “Signal propagation of wearable computer using human body as transmission channel,” *Proceedings of the International Symposium on Antennas and Propagation ISAP-02*, pp. 512–515, 2002.
- [24] M. Fukumoto and Y. Tonomura, ““body coupled fingerring”: wireless wearable keyboard,” *Proceedings of the ACM SIGCHI Conference on Human factors in computing systems*, pp. 147–154, 1997.
- [25] D. Gesbert, M. Shafi, D.-s. Shiu, P. J. Smith, and A. Naguib, “From theory to practice: an overview of mimo space-time coded wireless systems,” *IEEE Journal on Selected Areas in Communications*, vol. 21, no. 3, pp. 281–302, 2003.
- [26] A. Gorokhov, D. Gore, A. J. Paulraj *et al.*, “Receive antenna selection for mimo spatial multiplexing: theory and algorithms,” *IEEE Transactions on Signal Processing*, vol. 51, no. 11, pp. 2796–2807, 2003.

- [27] K. Hachisuka, A. Nakata, T. Takeda, Y. Terauchi, K. Shiba, K. Sasaki, H. Hosaka, and K. Itao, "Development and performance analysis of an intra-body communication device," *12th International Conference on Solid-State Sensors, Actuators and Microsystems (TRANSDUCERS)*, vol. 2, pp. 1722–1725, 2003.
- [28] T. Handa, S. Shoji, S. Ike, S. Takeda, and T. Sekiguchi, "A very low-power consumption wireless eeg monitoring system using body as a signal transmission medium," *International Conference on Solid State Sensors and Actuators (TRANSDUCERS)*, vol. 2, pp. 1003–1006, 1997.
- [29] J.-H. Hauer, "Leveraging human mobility for communication in body area networks," *ACM Transactions on Sensor Networks (TOSN)*, vol. 10, no. 3, p. 39, 2014.
- [30] V. Havary-Nassab, S. Shahbazpanahi, A. Grami, and Z.-Q. Luo, "Distributed beamforming for relay networks based on second-order statistics of the channel state information," *IEEE Transactions on Signal Processing*, vol. 56, no. 9, pp. 4306–4316, 2008.
- [31] W. W. Ho, T. Q. Quek, and S. Sun, "Distributed precoding for network MIMO," *IEEE International Conference on Communications (ICC)*, pp. 1–5, 2010.
- [32] B. M. Hochwald and S. Ten Brink, "Achieving near-capacity on a multiple-antenna channel," *IEEE Transactions on Communications*, vol. 51, no. 3, pp. 389–399, 2003.
- [33] A. Høst-Madsen and J. Zhang, "Capacity bounds and power allocation for wireless relay channels," *IEEE Transactions on Information Theory*, vol. 51, no. 6, pp. 2020–2040, 2005.
- [34] W.-J. Huang, Y.-W. P. Hong, and C.-C. J. Kuo, "Lifetime maximization for amplify-and-forward cooperative networks," *IEEE Transactions on Wireless Communications*, vol. 7, no. 5, pp. 1800–1805, 2008.

- [35] K.-S. Hwang and Y.-C. Ko, “An efficient relay selection algorithm for cooperative networks,” *IEEE 66th Vehicular Technology Conference (VTC-Fall)*, pp. 81–85, 2007.
- [36] A. T. James, “Distributions of matrix variates and latent roots derived from normal samples,” *The Annals of Mathematical Statistics*, pp. 475–501, 1964.
- [37] J. Jensen, “Sur les fonctions convexes et les inégalités entre les valeurs moyennes,” *Acta Mathematica*, vol. 30, no. 1, pp. 175–193, 1906.
- [38] Y. Jing and B. Hassibi, “Distributed space-time coding in wireless relay networks,” *IEEE Transactions on Wireless Communications*, vol. 5, no. 12, pp. 3524–3536, 2006.
- [39] Y. Jing and H. Jafarkhani, “Using orthogonal and quasi-orthogonal designs in wireless relay networks,” *IEEE Transactions on Information Theory*, vol. 53, no. 11, pp. 4106–4118, 2007.
- [40] Z. Jingmei, Z. Qi, S. Chunju, W. Ying, Z. Ping, and Z. Zhang, “Adaptive optimal transmit power allocation for two-hop non-regenerative wireless relaying system,” *IEEE 59th Vehicular Technology Conferenc (VTC-Spring)*, vol. 2, pp. 1213–1217, 2004.
- [41] E. Jovanov, A. Milenkovic, C. Otto, and P. C. De Groen, “A wireless body area network of intelligent motion sensors for computer assisted physical rehabilitation,” *Journal of NeuroEngineering and rehabilitation*, vol. 2, no. 1, p. 6, 2005.
- [42] M. Ju and I.-M. Kim, “Ml performance analysis of the decode-and-forward protocol in cooperative diversity networks,” *IEEE Transactions on Wireless Communications*, vol. 8, no. 7, pp. 3855–3867, 2009.
- [43] M. Kang and M.-S. Alouini, “Largest eigenvalue of complex wishart matrices and performance analysis of MIMO MRC systems,” *IEEE Journal on Selected Areas in Communications*, vol. 21, no. 3, pp. 418–426, 2003.

- [44] S. Kim, S. Kim, and D.-S. Eom, "Rssi/lqi-based transmission power control for body area networks in healthcare environment," *IEEE Journal of Biomedical and Health Informatics*, vol. 17, no. 3, pp. 561–571, 2013.
- [45] S. Krusevac, P. Rapajic, and R. A. Kennedy, "Channel capacity estimation for mimo systems with correlated noise," *IEEE Global Telecommunications Conference (GLOBECOM)*, vol. 5, pp. 5–pp, 2005.
- [46] J. N. Laneman, "Cooperative communications in mobile ad hoc networks," *IEEE Signal Processing Magazine*, vol. 1053, no. 5888/06, 2006.
- [47] J. N. Laneman and G. W. Wornell, "Energy-efficient antenna sharing and relaying for wireless networks," *IEEE Wireless Communications and Networking Conference (WCNC)*, vol. 1, pp. 7–12, 2000.
- [48] B. Latré, B. Braem, I. Moerman, C. Blondia, and P. Demeester, "A survey on wireless body area networks," *Wireless Networks*, vol. 17, no. 1, pp. 1–18, 2011.
- [49] B. Latre, B. Braem, I. Moerman, C. Blondia, E. Reusens, W. Joseph, and P. Demeester, "A low-delay protocol for multihop wireless body area networks," *Fourth Annual International Conference on Mobile and Ubiquitous Systems: Networking & Services (MobiQuitous)*, pp. 1–8, 2007.
- [50] D. P. Lindsey, E. L. McKee, M. L. Hull, and S. M. Howell, "A new technique for transmission of signals from implantable transducers," *IEEE Transactions on Biomedical Engineering*, vol. 45, no. 5, pp. 614–619, 1998.
- [51] K. Lorincz, D. J. Malan, T. R. Fulford-Jones, A. Nawoj, A. Clavel, V. Shnyder, G. Mainland, M. Welsh, and S. Moulton, "Sensor networks for emergency response: challenges and opportunities," *IEEE Pervasive Computing*, vol. 3, no. 4, pp. 16–23, 2004.
- [52] D. J. Love, R. W. Heath, V. K. Lau, D. Gesbert, B. D. Rao, and M. Andrews, "An overview of limited feedback in wireless communication systems," *IEEE Journal on Selected Areas in Communications*, vol. 26.

- [53] D. J. Love and R. W. Heath, "Limited feedback unitary precoding for spatial multiplexing systems," *IEEE Transactions on Information Theory*, vol. 51, no. 8, pp. 2967–2976, 2005.
- [54] J. Luo, R. S. Blum, L. J. Cimini, L. J. Greenstein, and A. M. Haimovich, "Decode-and-forward cooperative diversity with power allocation in wireless networks," *IEEE Transactions on Wireless Communications*, vol. 6, no. 3, pp. 793–799, 2007.
- [55] G. MADI, "Optimisation d'un réseau de capteurs par techniques MIMO coopératives. applications possibles : Smart grid, télédétection, ..." Ph.D. dissertation, University of Poitiers, 2012.
- [56] G. Madi, B. Vrigneau, A.-M. Poussard, R. Vauzelle *et al.*, "Cooperative MIMO precoders for energy-efficient transmission in wireless sensor network," *Proceedings of EusipCo*, 2011.
- [57] S. J. Marinkovic and E. M. Popovici, "Nano-power wireless wake-up receiver with serial peripheral interface," *IEEE Journal on Selected Areas in Communications*, vol. 29, no. 8, pp. 1641–1647, 2011.
- [58] D. Miniutti, L. Hanlen, D. Smith, A. Zhang, D. Lewis, D. Rodda, and B. Gilbert, "Narrowband channel characterization for body area networks," *IEEE P802*, pp. 15–08, 2008.
- [59] S. K. Mohammed, E. Viterbo, Y. Hong, and A. Chockalingam, "Mimo precoding with x-and y-codes," *IEEE Transactions on Information Theory*, vol. 57, no. 6, pp. 3542–3566, 2011.
- [60] A. Moldovan, G. Madi, B. Vrigneau, T. Palade, and R. Vauzelle, "Different Criteria of Selection for Quantized Feedback of Minimum-Distance Based MIMO Precoder," *ICWMC*, p. 254 to 258, Jun. 2012. [Online]. Available: <https://hal.archives-ouvertes.fr/hal-00714218>

- [61] S. Movassaghi, M. Abolhasan, J. Lipman, D. Smith, and A. Jamalipour, “Wireless body area networks: A survey,” *IEEE Communications Surveys & Tutorials*, vol. 16, no. 3, pp. 1658–1686, 2014.
- [62] Q. Ngo, O. Berder, and P. Scalart, “Minimum euclidean distance based precoders for MIMO systems using rectangular QAM modulations,” *IEEE Transactions on Signal Processing*, vol. 60, no. 3, pp. 1527–1533, 2012.
- [63] Q.-T. NGO, “Generalized minimum euclidean distance based precoders for mimo spatial multiplexing systems,” Ph.D. dissertation, University of Rennes 1, 2011.
- [64] Q.-T. Ngo, O. Berder, and P. Scalart, “Minimum euclidean distance-based precoding for three-dimensional multiple input multiple output spatial multiplexing systems,” *IEEE Transactions on Wireless Communications*, vol. 11, no. 7, pp. 2486–2495, 2012.
- [65] Q.-T. Ngo, O. Berder, B. Vrigneau, and O. Sentieys, “Minimum distance based precoder for MIMO-OFDM systems using a 16-qam modulation,” *IEEE International Conference on Communications (ICC)*, pp. 1–5, 2009.
- [66] T.-D. Nguyen, O. Berder, and O. Sentieys, “Cooperative MIMO schemes optimal selection for wireless sensor networks,” *IEEE Vehicular Technology Conference Spring (VTC-Spring)*, pp. 85–89, 2007.
- [67] ———, “Impact of transmission synchronization error and cooperative reception techniques on the performance of cooperative mimo systems,” *IEEE International Conference on Communications (ICC)*, pp. 4601–4605, 2008.
- [68] V.-H. Nguyen, O. Berder, C. Langlais, and B. Vrigneau, “Distributed minimum euclidean distance based precoding for wireless sensor network,” *International Conference on Computing, Networking and Communications (ICNC)*, pp. 918–923, 2015.
- [69] V.-H. Nguyen, B. Vrigneau, M. Bhatnagar, O. Berder, and C. Langlais, “Distributed precoding for decode-and-forward protocol based wireless sensor net-

- works,” *To be submitted to IEEE Transaction on Wireless Communication*, 2015.
- [70] V.-H. Nguyen, B. Vrigneau, C. Langlais, and O. Berder, “On the performance of distributed precoding amplify-and-forward in wireless body area sensor network,” *submitted to IEEE International Conference on Communications (ICC)*, 2016.
- [71] M. OBERLE, “Low power system-on-chip for biomedical application,” Ph.D. dissertation, IIS/ETH Zurich, 2002.
- [72] C. Otto, A. Milenkovic, C. Sanders, and E. Jovanov, “System architecture of a wireless body area sensor network for ubiquitous health monitoring,” *Journal of Mobile Multimedia*, vol. 1, no. 4, pp. 307–326, 2006.
- [73] O. J. Oyedapo, B. Vrigneau, and R. Vauzelle, “Performance analysis of closed-loop mimo precoder based on the probability of minimum distance,” *IEEE Transactions on Wireless Communications*, 2014.
- [74] L. H. Ozarow, S. Shamai, and A. D. Wyner, “Information theoretic considerations for cellular mobile radio,” *IEEE Transactions on Vehicular Technology*, vol. 43, no. 2, pp. 359–378, 1994.
- [75] A. Özgür, O. Lévêque, and D. N. Tse, “Hierarchical cooperation achieves optimal capacity scaling in ad hoc networks,” *IEEE Transactions on Information Theory*, vol. 53, no. 10, pp. 3549–3572, 2007.
- [76] S. Park and S. Jayaraman, “Enhancing the quality of life through wearable technology,” *IEEE Engineering in Medicine and Biology Magazine*, vol. 22, no. 3, pp. 41–48, 2003.
- [77] K. Partridge, B. Dahlquist, A. Veiseh, A. Cain, A. Foreman, J. Goldberg, and G. Borriello, “Empirical measurements of intrabody communication performance under varied physical configurations,” *Proceedings of the 14th annual ACM symposium on User interface software and technology*, pp. 183–190, 2001.

- [78] E. R. Post, M. Reynolds, M. Gray, J. Paradiso, and N. Gershenfeld, “Intrabody buses for data and power,” *iswc*, p. 52, 1997.
- [79] Q. Qu, L. B. Milstein, and D. R. Vaman, “Cooperative and constrained mimo communications in wireless ad hoc/sensor networks,” *IEEE Transactions on Wireless Communications*, vol. 9, no. 10, pp. 3120–3129, 2010.
- [80] M. Quwaider, J. Rao, and S. Biswas, “Body-posture-based dynamic link power control in wearable sensor networks,” *IEEE Communications Magazine*, vol. 48, no. 7, pp. 134–142, 2010.
- [81] N. E. Roberts and D. D. Wentzloff, “A 98nm wake-up radio for wireless body area networks,” *IEEE Radio Frequency Integrated Circuits Symposium (RFIC)*, pp. 373–376, 2012.
- [82] A. G. Ruzzelli, R. Jurdak, G. M. O’Hare, and P. Van Der Stok, “Energy-efficient multi-hop medical sensor networking,” *Proceedings of the 1st ACM SIGMOBILE international workshop on Systems and networking support for healthcare and assisted living environments*, pp. 37–42, 2007.
- [83] M. Safari and M. Uysal, “Cooperative diversity over log-normal fading channels: performance analysis and optimization,” *IEEE Transactions on Wireless Communications*, vol. 7, no. 5, pp. 1963–1972, 2008.
- [84] H. Sampath, P. Stoica, and A. Paulraj, “Generalized linear precoder and decoder design for MIMO channels using the weighted MMSE criterion,” *IEEE Transactions on Communications*, vol. 49, no. 12, pp. 2198–2206, 2001.
- [85] W. G. Scanlon and S. L. Cotton, “Understanding on-body fading channels at 2.45 ghz using measurements based on user state and environment,” *Loughborough Antennas and Propagation Conference (LAPC)*, pp. 10–13, 2008.
- [86] R. Schmidt, T. Norgall, J. Mörsdorf, J. Bernhard, and T. von der Grün, “Body area network ban—a key infrastructure element for patient-centered medical applications,” *Biomedizinische Technik/Biomedical Engineering*, vol. 47, no. s1a, pp. 365–368, 2002.

- [87] L. Schumacher, K. I. Pedersen, and P. E. Mogensen, “From antenna spacings to theoretical capacities-guidelines for simulating mimo systems,” *The 13th IEEE International Symposium on Personal, Indoor and Mobile Radio Communications*, vol. 2, pp. 587–592, 2002.
- [88] A. Sendonaris, E. Erkip, and B. Aazhang, “User cooperation diversity. part i. system description,” *IEEE Transactions on Communications*, vol. 51, no. 11, pp. 1927–1938, 2003.
- [89] —, “User cooperation diversity. part ii. implementation aspects and performance analysis,” *IEEE Transactions on Communications*, vol. 51, no. 11, pp. 1939–1948, 2003.
- [90] S. Simoens, O. Muñoz-Medina, J. Vidal, and A. d. Coso, “Compress-and-forward cooperative mimo relaying with full channel state information,” *IEEE Transactions on Signal Processing*, vol. 58, no. 2, pp. 781–791, 2010.
- [91] D. Smith, L. Hanlen, D. Miniutti, J. Zhang, D. Rodda, and B. Gilbert, “Statistical characterization of the dynamic narrowband body area channel,” *First International Symposium on Applied Sciences on Biomedical and Communication Technologies (ISABEL)*, pp. 1–5, 2008.
- [92] D. Smith, L. Hanlen, J. Zhang, D. Miniutti, D. Rodda, and B. Gilbert, “Characterization of the dynamic narrowband on-body to off-body area channel,” *IEEE International Conference on Communications (ICC)*, pp. 1–6, 2009.
- [93] D. B. Smith, L. W. Hanlen, J. A. Zhang, D. Miniutti, D. Rodda, and B. Gilbert, “First-and second-order statistical characterizations of the dynamic body area propagation channel of various bandwidths,” *annals of telecommunications-Annales des télécommunications*, vol. 66, no. 3-4, pp. 187–203, 2011.
- [94] J. M. Steele, *The Cauchy-Schwarz master class: an introduction to the art of mathematical inequalities*, 2004.

- [95] P. Stoica and G. Ganesan, "Maximum-SNR spatial-temporal formatting designs for MIMO channels," *IEEE Transactions on Signal Processing*, vol. 50, no. 12, pp. 3036–3042, 2002.
- [96] W. Su, A. K. Sadek, and K. Liu, "Ser performance analysis and optimum power allocation for decode-and-forward cooperation protocol in wireless networks," *IEEE Wireless Communications and Networking Conference*, vol. 2, pp. 984–989, 2005.
- [97] L. Sun, T. Zhang, L. Lu, and H. Niu, "Cooperative communications with relay selection in wireless sensor networks," *IEEE Transactions on Consumer Electronics*, vol. 55, no. 2, pp. 513–517, 2009.
- [98] A. Tajer and A. Nosratinia, "Opportunistic cooperation via relay selection with minimal information exchange," *IEEE International Symposium on Information Theory (ISIT)*, pp. 1926–1930, 2007.
- [99] R. Tannious and A. Nosratinia, "Spectrally-efficient relay selection with limited feedback," *IEEE Journal on Selected Areas in Communications*, vol. 26, no. 8, pp. 1419–1428, 2008.
- [100] E. Telatar, "Capacity of multi-antenna gaussian channels," *European transactions on telecommunications*, vol. 10, no. 6, pp. 585–595, 1999.
- [101] S. Ullah, H. Higgins, B. Braem, B. Latre, C. Blondia, I. Moerman, S. Saleem, Z. Rahman, and K. S. Kwak, "A comprehensive survey of wireless body area networks," *Journal of medical systems*, vol. 36, no. 3, pp. 1065–1094, 2012.
- [102] E. C. Van Der Meulen, "Three-terminal communication channels," *Advances in applied Probability*, pp. 120–154, 1971.
- [103] K. Vardhe, D. Reynolds, and B. D. Woerner, "Joint power allocation and relay selection for multiuser cooperative communication," *IEEE Transactions on Wireless Communications*, vol. 9, no. 4, pp. 1255–1260, 2010.

- [104] C.-L. Wang and S.-J. Syue, "An efficient relay selection protocol for cooperative wireless sensor networks," *IEEE Wireless Communications and Networking Conference (WCNC)*, pp. 1–5, 2009.
- [105] K. Y. Yazdandoost, K. Sayrafian-Pour *et al.*, "Channel model for body area network (BAN)," *IEEE P802.15*, 2009.
- [106] R. Zakhour and D. Gesbert, "Distributed multicell-MISO precoding using the layered virtual SINR framework," *IEEE Transactions on Wireless Communications*, vol. 9, no. 8, pp. 2444–2448, 2010.
- [107] T. G. Zimmerman, "Personal area networks: near-field intrabody communication," *IBM systems Journal*, vol. 35, no. 3.4, pp. 609–617, 1996.